bioRxiv preprint doi: https://doi.org/10.1101/479980; this version posted November 27, 2018. The copyright holder for this preprint (which was not certified by peer review) is the author/funder, who has granted bioRxiv a license to display the preprint in perpetuity. It is made available under aCC-BY-NC-ND 4.0 International license.

Title page

Integrated multiomic analysis from chromatin to translation of stimulus-regulated gene activity exposes dominant patterns of nuclear-level control

Running Head: Dynamics in Nuclear Gene Regulatory Control by Hypoxia

Travis A Lee[1,2] and Julia Bailey-Serres[1]
[1]Center for Plant Cell Biology and Botany and Plant Sciences Department, University of California, Riverside, California 92521, USA
[2]Plant Biology Laboratory, The Salk Institute for Biological Studies, La Jolla, CA 92037, USA

ORCID ID: 0000-0002-8352-8956 (T.A.L.)
ORCID ID: 0000-0002-8568-7125 (J.B.-S.)

Corresponding author: Julia Bailey-Serres

bioRxiv preprint doi: https://doi.org/10.1101/479980; this version posted November 27, 2018. The copyright holder for this preprint (which was not certified by peer review) is the author/funder, who has granted bioRxiv a license to display the preprint in perpetuity. It is made available under aCC-BY-NC-ND 4.0 International license.

Background

Limitations in molecular oxygen reduce ATP production and dramatically curtail energy demanding processes in eukaryotes. Little is known of the influence of hypoxia on nuclear regulatory mechanisms and their integration with mRNA accumulation and translation. Here we apply multomic technologies to evaluate epigenetic to translational regulation in response to hypoxic stress in seedlings of *Arabidopsis.* We focus on hypoxia-responsive (*HRG*) and *RIBOSOMAL PROTEIN* (*RP*) genes that encode actively and poorly translated mRNAs under hypoxia, respectively.

Results

Evaluation of hypoxia-induced dynamics in eight chromatin readouts including chromatin accessibility, histone modifications, RNA polymerase II (RNAPII) activity plus three RNA populations (nuclear, polyadenylated, and ribosome-associated) identified distinct patterns of nuclear regulation. *HRG*s coordinately increased promoter accessibility, Histone 2A.Z eviction, Histone 3-lysine 9 acetylation, and RNAPII engagement. Many *HRG* promoters were bound by HYPOXIA-RESPONSIVE ETHYLENE RESPONSIVE FACTOR (ERF) 2 (HRE2) or had *cis*-elements targeted by related ERFs. Hypoxia sustained *RP* transcription but the transcripts were largely retained in the nucleus. We discovered heat and oxidative stress genes with pronounced hypoxia-induced RNAPII engagement accompanied by elevated nuclear and ribosome-associated but not polyadenylated transcripts. These heat stress genes had *cis*-elements recognized by HEAT SHOCK FACTOR transcriptional activators, 5' biased histone marks, less H2A.Z eviction and Histone 3-lysine 4 trimethylation than genes bound by HRE2 and coordinately upregulated from transcription through translation. Genes of the circadian cycle, photosynthesis, and development also displayed notable nuclear regulation.

Conclusions

Hypoxia triggers dominant patterns in nuclear regulatory control that differentiate cohorts of genes associated with stress responses and growth.

Keywords: *Arabidopsis thaliana*, hypoxia, histone modification, H2A.Z, ATAC-seq, RNA Polymerase II, nascent RNA, polyadenylated RNA, transcriptome, TRAP-seq

bioRxiv preprint doi: https://doi.org/10.1101/479980; this version posted November 27, 2018. The copyright holder for this preprint (which was not certified by peer review) is the author/funder, who has granted bioRxiv a license to display the preprint in perpetuity. It is made available under aCC-BY-NC-ND 4.0 International license.

Background

The regulated expression of protein coding genes in eukaryotes involves processes within the nucleus including the remodeling of chromatin, recruitment of RNA polymerase II, co-transcriptional processing and the export of mature mRNA to the cytoplasm, after which it may be translated, sequestered or degraded. These processes are modulated in response to conditions that necessitate alterations in metabolism and management of energy reserves to maintain cell viability including oxygen deficiency. In *Arabidopsis thaliana*, cellular hypoxia promotes activation of anaerobic metabolism to sustain cell viability. This involves rapid activation in transcription followed by selective translation of a subset of cellular mRNAs, while others are transiently sequestered and stabilized whereas others are degraded [1–4]. The mRNAs that are well translated under hypoxic stress are not characterized by a sequence element or feature [1,3,4] but are likely to be transcriptionally upregulated by the stress.

Transcriptional activation in response to hypoxia involves the evolutionarily conserved group VII ethylene response factor (ERFVII) transcription factors (TFs) that are required for regulation of metabolism and survival of hypoxia [5–13]. The five members of this family are stabilized under hypoxia, due to attenuation of their oxygen-stimulated targeted proteolysis via the N-end rule pathway [7,8,12,14]. The constitutively synthesized ERFVIIs RELATED TO APETALA 2.2, 2.3, and 2.12 (RAP2.2, RAP2.3, RAP2.12) transactivate hypoxia-responsive gene (*HRG*) promoters in protoplasts [13,15,16] through a conserved *cis*-acting hypoxia-responsive promoter element (HRPE) identifiable in ~50% of the 49 *HRGs* expressed across cell types [7,15,17]. The two additional ERFVIIs, HYPOXIA-RESPONSIVE ERF 1/2 (HRE1/2) only weakly transactivate via the HRPE in protoplasts [15,18], suggesting they interact with a distinct *cis*-element or may otherwise influence gene transcription. Both *HRE1/2* are upregulated by hypoxia along with *ALCOHOL DEHYDROGENASE 1* (*ADH1*) and *PLANT CYSTEINE OXIDASE 1/2* (*PCO1/2*) that are required for anaerobic metabolism and negatively regulate the anaerobic response by catalyzing the oxygen-stimulated turnover of ERFVIIs, respectively [14,16,19,20].

Transcriptional activation requires access of TFs to specific *cis*-regulatory elements that are typically located near the 5' transcription start site (TSS) of genes and facilitate assembly of an RNAPII initiation complex. The distribution of nucleosomes across a genome can be assessed by DNAse I hypersensitivity site mapping [21,22] or the Assay for Transposase-Accessible Chromatin using sequencing (ATAC-seq) [21]. ATAC-seq leverages a Tn5 transposon that simultaneously inserts adaptor sequences and cleaves DNA in nucleosome-depleted chromatin regions [23]. The depletion of nucleosomes relative to the 5' TSS of each gene is controlled by a cadre of ATP dependent chromatin remodelers and can be influenced by interactions with certain TFs. The spatial distribution of nucleosomes with specific histones in their octamer core is routinely determined by chromatin immunopurification and sequencing (ChIP-seq). TF binding and RNAPII activity are influenced by and influence histone modifications and variants [24,25]. Tri-methylated Histone 3-lysine 27 (H3K27me3) and H3K4me3 are prevalent in the gene body of lowly and actively transcribed genes, respectively [25,26]. Acetylation of Histone H3 lysine residues (H3K9ac, H3K14ac) that reduce interactions between DNA and histones are associated with ongoing transcription [25]; these marks are also correlated with the active transcription of genes during environmental stress in plants [27–29]. Constitutive high levels of the Histone 2A variant H2A.Z are associated with stress-activated

bioRxiv preprint doi: https://doi.org/10.1101/479980; this version posted November 27, 2018. The copyright holder for this preprint (which was not certified by peer review) is the author/funder, who has granted bioRxiv a license to display the preprint in perpetuity. It is made available under aCC-BY-NC-ND 4.0 International license.

transcription and its presence at the first nucleosome within the gene body may reduce the energy required for commencement of transcriptional elongation on genes activated by elevated temperatures [30–34]. To date, there has been no genome-scale evaluation of coordinated dynamics in chromatin accessibility, histone alterations, transcription, and translation in a plant or other eukaryotes.

As transcription commences, the phosphorylation of specific residues within the heptad repeats of the carboxyl terminal domain (CTD) of RNAPII orchestrate interactions with factors that facilitate transcription-coupled histone modifications as well as co-transcriptional 5' capping, splicing, and polyadenylation of the nascent transcript [35,36]. RNAPII CTD phosphorylation at Serine 2 (Ser2P) demarks active elongation [37]. In animals, pausing of RNAPII downstream of the TSS is common among genes activated by heat stress [38]. Global nuclear run-on sequencing (GRO-seq) on *Arabidopsis* seedlings under optimal growth conditions found limited evidence of promoter-proximal pausing of RNAPII [39] but the mapping of the 5' end of nascent transcripts by Native Elongating Transcript sequencing (NET-seq) [40] indicated that elongation can be rate-limiting shortly after initiation. Both studies found transcription is rate-limited as RNAPII pauses just beyond the site of cleavage and polyadenylation. Nuclear splicing, polyadenylation and export to the cytoplasm is regulated during development and in response to environmental cues, and hypoxia promotes alternative splicing [2,3,17,41], alternative polyadenylation [42], and nuclear retention of transcripts [43] in plants. We hypothesized that the strong hypoxia-induced upregulation of *HRG*s and their prioritization for translation may be associated with specific features of their chromatin or transcriptional activation.

Here, we monitored dynamics in histones, chromatin accessibility, HRE2 binding and RNAPII-Ser2P distribution along gene bodies in response to hypoxic stress in seedlings. These nuclear readouts were compared with dynamics in nuclear RNA (nRNA), polyadenylated RNA (polyA RNA) and ribosome-associated RNA. An integrative analysis exposed distinct patterns of chromatin signatures, *cis*-element enrichment, and temporal regulation of nRNA accompanied by modulation of polyA or translated transcripts. This multiomic analysis provides a rich resource for evaluation of gene activity from epigenetic state and RNAPII activity through translation in a model organism.

Results

A multiscale dataset for analysis of dynamics from chromatin to translation

To better understand dynamics in gene regulatory variation following hypoxic stress, we developed chromatin and RNA-based genome-scale datasets in triplicate for seedlings treated with non-lethal hypoxic stress (2 h, 2HS; 9 h, 9HS) or normoxia (2NS, 9NS) consistent with prior high-throughput analysis of cell-type specific and translational regulation [2,3,17] (Fig. 1a; Figure S1a). The position and abundance of H3K9ac, H3K14ac, H3K4me3, H3K27me3, and H2A.Z was surveyed by ChIP-seq. The capture of nuclei by Isolation of Nuclei Tagged in Specific Cell Types (INTACT) was coupled with mapping of chromatin accessible regions by ATAC-seq [44,45] and ChIP-seq to monitor binding of the TF HRE2 and elongating RNAPII-Ser2P. Three transcript populations were compared including nRNA obtained by INTACT (rRNA subtracted nascent transcriptome [46]), polyA RNA obtained by oligo dT affinity purification (transcriptome) and polyA RNA associated with ribosomes obtained by Translating Ribosome Affinity Purification (TRAP RNA; translatome) [3,47]. The sequence reads mapped across

bioRxiv preprint doi: https://doi.org/10.1101/479980; this version posted November 27, 2018. The copyright holder for this preprint (which was not certified by peer review) is the author/funder, who has granted bioRxiv a license to display the preprint in perpetuity. It is made available under aCC-BY-NC-ND 4.0 International license.

annotated gene transcripts for each library type and treatment was reproducible but distinguishable by t-Distributed Stochastic Neighbor Embedding analysis (Fig. 1b) and the distribution of read abundance (Fig. 1c; Figure S1b-c). Because the ATAC-seq reads mapped primarily to non-transcribed regions (Fig 1g) these data were assayed separately. These assays of gene activity were used collectively to explore the integration of nuclear and cytoplasmic gene regulatory processes following hypoxic stress.

Stress- and growth-associated genes contrast in chromatin accessibility, histone, modifications and RNA modulation under hypoxia

For the nucleosome level evaluation, H3K9ac, H3K14ac, H3K4me3, H2A.Z, and H3K27me3 were plotted along each annotated protein-coding gene and global averages were compared for each condition (Fig. 1d; Figure S2a). H3 modifications associated with transcription (H3K9ac, H3K14ac, H3K4me3) and stress-activated transcription (H2A.Z) were enriched just 3' of TSS and tapered off at the primary site of polyadenylation (TES), whereas H3K27me3 was distributed more evenly across gene bodies. Hypoxia had little effect on these modifications at the global level, with the exception of a slight elevation of H3K14ac and reduction of H3K4me3 near the TSS. Meaningful alterations were apparent when histone abundance and distribution was surveyed for two gene cohorts with opposing transcript accumulation and translation under hypoxia, the induced and translated *HRG*s (n=49) and stable but poorly translated cytosolic *RPs* (n=246). *HRGs* significantly increased in H3K9ac and decreased in H2A.Z association at 2HS, with limited change in these marks on *RP*s (Fig. 1e, f; Figure S3a-c). We extended the stress to 9 h (9HS) to evaluate H3K9ac and the more slowly changing H3K14ac associated with active transcription. At the global scale, hypoxia increased H3K9ac on 863 and 3,646 genes and H3K14ac on 2 and 1,216 genes and after brief and prolonged hypoxia, respectively (Figure S1b; Table S2). Notably, H3K14ac but not H3K9ac levels progressively increased on *RPs* (Fig. 1f; Figure S1c; Figure S3a,c).

Next, we evaluated dynamics in chromatin accessibility in genic regions by use of ATAC-seq. Accessibility in 5' promoter regions is associated with depletion of nucleosomes and binding of TFs and other transcriptional machinery [45,48,49], whereas accessibility in 3' flanking regions is associated with formation of chromatin loops and transcriptional termination [50,51]. Our ATAC-seq reads mapped almost exclusively within 1000 bp 5' of the TSS and ~300 bp 3' of the major TES of genes in all four conditions (Fig. 2c). At 2HS the summative ATAC-seq peak height was higher than at 2NS, with the opposite trend observed for 9NS and 9HS (Fig. 2a). With respect to the opposingly regulated *HRGs* and *RP*s, the average ATAC signal within promoters rose by 1.8- and 1.4-fold by 2HS, respectively (Fig. 2b). Chromatin remodeling by the stress was evident from the expansion into more 5' and 3' flanking regions of the *HRG*s at both 2HS and 9HS. We also performed peak-calling to recognize Tn5 hypersensitive insertion sites (THSs) in order to quantify localized dynamics in chromatin accessibility, identifying both constitutively present (8,072) and stress-specific THSs (25,795) (Fig. 2c-f; Table S1a).

To complete our integrative survey of gene activity, we compared the distribution of the $\log_2$ fold change (FC) (2HS/2NS) values of the chromatin, RNAPII and RNA readouts genome-wide and for the *HRG*s and *RP*s (Fig. 3a; Table S2a). We found that stress-induced RNAPII-Ser2P engagement was positively correlated with increased H3K9ac and negatively correlated with H2A.Z eviction as demonstrated by the *HRG*s (global R = -0.27, *HRGs* R = -0.79) (global R

bioRxiv preprint doi: https://doi.org/10.1101/479980; this version posted November 27, 2018. The copyright holder for this preprint (which was not certified by peer review) is the author/funder, who has granted bioRxiv a license to display the preprint in perpetuity. It is made available under aCC-BY-NC-ND 4.0 International license.

= 0.43; *HRGs* R = 0.17; Fig. 3 b,c; Figure S4). *RPs* displayed minor changes in RNAPII-Ser2P association at 2HS, yet H3K14ac and nRNA abundance was elevated at the majority of these genes by 9HS (Fig. 3a; Figure S3c; Table S2a). These results demonstrate patterns of stress-induced epigenetic regulation distinct to stress-induced and growth-associated genes.

Regulation at nuclear and cytoplasmic scales can be concordant or discordant

To explore possible coordination of transcriptional and posttranscriptional gene regulation in response to hypoxia we performed a systematic analyses of the Ser2P, nRNA, polyA and TRAP RNA datasets. First, we surveyed whether significantly up- and downregulated genes (DRGs) in one readout were similarly regulated in other readouts. Second, we performed gene clustering to group genes that were co-regulated based on one or more readout.

A four-way comparison of DRGs identified nRNA with the greatest (1,722) and polyA RNA the fewest (602) up-DRGs (Fig. 4a). The vast majority (92%) of the polyA up-DRGs were upregulated in at least one other readout, whereas only 213 (13%) were significantly elevated in all four readouts. Notably, the coordinately upregulated genes included 38 of the 49 *HRG*s. A parallel analysis found 72% of the polyA down-DRGs were significantly reduced in at least one other dataset, with nRNA again displaying the greatest number of DRGs (down-DRGs: Ser2P [206], nRNA [2,608], polyA [291], TRAP [578]) (Fig. 4b). The lack of consensus in nRNA and polyA transcript dynamics suggests these RNA populations of are not equivalent. Indeed, a pairwise comparison of nRNA and polyA RNA abundance in the 2NS and 2HS samples identified transcripts enriched in the nRNA (nucleus-localized transcripts) and polyA RNA fractions (Figure S5a,b; Table S3).

Patterns of differential gene regulation were resolved further by identifying genes that were co-regulated in response to 2HS. Log_2 fold change (FC) values for all DRGs identified in at least one of the four datasets were sorted into 16 groups by partition around medoids (PAM) clustering and evaluated by Gene Ontology (GO) term enrichment (Fig 4c; Table S4a). This identified four clusters of coordinately upregulated (clusters 1-4) and one cluster of coordinately downregulated (cluster 16) genes. Other clusters differed in dynamics in one or more of the readouts. These analyses confirm that hypoxia impacts gene regulatory processes in both the nucleus and cytoplasm. This finding motivated us to consider whether changes in histones were characteristic of the patterns observed in RNAPII-Ser2P and RNA accumulation.

Patterns of histone alteration are associated with concordant and discordant regulation

To explore associations between regulatory variation at the chromatin, RNAPII and RNA scales, the average signal value for each data type of each cluster was plotted along genic regions (Fig. 4d; Figure S6). To appreciate the dynamic regulation of these genes over time, the same clusters were plotted using the 9NS and 9HS chromatin and RNA data (Fig. S7). We found the coordinate (concordant) upregulation of cluster 1-3 gene transcripts at 2HS was accompanied by enhanced chromatin accessibility, eviction of H2A.Z, as well as elevation of H3K9ac and RNAPII-Ser2P across the gene body. The coordinate rise in TRAP RNA level indicated these transcripts were translated in proportion to their increased abundance, as determined previously for the *HRG*s by high-resolution ribosome footprinting analyses [3]. Nearly all *HRGs* were present in the first two clusters, which were enriched for the the GO categories decreased oxygen level (cluster 1, p-adj. $<6.73e^{-22}$) and general stress (cluster 2, $<1.06e^{-21}$) (Table S4a).

bioRxiv preprint doi: https://doi.org/10.1101/479980; this version posted November 27, 2018. The copyright holder for this preprint (which was not certified by peer review) is the author/funder, who has granted bioRxiv a license to display the preprint in perpetuity. It is made available under aCC-BY-NC-ND 4.0 International license.

Genome browser views of two representative *HRGs, ADH1* and *PCO2,* illustrate the coordinate upregulation across the assays of gene activity (Fig. 5a,b).

Cluster 4-8 genes were not coordinately upregulated, indicating they are targets of post-transcriptional regulation. The rise in cluster 4 nRNA coincided with elevation of H3K9ac and RNAPII-Ser2P that is indicative of increased transcription, yet this was not accompanied by a similar rise in polyA or TRAP RNA (Fig. 4c; Figure S6). This discordant pattern could reflect nuclear retention or cytoplasmic destabilization of these transcripts. Clusters 6 and 7 genes were elevated primarily in nRNA at 2HS, a pattern that could reflect nuclear retention of previously synthesized transcripts in response to the stress. Yet another pattern was observed for Cluster 8, which was enriched for genes encoding *RPs* ($<8.06e^{-16}$). As noted for the *RP* cohort (Fig 3a,b; Figure S1b), these genes had limited change in H3K9ac but a rise in H3K14ac and nRNA at 2HS and 9HS (Figures S6 and S7), as illustrated by *RPL37B* (Fig. 3a; Fig. 5d; Figure S1b).

One of the most intriguing clusters was 9, which was notably distinct for the hypoxia-induced engagement of RNAPII-Ser2P without a similar rise in nRNA or polyA RNA. By comparison to cluster 1, cluster 9 had lower and more 5' skewed H2A.Z at 2NS that was only slightly reduced at 2HS (Fig 4d; Figure S9a). In addition, H3K4me3 association was significantly lower for cluster 9 than cluster 1 at 2HS (Figure S9c,d). The status of cluster 9 gene regulation changed between 2HS and 9HS, at which time their promoter region accessibility was elevated, along with H3K9ac, H3K14ac, nRNA and polyA RNA (Figure S7). Both cluster 2 and 9 genes were enriched for heat (cluster 2, $<7.74e^{-14}$; cluster 9, $<6.20e^{-13}$) and oxidative stress (cluster 2, $<1.13e^{-12}$; cluster 9, $<8.23e^{-11}$). The cluster 2 gene *HEAT SHOCK PROTEIN 70-4* (*HSP70-4*), as an example, displayed a 3.4-fold increase in RNAPII-Ser2P across the genic region with a very limited increase in polyA RNA at 2HS but a pronounced increase by 9HS (Fig. 5c). Notably, TRAP mRNA levels were higher than polyA RNA for *HSP70-4* at 2HS, as observed for *ADH1* and *PCO2*.

Highly downregulated genes have distinct stimulus-regulated histone modifications

Survey of the down-DRG genes (clusters 10-16) also showed stimulus-driven dynamics of chromatin, RNAPII and RNAs (Fig. 4a; Figure S6). These clusters displayed two dominant patterns. Cluster 10-14 were distinguished by significant reductions in nRNA at 2HS to 9HS that were accompanied by progressive increases in H3K14ac but limited changes in H2A.Z and H3K9ac. By 9HS, levels of H3K14ac had clearly increased in all but cluster 13, particularly near the TSS (Figure S6; Figure S7). Cluster 15 and 16 genes were strongly and coordinately reduced in RNAPII-Ser2P engagement and all three RNA readouts at 2HS (Fig. 4a; Figure S6). This was accompanied by slight elevation of H2A.Z incorporation and a strong decline in H3K9ac, all antithetical to the changes observed for cluster 1-3 (Figure S9a,c). These genes also had limited change in chromatin accessibility. Of the down-DRGs, only clusters 15 and 16 were strongly enriched for GO categories, including root development (cluster 15, $<3.7e^{-8}$) and regulation of transcription and RNA biosynthesis (cluster 16, $<7.78e^{-7}$). The reduced transcription and translation of these genes would contribute to energy conservation during hypoxia, as reported for the *RP*s [2]. Despite their opposing regulation, we noted that the most highly up- (cluster 1-2) and down-DRGs (cluster 15-16) were characterized by H3 modifications (H3K4me3, H3K9ac, H3K14ac) broadly distributed along the gene body, as opposed a more 5'

bioRxiv preprint doi: https://doi.org/10.1101/479980; this version posted November 27, 2018. The copyright holder for this preprint (which was not certified by peer review) is the author/funder, who has granted bioRxiv a license to display the preprint in perpetuity. It is made available under aCC-BY-NC-ND 4.0 International license.

biased distribution of H3 and H2A.Z in the other clusters. This indicates that H2A.Z distributed across a gene body limits chromatin accessibility and engagement of RNAPII under non-stress conditions.

H3K14 acetylation accompanied by limited H3K9 acetylation is characteristic of synthesized but nuclear-retained transcripts

To assess the impact of prolonged sub-lethal hypoxic stress we monitored the progressive change in H3K9ac, H3K14ac, nRNA, and polyA RNA at 2HS and 9HS by evaluation of $\log_2$ FC distribution again using multiple methods to visualize these genome-scale data (Fig. 6a,b; Figure S8; Table S2a). H3K9ac and H3K14ac levels were progressively and distinctly altered for the *HRG* and *RP* cohorts (Fig. 6a). We observed a coordinated rise in H3K9ac, nRNA and polyA RNA at 2HS and 9HS for clusters 1b-2b, identifying over 360 genes (38 *HRG*s) that were progressively upregulated. By contrast, we resolved patterns of discordant up- and downregulation between clusters 4b-11b, confirming that regulation of these changed as hypoxia was prolonged. Many genes with elevated nRNA at 9HS were enriched for H3K14ac near their TSS (clusters 2b-8b) (Figure S8), as exemplified by the *RPs* (Fig. 1f). Of the 228 cytosolic *RP*s monitored, 149 significantly increased in nRNA abundance at 9HS. Their progressive increase in nRNA demonstrates that genes scored as unchanged or downregulated by polyA transcriptomics may be actively transcribed during the stress but retained in the nucleus as near-full length (non-polyadenylated) nascent or mature transcripts. Other genes were more up- (cluster 6b) or downregulated after 9HS (clusters 8b-11b). Pronounced downregulation at 9HS included the GO categories photosynthesis (cluster 8b, $<5.8e^{-7}$ and $<1.5e^{-6}$), root development (cluster 10b, $<1.7e^{-6}$) and transcription (cluster 11b, $<7.6e^{-6}$) (Table S4b). A key finding was that regulation of transcript abundance may be distinct within the nucleus and the cytoplasm, where the vast majority of polyA RNA is located and undergoes translation, sequestration, or degradation.

Notably, genes associated with phasing of the circadian clock were perturbed by prolonged hypoxic stress. This included maintenance of mRNAs with peak abundance towards the end of the light cycle (cluster 6b; evening genes, circadian rhythm $<7.9e^{-10}$) and reduced upregulation of morning gene transcripts. For example, *TIMING OF CAB EXPRESSION* (*TOC1*) and other evening gene polyA RNAs remained elevated after 9HS (Fig. 6c,d). By contrast, transcripts of the key morning expressed clock regulators *CIRCADIAN CLOCK ASSOCIATED 1* (*CCA1*) (cluster 16b) and *LATE ELONGATED HYPOCOTYL* (*LHY*) (cluster 15b) as well as the midday *PSEUDO RESPONSE REGULATOR 7/9* (*PRR7/9*) were dampened in nRNA and/or polyA RNA at 9HS. Thus, hypoxia imposed in at the end of the day extremely delays or arrests the phasing of the circadian cycle. Low energy stress is known to extend the circadian cycle via SnRK1-mediated enhancement of *PPR7* transcriptional activation just prior to dawn [52]. This mechanism, however, does not seem to be relevant when hypoxia is initiated at the end of the light cycle and continued overnight, as *PPR7* nRNA and polyA RNA was significantly lower at 9HS relative to 9NS. This difference between the effect of hypoxia and conditions that invoke an energy stress could be our imposition of hypoxia at the end of the light cycle or inclusion of sucrose in the medium.

Many coordinately hypoxia-upregulated genes are targets of ERFVII regulation

bioRxiv preprint doi: https://doi.org/10.1101/479980; this version posted November 27, 2018. The copyright holder for this preprint (which was not certified by peer review) is the author/funder, who has granted bioRxiv a license to display the preprint in perpetuity. It is made available under aCC-BY-NC-ND 4.0 International license.

We hypothesized that the 215 coordinately up-DRGs might be transcriptionally activated by the low-oxygen stabilized ERFVIIs. We therefore searched for the presence of the HRPE in genes of each cluster resolved in the 2HS analysis (Fig. 4c) and found it was significantly enriched in cluster 1 promoters (Fig. 7a; Table S5), including the genes with the strongest and most coordinate upregulation. The constitutively expressed ERFVIIs (RAP2.2, RAP2.3 and RAP2.12) activate transcription via the HRPE in transfected protoplasts assays and based on targeted ChIP-qPCR [15,16], whereas the hypoxia-induced ERFs HRE1 and HRE2 do not. Of these, HRE2 is encoded by an *HRG* and is stabilized in seedlings after 2HS [7]. To gain more insight into the role of HRE2, ChIP-seq was performed on 2HS seedlings overexpressing a stabilized version of this ERFVII. Over 75% of the reads mapped within 1 kb upstream of TSSs, with clear enrichment of binding within 500 bp of the TSS (Figure S10; Table S2a). Binding of HRE2 to promoter regions was significant for clusters 1-3 (Fig. 7b). An unsupervised search for motifs enriched in HRE2 peak regions discovered an overrepresented multimeric 5'-GCC-3' element (p-value $<1e^{-351}$) (Fig. 7c; Table S5). This motif did not correspond to the HRPE, rather it resembled the GCC-rich EBP box bound by ERFs including ERFVII RAPs. Indeed, RAP2.12 bound a nearly identical motif based on the *in vitro* DNA affinity purification and sequencing (DAP-seq) assay [53] and stabilized RAP2.3 associated *in vivo* with promoter regions with this element based on ChIP-qPCR [54] and bound *in vitro* to DNA oligos with this sequence in electrophoretic mobility shift assays [55]. Although the HRE2 motif was enriched in cluster 1, it was more prevalent than the HRPE in other clusters (Fig. 7c), leading us to consider HRE2 binding to a promoter and HRPE presence over the HRE2 motif presence as relevant to hypoxia. The binding of HRE2 to the promoter was observed for 60 of the 49 coordinately upregulated genes, of which 23 contained an HRPE (Fig. 7e; Table S2a). Overall, 50% of the 215 coordinately up-DRGs were bound by HRE2 in their promoter region or are likely RAP-ERFVII targets based on the presence of an HRPE in their promoters (Fig. 7e). These results support the conclusion that many of the coordinately up-DRGs are transcriptionally activated by one or more ERFVII.

Hypoxic-stress progressively activates genes in heat and oxidative stress networks

The regulatory variation of oxidative stress and heat response genes displayed at 2HS in clusters 2-3 and 9 was of interest as genes in these categories are upregulated by rapid onset anoxia or prolonged hypoxia [2,3,17,41,56]. Both the onset of hypoxia and reoxygenation trigger a reactive oxygen species (ROS) burst that contributes to signaling [57]. The upregulation of *RESPIRATORY BURST OXIDASE* (*RBOH*) genes including *RBOHD* contributes to survival of hypoxia, submergence and post-submergence recovery [58–61]. The relationship between hypoxia and heat stress is not clearly understood but a brief heat shock protects *Arabidopsis* seedlings from anoxia via cooperative action of the HEAT SHOCK FACTOR (HSF) transcriptional activators HSFA1A/B and HSFA2 [56,62]. Elevation of RNAPII-Ser2P without a commensurate increase in polyA RNA was characteristic of *HSP*s, *RBOH*s and transcriptional co/activators associated with heat and oxidative stress (i.e., *MULTIPROTEIN BRIDGING FACTOR 1C* (*AtMBP1C*), *DEHYDRATION-RESPONSIVE 2A* (*DREB2A*), *ZINC FINGER PROTEIN 12* (*ZAT12*)).

Because strong and coordinate upregulation of genes in response to hypoxia was associated with activation by ERF-VIIs, we considered that the more gradual activation of

bioRxiv preprint doi: https://doi.org/10.1101/479980; this version posted November 27, 2018. The copyright holder for this preprint (which was not certified by peer review) is the author/funder, who has granted bioRxiv a license to display the preprint in perpetuity. It is made available under aCC-BY-NC-ND 4.0 International license.

cluster 9 genes may be mediated by members of HSF transcriptional activators. This led to the discovery that clusters 2 and 3 included several *HSF*s that were elevated in TRAP RNA at 2HS (*HSFA2, HSFA4A,* and *HSFA7A*) and HSF *cis*-elements (HSEs) were significantly enriched in promoters of cluster 2, 3 and 9 genes (Fig. 7d). The pronounced increase in RNAPII-Ser2P engagement on these genes at 2HS corresponded with a rise in nRNA but limited elevation of polyA RNA at either 2HS and 9HS (Figure S11). These genes were distinguishable from the HRE2-bound up-DRGs by a (1) 5' bias in nucleosomes across gene bodies, (2) more 5' localized H2A.Z that was less dramatically evicted by 2HS, (3) reduced H3K4me3, (4) increased H3K14ac that preceded the rise in H3K9ac, (5) and an increase in nRNA not necessarily mirrored in polyA RNA. Collectively, these results resolve patterns of nuclear gene regulatory control that distinguish stress-activated genes regulated by different transcriptional activators.

Discussion

Gene regulation in response to hypoxic stress involves regulation of chromatin, transcription, and post-transcriptional processes in the nucleus and cytoplasm

This study assembled a dataset of genome-wide measurements of chromatin state and intermediary steps of gene expression in seedlings exposed to sub-lethal hypoxic stress and identified time-dependent chromatin and transcript dynamics, the latter not captured by standard transcriptomics. We found that hypoxic stress modulates the (1) position and degree of open chromatin near the TSS, (2) trimethylation and acetylation of H3 lysines, (3) eviction of H2A.Z, (4) engagement of RNAP II-Ser2P, and (5) the abundance of nuclear, polyadenylated and ribosome-associated gene transcripts. Here, we demonstrate that steady-state nuclear and polyA transcriptomes are distinct, as shown by a similar comparison for rice [46]. Our findings of translational regulation are also consistent previous reports [1,63,64]. The use of RNAPII-Ser2P association as a proxy for transcriptional elongation suggests that global levels of transcription were not dramatically dampened by 2HS (Fig. 1c), although there was considerable regulation of individual genes (Fig 1c; Fig. 4c). Remarkably, we discovered that less than 10% of all DRGs were coordinately up- or downregulated at 2HS from transcription (RNAPII-Ser2P) through translation. Four patterns of discontinuous gene regulation were apparent: (1) partial upregulation, characterized by high RNAPII-Ser2P engagement and delayed elevation of polyA RNA, as observed for many heat and oxidative stress genes, (2) compartmentalized downregulation, characterized by maintained RNAPII-Ser2P engagement and increased nRNA abundance with limited change in polyA RNA, as observed for *RP*s; and (3) enhanced or reduced translational status, measured by comparison of TRAP RNA and polyA RNA abundance as described previously [2,3,17]. We also identified variations in nuclear regulation (chromatin accessibility, histone modification, RNAPII engagement and nRNA abundance) that were a talisman of changes in polyA RNA abundance and translation.

Coordinate upregulation of hypoxia-responsive genes is characterized by nucleosome dynamics associated with histone modification, histone variant eviction, and increased chromatin accessibility

Hypoxia affected the position, composition, and modifications of specific histones of nucleosomes. The genes that were coordinately upregulated at the level of RNAPII-Ser2P engagement through ribosome association included the *HRG*s critical to low-oxygen stress

bioRxiv preprint doi: https://doi.org/10.1101/479980; this version posted November 27, 2018. The copyright holder for this preprint (which was not certified by peer review) is the author/funder, who has granted bioRxiv a license to display the preprint in perpetuity. It is made available under aCC-BY-NC-ND 4.0 International license.

384 survival [7,13,15–17,65]. The strong and coordinate upregulation of *HRG*s was characterized by
385 pronounced eviction of H2A.Z and enrichment of H3K9ac across the gene body as well as
386 elevation of chromatin accessibility RNAP-Ser2P engagement, nRNA, polyA and ribosome-
387 associated mRNAs (Fig. 8). The co-transcriptional histone acetyltransferase (HAT)-catalyzed
388 placement of a positive charge on the N-terminus of H3K9 is considered a reliable signature of
389 active transcription [27] and is common for stress-activated genes [28,29,66].
390 In animals, the H3K9ac modification is promoted by the presence of H3K4me3 and
391 stimulates the recruitment of the super elongation complex for release of poised RNAPII
392 complexes [38]. Although H3K4me3 generally rose on *HRG*s in response to 2HS, it was not as
393 strongly correlated with RNAPII-Ser2P engagement as H3K9ac (Fig 3b; Figure S4d), raising the
394 possibility that the co-upregulated genes may be activated by releasing polymerase pausing.
395 This could relate to the stress-activated eviction of H2A.Z that is broadly distributed across
396 these gene bodies at 2NS. The presence of H2A.Z in nucleosomes of gene bodies is associated
397 with limited transcription [30,31] and its eviction is characteristic of temperature-responsive
398 genes [30–34].
399 The mechanisms of H2A.Z deposition, eviction, and the impact on transcriptional
400 regulation are complex and not fully understood. This process requires ACTIN-RELATED
401 PROTEIN 6 (ARP6), a component of the SWR1 remodeling complex complex, and other factors
402 in *Arabidopsis* [26,67]. Yet disruption of H2A.Z deposition in an *arp6* mutant has limited effect
403 on regulation of *HRG*s under aerated growth conditions [34]. Other chromatin remodeling
404 proteins or specific TFs could be important. In response to small increases in temperature;
405 displacement of H2A.Z was facilitated by HSF1A in the activation of the heat response network
406 [32]. H2A.Z eviction from *HRG*s could involve ERFVIIs. Indeed, RAP2.2 reportedly interacts with
407 the SWI-SNF remodeler BRAHMA leading to the hypothesis that it that may contribute to H2A.Z
408 eviction or chromatin remodeling associated with increased chromatin accessibility [68]. Of the
409 >200 coordinately up-DRGs, 69 had one or more HRPE within 1 kb of their TSS and many
410 bound by HRE2 at 2HS (Fig. 7e; Table S2). RAP2.12 is stabilized and nuclear localized as
411 external oxygen levels decline below 10 kPa [69]. The stabilization of RAP2.12 and other
412 ERFVIIs may coordinate RNAPII initiation and facilitate H2A.Z eviction to promote productive
413 transcription that is coupled with H3K9 acetylation. If ERFVIIs interact with the ATP-dependent
414 chromatin remodeling machinery, they could also contribute to the stabilization or expansion of
415 regions of accessible chromatin to facilitate high levels of transcriptional activation, resulting in
416 transcripts that are efficiently processed, exported and translated under hypoxia. This
417 continuum of effective upregulation from transcription to translation is reminiscent of the
418 production of translationally competent mRNAs during nutrient starvation in yeast that is
419 associated with specific transcription factors [70].
420
421 **Genes associated with heat and oxidative stress are progressively activated by hypoxia**
422 The stress distinctly activated genes associated with heat and oxidative stress. The progressive
423 upregulation of genes in cluster 9 (Fig. 4c; Figure S7) became more evident when their activity
424 was compared at 2HS and 9HS with two chromatin and two RNA readouts (Fig. 7g). A
425 significant proportion of these genes had HSEs within their promoters (Fig. 7d). Their pattern of
426 regulatory variation included a 5' bias in histone marks and moderate to very high RNAPII-
427 Ser2P engagement at 2HS accompanied by elevated nRNA and TRAP RNA, but little to no full-

bioRxiv preprint doi: https://doi.org/10.1101/479980; this version posted November 27, 2018. The copyright holder for this preprint (which was not certified by peer review) is the author/funder, who has granted bioRxiv a license to display the preprint in perpetuity. It is made available under aCC-BY-NC-ND 4.0 International license.

length polyA RNA (Fig. 8). The increase in H3K9ac, H3K14ac and nRNA confirms these are progressively upregulated by hypoxia, whereas the pronounced 3' bias in polyA RNA suggests susceptibility to 5' to 3' degradation, as evident for *HSP70-4* (Fig. 5) and other members of cluster 9 (Figure S11).

Previously, heat stress-responsive genes were recognized as highly induced in *Arabidopsis* seedlings directly transferred to anoxia [56,62]. Remarkably, a brief pre-treatment with heat stress increased the resilience to anoxia of wild-type seedlings but not loss-of-function *hsfa2* or *hsf1a hsf1b* mutant seedlings [71]. This is enigmatic because high temperatures do not typically precede flooding in natural environments, but the availability of HSPs could reduce cellular damage under extreme stress conditions such as anoxia. Indeed, *HSPs* were plentiful in cluster 9. The limited synthesis of ATP-dependent chaperones during early hypoxia by nuclear sequestration/physical compartmentalization of their transcripts could minimize demands on limited energy reserves. However, as the stress is prolonged or upon reoxygenation, the synthesis of chaperones and proteins that provide protection from ROS could aid survival.

The nucleosome dynamics of cluster 2 and 9 genes included similar modifications with notable exceptions (Fig. 4c,d; Figures S7 and S11). Genes of both clusters underwent a loss of H2A.Z near the TSS of the gene body in conjunction with increased H3K9ac, but cluster 9 showed a loss of H3K4me3 proximal to the TSS that was not evident for cluster 2 or other genes with strong coordinate upregulation. The decrease in H3K4me3 may be an indication of non-productive RNAPII-Ser2P engagement, as this modification is associated with RNAPII elongation [72,73]. We found a significant enrichment of HSEs in the promoters of both rapidly and progressively upregulated genes (Fig. 7d). The heat-mediated upregulation of *HSFA2* (cluster 2) but not *HSFB1* (cluster 9) is dependent on recruitment of ANTI-SILENCING FUNCTION 1 that was associated with RNAPII engagement [74]. We predict that recruitment of specific TFs and chromatin modifying enzymes may influence histone or RNAPII CTD modifications that have ramifications on the rate of RNAPII elongation, termination, or post-transcriptional processing, thereby tuning the timing and production of cohorts of stress induced transcripts. The progressive upregulation of heat and oxidative stress networks could be mediated by the upregulation of TF genes encoding HSFs (i.e., HSFB2B) and ZINC FINGER PROTEIN 10 (ZAT10), and others during the early hours of the stress. Our datasets provide an opportunity for further meta-analyses of heat and oxidative stress gene regulatory networks.

Transcription of genes associated with major cellular processes during hypoxia

Intriguing patterns of transcriptional and RNA regulation of genes associated with cellular housekeeping became evident from our multi-tier evaluation (Fig. 8). Our prior comparisons of the transcriptome and translatome determined that hypoxic stress limits the investment of energy into the production of abundant cellular machinery such as ribosomes. mRNAs encoding *RPs* and some other abundant proteins are maintained but poorly translated under hypoxic stress [1–4]. This stress-limited translation of *RP*s is associated with their sequestration in UBP1C-associated macromolecular complexes [4]. Upon reoxygenation, *RP* mRNAs became rapidly associated with polysomes [2–4]. Although nuclear run-on transcription assays demonstrated that transcription of housekeeping genes continues during hypoxia in roots of maize seedlings [75], it was not known if *RP*s or other *UBP1C*-sequestered mRNAs continue to be synthesized during hypoxia in *Arabidopsis* seedlings. Here, the profiling of RNAP-Ser2P and

bioRxiv preprint doi: https://doi.org/10.1101/479980; this version posted November 27, 2018. The copyright holder for this preprint (which was not certified by peer review) is the author/funder, who has granted bioRxiv a license to display the preprint in perpetuity. It is made available under aCC-BY-NC-ND 4.0 International license.

nRNA confirmed that genes encoding RPs, metabolic enzymes and some photosynthetic apparatus are synthesized and retained as partially or completely processed transcripts in the nucleus during hypoxia (Fig. 6, *e.g.,* cluster 8b), regulatory variation characterized by progressive increase in H3K14ac but not H3K9ac. The cause of the limited increase in polyA RNA is unknown but could be due to limited cleavage and polyadenylation. The uncoupling of the H3K9ac and H3K14ac marks associated with active transcription but limited polyA RNA accumulation was reported in pluripotent embryonic stem cells of mice on a cohort of promoters deemed inactive but primed for future activation [76]. We propose that many housekeeping genes continue to be transcribed and accumulate in the nucleus during the stress. This compartmentalized downregulation may poise cells for the observed rapid recovery of the transcriptome and translatome upon reoxygenation [2,4].

Our genome-scale analysis support evidence of nuclear retention of transcripts that was visualized in response to hypoxic stress in *Arabidopsis* and lupine [43]. Moreover, mRNAs associated with the cell cycle are enriched in the nucleus under control conditions in *Arabidopsis [77]*. Our comparison of the nRNA and polyA RNA transcriptomes (Figure S5) validated the bias in nuclear enrichment of transcripts associated with the cell cycle (Figure S5), firmly indicating nuclear export is a point of regulation under control and stress conditions. During hypoxia, enhanced nuclear compartmentalization of the abundant transcripts associated with ribosome biogenesis, primary metabolism and photosynthesis would contribute to energy conservation by limiting translation, similar to the cytoplasmic sequestration associated with UBP1C. Nuclear retention and cytoplasmic sequestration could provide two reservoirs of transcripts that can be deployed upon reaeration, enabling rapid restoration of cellular processes. The RNA helicase eIF4AIII [78] as well as the RNA binding proteins UBP1A/B/C and the *HRG*-encoded CML38 form macromolecular ribonucleoprotein complexes that are primarily cytoplasmic but also present within the nucleus in response to hypoxia [4,79]. These complexes could orchestrate the nuclear co- and post-transcriptional processes during the stress. Hypoxia promotes alternative splicing including intron retention [3] and alternative polyadenylation site selection [42] and some of these transcripts are found in association with ribosomes. Nonetheless, there is no clear evidence of a general disruption of splicing or polyadenylation by hypoxia [3,42,78]. Further experimentation is required to understand the mechanisms responsible for the distinctive elevation in H3K14ac and nuclear-retained transcripts observed for many genes under hypoxic stress.

An ERFVII hierarchy drives transcriptional activation in response to hypoxia

This study included the first genome-wide analysis of the *cis*-element targets of an ERFVII. Enigmatically, ChIP-seq of the hypoxia-induced ERFVII HRE2 led to the identity of a multimeric GCC *cis*-element that did not correspond to the HRPE found in many *HRG*s and sufficient for transactivation by RAP ERFVIIs in protoplasts [15]. The HRE2 binding motif strongly resembled the double GCC motif of the EBP box first defined for an ERF of *Nicotiana tabacum* [80]. Strikingly, RAP2.3 was shown to bind the *ACID INSENSITIVE 5* (*ABI5*) promoter in the region of its two EBP boxes and transactivation of the *ABI5* promoter was demonstrated in protoplasts by all three constitutively expressed ERFVIIs (RAP2.2/2.3/2.12) in an EBP box-dependent manner [54]. It remains to be determined if HRE2 binds directly to the HRPE *in planta*, as neither HRE1 or HRE2 interacted with a 33 bp region containing the HRPE in a Yeast-1 hybrid assay, and

bioRxiv preprint doi: https://doi.org/10.1101/479980; this version posted November 27, 2018. The copyright holder for this preprint (which was not certified by peer review) is the author/funder, who has granted bioRxiv a license to display the preprint in perpetuity. It is made available under aCC-BY-NC-ND 4.0 International license.

both provided 40-fold lower transactivation via the HRPE in protoplasts than the RAP-ERFs [15]. This supports the conclusion that these these two subgroups of ERFVIIs are not genetically redundant. Yet the predicted HRPE contains 5'-GCC-3' followed by a lower frequency 5'-GCC-3' and perhaps more significantly, the 33 bp sequence used to define the HRPE contained a tandem 5'-GCC-3'. In addition we found that promoter regions with high scores for the HRPE and HRE2 motif coincided in 40 of the 213 coordinately upregulated genes, of which 13 were bound at 2HS by HRE2. Finally, the region of the *Arabidopsis ADH1* promoter that is necessary and sufficient for hypoxic upregulation contains both of these motifs, as discussed by [15]. Our data do not conflict with the model that the low-oxygen-mediated stabilization of the constitutively-expressed RAP-type ERFVIIs is responsible for rapid transactivation of *HRG*s that include *HRE2* [81,82], which is synthesized and stabilized under hypoxia [7]. It seems likely that HRE2 production and binding to promoters may bolster upregulation of HRGs, as an *hre1 hre2* double mutant fails to maintain the upregulation of these genes after 4 h of anoxia [83]. Still, further analyses are required to more fully comprehend the independent or overlapping roles of the low abundant HRE2 and RAP-type ERFVIIs in the temporal activation of transcription in response to hypoxia.

In mammalian systems, the response to hypoxia involves regulation of histone modifications and transcriptional activity [84]. The similarity to plants is remarkably analogous. Hypoxia-responsive genes are activated by the two-subunit Hypoxia Inducible Factor (HIF) transcription factor complex, that includes the oxygen-destabilized HIF1A subunit [85]. Similar to the three RAP-ERFVIIs, HIF1A is a constitutively synthesized protein that is unstable when oxygen is replete. It is the oxygen-dependent activity of a group of prolylhydroxlases that govern the hydroxylation of specific residues of HIF1A that triggers its oxygen-dependent ubiquitylation and protoeasome-mediated turnover. In animals, the chromatin landscape is additionally regulated through chromatin accessibility [86] and the post-translational modification of histones [87] in an oxygen-sensitive manner. It has been shown that HIF signaling itself directly mediates histone modification of target genes through the interaction with chromatin modifying enzymes [84]. Additionally, several histone modifying enzymes are directly targeted by HIF transcriptional activation, and HIF1A expression itself is regulated by histone acetylation [88], confirming the integration of epigenetic regulation. The analogy of low-oxygen stabilized transcriptional regulators and their coordination with chromatin modifications hints of convergent mechanisms of hypoxia signaling in plants and animals. Indeed, this may extend in a concerted manner beyond transcriptional regulation as cytoplasmic sequestration and selective translation of mRNAs is also observed in plants and metazoa [2,3,89,90]. It remains to be explored if hypoxia influences the synthesis and accumulation of nascent transcripts associated with growth in animals, as demonstrated in this multiomic analysis of *Arabidopsis*.

Conclusions

This deep investigation into gene regulatory processes in hypoxic stress revealed distinct regulation within the nucleus that fine tune cellular and physiological acclimation to transient deficiencies in oxygen availability. We determined that rapid regulation of the epigenome in response to short-term hypoxic stress continues as the stress becomes more severe. Coordinate regulation from chromatin accessibility, to RNAPII engagement, polyadenylated mRNA accumulation, and translation is observed for over 200 hypoxia-upregulated genes, while

bioRxiv preprint doi: https://doi.org/10.1101/479980; this version posted November 27, 2018. The copyright holder for this preprint (which was not certified by peer review) is the author/funder, who has granted bioRxiv a license to display the preprint in perpetuity. It is made available under aCC-BY-NC-ND 4.0 International license.

more discontinuous upregulation of nascent transcript production, export to the cytoplasm, and recruitment to ribosomes is observed for other gene cohorts. These findings uncover dynamic patterns of nuclear gene activity control that operate in response to an environmental challenge.

Methods

Genetic Material

The following genotypes were used for genome wide experiments: Col-0, Histone modification ChIP-seq, RNAP II ChIP-seq; *pHTA11:HTA11-3xFLAG [32]*, H2A.Z ChIP-seq; *pUBQ10:NTF/pACT2:BirA [21]*, ATAC-seq, nRNA-seq, polyA mRNA-seq; *p35S:HF-RPL18* [47], TRAP-seq, mRNA-seq; and HRE ChIP-seq *p35S:C2A-HRE2-HA* [7].

Growth and Treatment Conditions

Arabidopsis seeds were surface sterilized by incubation in 70% EtOH for 5 min, followed by incubation in 20% (v/v) bleach, 0.01% (v/v) TWEEN-20, followed by three washes in ddH_2O for 5 min, in triplicate. Sterilized seeds were placed onto 1x MS media (1.0x Murishige Skoog (MS) salts, 0.4% (w/v) Phytagel (Sigma-Aldrich), and 1% (w/v) Suc, pH 5.7) in 9 cm^2 Petri dishes and stratified by incubation at 4°C for 3 d in complete darkness. Following stratification, plates were placed vertically into a growth chamber (Percival) with 16 h light / 8 h dark cycle at ~120 µmol photons$\cdot s^{-1} \cdot m\text{-}^{2}$, at 23 °C for 7 d.

Seedling Treatments

For hypoxic stress, seedlings were removed from the growth chamber at Zeitgeber time (ZT) 16 and were subjected to hypoxic stress by bubbling argon gas into sealed chambers in complete darkness for 2 or 9 h at 24 °C. The chamber set-up was as described by [2]. Oxygen partial pressure in the chamber was measured with the NeoFox Sport O_2 sensor and probe (Ocean Optics). Hypoxia ($[O_2] < 2\%$) was attained within 15 min of initiation of the stress. Control samples were placed in an identical chamber that was open to ambient air under the same light and temperature conditions. Post hypoxia aeration was achieved by removing plates from the chamber and placing them into identical chambers in ambient air. Tissue was rapidly harvested into liquid N_2 and stored at -80 °C.

Chromatin Immunopurification (ChIP)

ChIP was performed according to [44] with minor modifications. Seedlings were grown on Petri dishes and treated as described above. For the HRE2 ChIP experiments, seedlings were pre-treated by flooding with 10 mL of 100 µM Calpain inhibitor IV (American Peptide) and 1% (v/v) DMSO for 2 h prior to the hypoxia treatment. For all genotypes, following hypoxia treatment, seedlings were immediately cross-linked in 1% (v/v) formaldehyde nuclei purification buffer (NPB: 20 mM MOPS, pH 7.0, 40 mM NaCl, 90 mM KCl, 2 mM EDTA, and 0.5 mM EGTA) in a vacuum chamber under house vacuum for 10 min. The reaction was quenched by addition of 5M glycine to reach a concentration of 125 mM followed by vacuum infiltration for 5 min. This was followed by three washes in 30 mL ddH_2O. Seedlings were blotted dry and then pulverized under liquid N_2. To isolate nuclei, 0.5 g tissue was thawed to 4°C in 10 mL NPB that additionally contained 0.5 mM spermidine, 0.2 mM spermine, and 1 X Plant Protease Inhibitor Cocktail

bioRxiv preprint doi: https://doi.org/10.1101/479980; this version posted November 27, 2018. The copyright holder for this preprint (which was not certified by peer review) is the author/funder, who has granted bioRxiv a license to display the preprint in perpetuity. It is made available under aCC-BY-NC-ND 4.0 International license.

(Sigma-Aldrich P9599). Nuclei were pelleted by centrifugation in 4°C at 1200*g* for 10 min. The nuclei were washed in 10 mL NPBt (NPB, 0.1% Triton X-100) and pelleted by centrifugation in 4°C at 1200*g* for 10 min in triplicate. Following the final NPBt wash, the supernatant was aspirated and the nuclei pellet was resuspended in 120 µL NPB, and lysed with the addition of 120 µL 2X nuclei lysis buffer (NLB: 100 mM Tris, pH 8.0, 20 mM EDTA, 2% [w/v] SDS, and 2X Plant Protease Inhibitor Cocktail) by vortexing for 2 min at 24 °C. The chromatin was sheared into 200 to 600 bp fragments by sonication (Diagenode, Denville, NJ) with 33 cycles of 30 s ON and 30 s OFF at 4°C. The sample was cleared by centrifugation at 16,000*g* at 4°C for 2 min and the supernatant was diluted ten-fold with dilution buffer (DB: 16.7 mM Tris, pH8.0, 167 mM NaCl, 1.1% (v/v) Triton X-100, 1.2 mM EDTA). The entire chromatin fraction was precleared by incubation with uncoupled Protein G Dynabeads (ThermoFisher) for 30 min followed by collection of the supernatant. Three hundred microliters of the input chromatin (1 mL for HRE2) was incubated with 3 µL of anti-H3K4me3 (ab8580, Abcam), anti-H3K27me3 (07-449, EMD Millipore), anti-H3K9ac (ab4441, Abcam), anti-H3K14ac (ab52946, Abcam), anti-p-CTD RNA Polymerase II (ab5095, Abcam), anti-FLAG (F1804, Sigma), or anti-HA (h3663, Sigma) for 4 h (overnight for HRE2) while rocking at 4°C. Protein G Dynabeads (30 µL) were washed in DB, added to the chromatin fraction and allowed to incubate for 2 h while rocking at 4°C. Beads were magnetically captured and washed sequentially in 1 mL for 5 min with four buffers: low $NaCl_2$ wash buffer (20 mM Tris, pH 8.0, 150 mM NaCl, 0.1% [w/v] SDS, 1% [v/v] Triton X-100, 2mM EDTA), high $NaCl_2$ wash buffer (20 mM Tris, pH 8.0, 500 mM $NaCl_2$, 0.1% [w/v] SDS, 1% [v/v] Triton X-100, 2mM EDTA), LiCl wash buffer (10 mM Tris, pH 8.0, 250 mM LiCl, 1% [w/v] sodium deoxycholate, 1% [v/v] Nonidet P-40, 1 mM EDTA), and standard TE buffer (10 mM Tris, pH 8.0, 1 mM EDTA). The beads were then washed twice with 10 mM Tris, pH 8.0 and resuspended in 25 µL of tagmentation reaction mix (10 mM Tris, pH 8.0, 5 mM $MgCl_2$, 10% [w/v] dimethylformamide) containing 1 µL of Tagment DNA Enzyme (Illumina) and incubated at 37°C for 1 minute. Beads were washed twice with low $NaCl_2$ wash buffer and then once in standard TE buffer. The chromatin was eluted from the beads by heating for 15 min at 65°C in elution buffer (EB: 100 mM $NaHCO_3$ and 1% [w/v] SDS) and reverse cross-linked by the addition of 20 µL 5 M $NaCl_2$ with heating at 65°C overnight. Following reverse cross-linking, Proteinase K (0.8 units; New England Biolabs) was added and the sample was incubated at 55°C for 15 min. The final tagged ChIP-DNA sample was purified using Qiagen MinElute columns according to the manufacturer's instructions and eluted with 14 µL of EB.

ChIP-seq Library Preparation

Library preparation for short-read sequencing (ChIP-seq) with tagmentation was performed according to [92], with minor modifications. Final library enrichment was performed in a 50 µL reaction containing 12 µL ChIP DNA, 0.75 µM primers, and 25 µL 2X NEBNext PCR Master Mix. To determine the appropriate amplification cycle number, a qPCR reaction was performed on 1 µL of tagmented ChIP DNA in a 10 µL reaction volume containing 0.15 µM primers, 1X SybrGreen (ThermoFisher), and 5 µL 2X NEBNext PCR Master Mix (New England Biolabs) with the following program: 72°C for 5 min, 98°C for 30 s, 24 cycles of 98°C for 10 s, 63°C for 30 s, 72°C for 30 s, and a final elongation at 72°C for 1 min. Libraries were amplified for *n* cycles, where *n* is equal to the rounded up Cq value determined in the qPCR reaction. Amplified libraries were purified and size selected using SPRI AMPure XP beads (Beckman). AMPure XP

bioRxiv preprint doi: https://doi.org/10.1101/479980; this version posted November 27, 2018. The copyright holder for this preprint (which was not certified by peer review) is the author/funder, who has granted bioRxiv a license to display the preprint in perpetuity. It is made available under aCC-BY-NC-ND 4.0 International license.

beads were added at a 0.7:1.0 bead to sample ratio, and the remaining DNA was recovered by the addition of AMPure XP beads at a 2.0:1.0 bead to sample ratio and eluted in 13 µL of EB. Quantification of the final libraries was performed with Quant-iT PicoGreen (ThermoFisher), and library fragment distribution was evaluated by use of the the Agilent 2100 Bioanalyzer using the high sensitivity DNA chip. Final libraries were multiplexed to >5 nM final concentration and sequenced on the HiSeq 3000/4000 at the UC Davis DNA Technologies Core.

Isolation of Nuclei Tagged in Specific Cell Types (INTACT)

INTACT was performed according to [44] with modifications. Frozen pulverized tissue (0.5 g) of *pUBQ:NTF/pACT2:BirA* seedlings was thawed in 10 mL of cold NPB buffer and filtered through 30 µm filters (Sysmex). Nuclei were pelleted by centrifugation at 1200*g* for 7 min at 4°C, and the nuclear pellet was resuspended and washed twice in NPB containing 0.1% (v/v) Tween-20 (NPBt), and the washed pellet was resuspended in 1 mL of NPB. M280 Streptavidin Dynabeads (10 µL; Invitrogen) washed with 1 mL NPB and resuspended in the original volume were added to the nuclei and the sample was allowed to rock for 30 min at 4°C. The bead-nuclei mixture was diluted to 14 mL with NPBt and incubated with rocking for 30 s at 4°C. The beads were magnetically collected, the supernatant removed, the beads washed twice with NPBt, and resuspended in 1 mL of NPBt. A 25 µL fraction was removed to quantify nuclei following addition of 1 µL of 1.0 µg/µL Propidium Iodide following incubation on ice for 5 min before visualization and quantification with a C-Chip hemocytometer (Incyto) using a fluorescence microscope.

Assay for Transposase Accessible Chromatin (ATAC)

Fifty-thousand INTACT-purified nuclei from root tissue were magnetically captured. Any remaining NPB was removed and the nuclei were resuspended in 50 µL of transposition mix (1X TD buffer, 2.5 µL TDE1 transposase) and were incubated for 30 min at 37°C with occasional mixing. The transposed DNA was purified with Qiagen MinElute PCR purification columns, and the purified DNA was eluted in 11 µL of EB. For library construction, a reaction was prepared to amplify the sample in a two step process. The reaction was assembled containing transposed DNA (10 µL), 5 µM Ad1.1 and an indexing primer [23], 1X NEBNext High Fidelity PCR mix and cycled in the following program: 72°C 5 min; 98°C 30 s; 3 cycles of 98°C 10 s, 63°C 30s, 72°C 1 min; 4°C and the samples were placed on ice. Then a qPCR was performed using an aliquot of the amplified library with the following program: 98°C for 30 s; 20 cycles of 98°C for 10 s, 63°C for 30 s, 72°C for 1 min. The original PCR reaction was resumed for *n* additional cycles, where *n* is the cycle at which the qPCR reaction was at 1/3 of its maximum fluorescence intensity. Amplified DNA was then purified with Qiagen MinElute PCR purification columns and eluted in 20 µL of EB. Amplified libraries were purified and size selected for fragments between 200 to 600 bp using SPRI AMPure XP beads (Beckman). AMPure XP beads were added at a 0.55:1.0 bead to sample ratio, and the remaining DNA was recovered by the addition of AMPure XP beads at a 1.55:1.0 bead to sample ratio and eluted in 13 µL of EB. Library concentration was determined using the NEBNext (New England Biolabs) library quantification kit. Final libraries were multiplexed to >5 nM final concentration and sequenced on the HiSeq 3000/4000 at the UC Davis DNA Technologies Core.

bioRxiv preprint doi: https://doi.org/10.1101/479980; this version posted November 27, 2018. The copyright holder for this preprint (which was not certified by peer review) is the author/funder, who has granted bioRxiv a license to display the preprint in perpetuity. It is made available under aCC-BY-NC-ND 4.0 International license.

INTACT followed by Nuclear RNA Extraction

Fifty-thousand INTACT-purified nuclei were collected magnetically and the supernatant was removed, and resuspended in 20 µL of NPB. Nuclear RNA was extracted and purified using the Qiagen RNeasy Micro kit, and eluted in 20 µL of H_2O. The RNA was then DNaseI digested with with 1 µL (2U/µL) of Turbo DNAseI (Ambion) and incubated for 30 min at 37°C. DNaseI was inactivated by adding EDTA to 15 mM, and heated at 75°C for 10 min, centrifuged at 2000*g* for 5 min and transferred to a new tube. The RNA was then purified using AMPure XP beads, and eluted in 15 µL H_2O. Ribosomal RNA was depleted from the sample using the plant Ribo-Zero rRNA removal kit (Illumina) according to the manufacturer's instructions.

Total RNA Isolation and PolyA RNA Affinity Purification

Total RNA was extracted from 50 mg frozen pulverized tissue by addition of 800 µL Trizol (Life Sciences) and incubation for 5 min at room temperature. Chloroform (200 µL) was added and the sample briefly vortexed and incubated at room temperature for 3 min. Following incubation, the samples were centrifuged at 12,000*g* for 15 min at 4°C, and the clear phase was transferred to a new tube. RNA was precipitated by addition of 500 µL isopropanol, vortexing briefly, and incubation at room temperature for 10 min, and pelleted by centrifugation at 12,000*g* for 10 min at 4°C. Purified RNA was resuspended in 50 µl EB and DNaseI digested with 2.5 µL of TURBO DNaseI (Ambion) for 30 min at 37°C. DNaseI was inactivated by addition of EDTA to 15 mM and heat treatment at 75°C for 10 min. The RNA was pelleted by centrifugation at 2000*g* for 5 min and transferred to a new tube. The RNA was then purified using AMPure XP beads, and eluted in 50 µL H_2O. For polyA RNA selection, the total RNA sample was heated for 2 min at 65°C and placed on ice, after which 50 µl of Dynabeads Oligo $(dT)_{25}$ pre-washed with wash buffer (WB: 10 mM Tris, pH 7.5, 150 mM LiCl, 1 mM EDTA) were added and the sample incubated at room temperature for 15 min with agitation. The beads were magnetically separated and washed twice with WB. For RNA elution, 50 µl EB was added and the sample heated for 2 min at 80°C and the eluted RNA was transferred to a new tube. The polyA RNA selection was repeated a second time and eluted in a volume of 16 µl.

Translating Ribosome Affinity Purification (TRAP)-seq

TRAP of mRNA-ribosome complexes was performed following the procedure of [17]. Briefly, pulverized tissue (1 mL) from the *35S:HF-RPL18* genotype was added to 5 mL of polysome extraction buffer (PEB: 200 mM Tris, pH 9.0, 200 mM KCl, 25 mM EGTA, 35 mM $MgCl_2$, 1% PTE, 1 mM DTT, 1 mM PMSF, 100 µg/mL cycloheximide, 50 µg/mL chloramphenicol) containing 1% detergent mix (20% (w/v) polyoxyethylene(23)lauryl ether, 20% (v/v) Triton X-100, 20% (v/v) Octylphenyl-polyethylene glycol, 20% (v/v) Polyoxyethylene sorbitan monolaurate 20) and homogenized with a glass homogenizer on ice The homogenized mixture was allowed to stand for 10 min on ice and then centrifuged at 16,000*g* at 4°C for 15 min. Following centrifugation, the supernatant was transferred to a new tube and filtered through one layer of Miracloth (Millipore) to produce the clarified extract.

Protein G Dynabeads (50uL; ThermoFisher) were prewashed twice with 1.5 mL of wash buffer (WB-T: 200 mM Tris, pH 9.0, 200 mM KCl, 25 mM EGTA, 35 mM $MgCl_2$, 5 mM PMSF, 50 µg/mL cycloheximide, 50 µg/mL chloramphenicol) by suspension and magnetic collection, with final re-suspension in the original volume. These were added to the clarified tissue extract and

bioRxiv preprint doi: https://doi.org/10.1101/479980; this version posted November 27, 2018. The copyright holder for this preprint (which was not certified by peer review) is the author/funder, who has granted bioRxiv a license to display the preprint in perpetuity. It is made available under aCC-BY-NC-ND 4.0 International license.

incubated at 4°C for 2 h with gentle rocking. The beads were collected magnetically, the supernatant was removed, and the beads were gently resuspended in 6 mL WB-T for 5 min at 4°C with rocking. This wash step was repeated two additional times, after which the beads were resuspended in 1 mL WB-T and transferred to a new tube and the supernatant was removed.

RNA was purified from the sample and the reserved clarified extract by addition of 105 µl of LBB (LBB: 100 mM Tris, pH 8.0, 500 mM LiCl, 10 mM EDTA, 1% (w/v) SDS, 5 mM DTT, 1.5% (v/v) Antifoam A, 5 µl/mL 2-mercaptoethanol) followed by vortexing for 5 min. Samples were incubated at room temperature for 10 min, centrifuged at 13,000*g* for 10 min and transferred to a new tube. Poly(A)$^+$ RNA selection was performed by addition of 1 µl of 12.5 µM biotin-20nt-dT oligos (Integrated DNA Technologies) to 200 µl of the TRAP or RNA lysate sample, followed by incubation at room temperature for 10 min. In a separate tube 20 µl magnetic streptavidin beads (New England Biolabs) were washed with 200 µl LBB. The lysate was added to the washed beads and incubated at room temperature for 10 min with gentle agitation. The beads were magnetically separated and washed sequentially with wash buffer A (WBA:10 mM Tris, pH 8.0, 150 mM LiCl, 1 mM EDTA, 0.1% (w/v) SDS), wash buffer B (WBB:10 mM Tris, pH 8.0, 150 mM LiCl, 1 mM EDTA), and low salt buffer (LSB: 20 mM Tris, pH 8.0, 150 mM NaCl, 1 mM EDTA). Following washes, the pellet was resuspended in 16 µl 10 mM Tris, pH 8.0 containing 1 mM 2-Mercaptoethanol and heated at 80°C for 2 min. The beads were magnetically collected, the supernatant was transferred to a new tube, and the poly(A)$^+$ RNA selection process was repeated, and the samples combined in a new tube before storage at -80°C.

RNA-seq Library Preparation

RNA-seq library preparation for nRNA, polyA, and TRAP RNA was performed as described in Kumar et al., 2012 [93]. In brief, RNA was fragmented and primed for first strand synthesis with random hexamers (Invitrogen). First strand synthesis was performed, followed by second strand synthesis, end repair, and A-tailing. Universal sequencing adapters were ligated to cDNA molecules. An initial enrichment and adapter extension PCR was first performed on 0.25x volume of the ligated products for each sample to determine amplification cycle number to prevent overamplification of sequencing libraries. A final enrichment and adapter extension PCR was performed with 0.25x starting volume for the specified cycle number (13-15 cycles) for each sample. Following enrichment, purification, size selection of libraries, and sequencing was performed as described for ChIP-seq.

Bioinformatic Analyses

For all high throughput outputs, short reads were trimmed using FASTX-toolkit to remove barcodes and filter short and low quality reads prior to alignment to the TAIR10 genome with Bowtie2/Tophat2. Read quality reports were generated using fastqc. For all datasets, counting of aligned reads was performed on entire transcripts [94] using the latest Araport 11 annotation (201606) and reads per kilobase of transcript per million mapped reads (RPKM) values were calculated. Differentially expressed genes were determined by edgeR, $|FC| > 1$, FDR < 0.01.

Data visualization and file generation: Bigwig files for Integrated Genome Viewer (IGV) visualization were generated from aligned bam files and normalized by RPKM values using the deepTools command bamCoverage with the -normalizeUsingRPKM specification. Within IGV,

bioRxiv preprint doi: https://doi.org/10.1101/479980; this version posted November 27, 2018. The copyright holder for this preprint (which was not certified by peer review) is the author/funder, who has granted bioRxiv a license to display the preprint in perpetuity. It is made available under aCC-BY-NC-ND 4.0 International license.

all chromatin based outputs were normalized to the same scale and all RNA outputs were normalized to a separate scale.

Peak calling: For ChIP-seq and ATAC-seq datasets, peak calling was performed using independent replicates in combination as input for HOMER using the findPeaks command [95]. For downstream analyses, peaks identified from each time point comparison were combined and counting was performed on individual replicates. Peaks were annotated using the HOMER command annotatePeaks.pl. Differential regulation of peaks was performed using edgeR.

Motif discovery: HRE2 peaks identified by HOMER command findPeaks were used as an input for the HOMER command findMotifsGenome.pl. The matrix for the top HRE2 motif (p: 1e-69) was used as input the MEME command ceqlogo to generate the motif logo.

DAP-seq motif analysis: Sequences of promoter regions spanning 1 kb upstream to 500 bp downstream of the TSS were extracted for genes within each cluster. The promoter sequences were compared against each TF, per TF family, using motif matrices identified by [53]. The number of significant motifs identified within the promoters of each cluster were quantitated and normalized to the number of genes within each cluster.

t-distributed stochastic neighbor embedding (t-SNE): t-SNE analysis was performed according to [96]. Briefly, a principal component analysis was performed using RPKM values for each replicated dataset and timepoint. t-SNE was then performed on PCs 1-10 and the results were plotted using ggplot2.

Wilcoxon signed rank sum test: Wilcoxon signed rank sum test was performed by comparing the RPKM values of one genomic output for each gene within a cluster to the genes of another cluster. Each cluster was compared individually to all other clusters to determine significance, $p < 0.05$.

Fisher's exact test: Fisher's exact test was performed by comparing the number of motifs / peaks associated with genes within a cluster to the total number of motifs / peaks identified for all DRGs. Significance

Bioinformatic Tools

Analyses were performed with Bioconductor R packages particularly the Next Generation Sequencing analysis software of systemPipeR [97]. Programs used within Bioconductor included: BiocParallel [98], BatchJobs [99], GenomicFeatures [94], GenomicRanges [94], edgeR [100], gplots [101], ggplot2 [102], RColorBrewer [103], Dplyr [104], biomaRt [105], ChIPseeker [106], rtracklayer [107], Rtsne [108], Pheatmap [109], e1071 [110], cluster [111], ShortRead [112], and Rsamtools [113]. The Publically available UNIX/Python/Perl packages used included Tophat [114], fastx_toolkit [115], Fastqc [116], MEME [117], HOMER [95], deepTools [118], circos [119], Bedtools [120], samtools [121].

bioRxiv preprint doi: https://doi.org/10.1101/479980; this version posted November 27, 2018. The copyright holder for this preprint (which was not certified by peer review) is the author/funder, who has granted bioRxiv a license to display the preprint in perpetuity. It is made available under aCC-BY-NC-ND 4.0 International license.

Declarations

Ethics approval and consent to participate

Not applicable

Consent for publication

Not applicable

Availability of data and material

The datasets generated and/or analysed during the current study are available in the NCBI GEO repository

Competing interests

The authors declare that they have no competing interests.

Funding

This work was supported by U.S. National Science Foundation (Grant Nos. IOS−1121626, IOS-1238243, MCB-1716913) and the U.S. Department of Agriculture, National Institute of Food and Agriculture - Agriculture and Food Research Initiative (Grant No. 2011−04015) to J.B.-S..

Authors' contributions

T.L. and J.B.-S. designed research; T.L. performed research; T.L. and J.B.-S. analyzed data; and T.L. and J.B.-S. wrote the paper.

Acknowledgements

We thank Mauricio Reynoso, Roger Deal, Marko Bajic, Seung-Cho Lee, Maureen Hummel, Lauren Dedow, Sonja Winte, Jérémie Bazin, Thomas Girke, and Thomas Eulgem for helpful discussions. This work was supported by U.S. National Science Foundation (Grant Nos. IOS−1121626, IOS-1238243, MCB-1716913) and the U.S. Department of Agriculture, National Institute of Food and Agriculture - Agriculture and Food Research Initiative (Grant No. 2011−04015) to J.B.-S..

Authors' information (optional)

The current location of T.L. is: Plant Biology Laboratory, The Salk Institute for Biological Studies, La Jolla, CA 92037, USA

Supplemental Tables

Table S1: Tabulation of ATAC and HRE2-ChIP peaks on chromatin

Table S2: Survey of histones, RNAPII, HRE2 and three RNA sub-populations in response to two durations of hypoxic stress

bioRxiv preprint doi: https://doi.org/10.1101/479980; this version posted November 27, 2018. The copyright holder for this preprint (which was not certified by peer review) is the author/funder, who has granted bioRxiv a license to display the preprint in perpetuity. It is made available under aCC-BY-NC-ND 4.0 International license.

Table S3: nRNA Enrichment and Gene Ontology Analysis
Table S4: Gene Ontology Analysis for two durations of hypoxic stress in Table S2
Table S5: List of Arabidopsis Blacklisted Chromatin (ABC)

Supplemental Note

***Arabidopsis* blacklisted chromatin**

The variety of genome-wide outputs in this study recording dynamics at the level of chromatin and RNA has permitted the identification of Tn5 bias/genomic regions with high nonspecific background and/or high signal/read counts in Arabidopsis irrespective of experiment, similar to regions identified by the ENCODE project for other organisms [91]. The identification and filtering of genomic blacklisted regions is especially important for calculation of genome wide Pearson correlations and the generation of signal tracks used for accurate browser views. The *Arabidopsis* Blacklisted Chromatin (ABC) regions (Table S5) can be used to remove these defined regions that create statistical artefacts of the nuclear genome prior to performing analyses of chromatin-based data.

bioRxiv preprint doi: https://doi.org/10.1101/479980; this version posted November 27, 2018. The copyright holder for this preprint (which was not certified by peer review) is the author/funder, who has granted bioRxiv a license to display the preprint in perpetuity. It is made available under aCC-BY-NC-ND 4.0 International license.

References

1. Branco-Price C, Kawaguchi R, Ferreira RB, Bailey-Serres J. Genome-wide analysis of transcript abundance and translation in Arabidopsis seedlings subjected to oxygen deprivation. Ann Bot. Oxford University Press; 2005;96:647–60.
2. Branco-Price C, Kaiser KA, Jang CJH, Larive CK, Bailey-Serres J. Selective mRNA translation coordinates energetic and metabolic adjustments to cellular oxygen deprivation and reoxygenation in Arabidopsis thaliana. Plant J. 2008;56:743–55.
3. Juntawong P, Girke T, Bazin J, Bailey-Serres J. Translational dynamics revealed by genome-wide profiling of ribosome footprints in Arabidopsis. Proc Natl Acad Sci U S A. 2014;111:E203–12.
4. Sorenson R, Bailey-Serres J. Selective mRNA sequestration by OLIGOURIDYLATE-BINDING PROTEIN 1 contributes to translational control during hypoxia in Arabidopsis. Proc Natl Acad Sci U S A. 2014;111:2373–8.
5. Xu K, Xu X, Fukao T, Canlas P, Maghirang-Rodriguez R, Heuer S, et al. Sub1A is an ethylene-response-factor-like gene that confers submergence tolerance to rice. Nature. 2006;442:705–8.
6. Hattori Y, Nagai K, Furukawa S, Song X-J, Kawano R, Sakakibara H, et al. The ethylene response factors SNORKEL1 and SNORKEL2 allow rice to adapt to deep water. Nature. 2009;460:1026–30.
7. Gibbs DJ, Lee SC, Isa NM, Gramuglia S, Fukao T, Bassel GW, et al. Homeostatic response to hypoxia is regulated by the N-end rule pathway in plants. Nature. 2011;479:415–8.
8. Licausi F, Kosmacz M, Weits DA, Giuntoli B, Giorgi FM, Voesenek LACJ, et al. Oxygen sensing in plants is mediated by an N-end rule pathway for protein destabilization. Nature. 2011;479:419–22.
9. Yang C-Y, Hsu F-C, Li J-P, Wang N-N, Shih M-C. The AP2/ERF transcription factor AtERF73/HRE1 modulates ethylene responses during hypoxia in Arabidopsis. Plant Physiol. 2011;156:202–12.
10. Abbas M, Berckhan S, Rooney DJ, Gibbs DJ, Vicente Conde J, Sousa Correia C, et al. Oxygen sensing coordinates photomorphogenesis to facilitate seedling survival. Curr Biol. 2015;25:1483–8.
11. Eysholdt-Derzsó E, Sauter M. Root Bending Is Antagonistically Affected by Hypoxia and ERF-Mediated Transcription via Auxin Signaling. Plant Physiol. 2017;175:412–23.
12. Paul MV, Iyer S, Amerhauser C, Lehmann M, van Dongen JT, Geigenberger P. Oxygen Sensing via the Ethylene Response Transcription Factor RAP2.12 Affects Plant Metabolism and Performance under Both Normoxia and Hypoxia. Plant Physiol. 2016;172:141–53.
13. Giuntoli B, Perata P. Group VII Ethylene Response Factors in Arabidopsis: regulation and physiological roles. Plant Physiol [Internet]. 2017; Available from: http://dx.doi.org/10.1104/pp.17.01225
14. White MD, Klecker M, Hopkinson RJ, Weits DA, Mueller C, Naumann C, et al. Plant cysteine oxidases are dioxygenases that directly enable arginyl transferase-catalysed arginylation of N-end rule targets. Nat Commun. 2017;8:14690.
15. Gasch P, Fundinger M, Müller JT, Lee T, Bailey-Serres J, Mustroph A. Redundant ERF-VII transcription factors bind an evolutionarily-conserved cis-motif to regulate hypoxia-responsive gene expression in Arabidopsis. Plant Cell [Internet]. American Society of Plant Biologists; 2015; Available from: http://www.plantcell.org/content/early/2015/12/14/tpc.15.00866
16. Giuntoli B, Lee SC, Licausi F, Kosmacz M, Oosumi T, van Dongen JT, et al. A trihelix DNA binding protein counterbalances hypoxia-responsive transcriptional activation in Arabidopsis. PLoS Biol. 2014;12:e1001950.

bioRxiv preprint doi: https://doi.org/10.1101/479980; this version posted November 27, 2018. The copyright holder for this preprint (which was not certified by peer review) is the author/funder, who has granted bioRxiv a license to display the preprint in perpetuity. It is made available under aCC-BY-NC-ND 4.0 International license.

17. Mustroph A, Zanetti ME, Jang CJH, Holtan HE, Repetti PP, Galbraith DW, et al. Profiling translatomes of discrete cell populations resolves altered cellular priorities during hypoxia in Arabidopsis. Proc Natl Acad Sci U S A. 2009;106:18843–8.
18. Bui LT, Giuntoli B, Kosmacz M, Parlanti S, Licausi F. Constitutively expressed ERF-VII transcription factors redundantly activate the core anaerobic response in Arabidopsis thaliana. Plant Sci. 2015;236:37–43.
19. Giuntoli B, Licausi F, van Veen H, Perata P. Functional Balancing of the Hypoxia Regulators RAP2.12 and HRA1 Takes Place in vivo in Arabidopsis thaliana Plants. Front Plant Sci. 2017;8:591.
20. Weits DA, Giuntoli B, Kosmacz M, Parlanti S, Hubberten H-M, Riegler H, et al. Plant cysteine oxidases control the oxygen-dependent branch of the N-end-rule pathway. Nat Commun. 2014;5:3425.
21. Sullivan AM, Arsovski AA, Lempe J, Bubb KL, Weirauch MT, Sabo PJ, et al. Mapping and dynamics of regulatory DNA and transcription factor networks in A. thaliana. Cell Rep. 2014;8:2015–30.
22. Sullivan AM, Bubb KL, Sandstrom R, Stamatoyannopoulos JA, Queitsch C. DNase I hypersensitivity mapping, genomic footprinting, and transcription factor networks in plants. Current Plant Biology. 2015;3-4:40–7.
23. Buenrostro JD, Giresi PG, Zaba LC, Chang HY, Greenleaf WJ. Transposition of native chromatin for fast and sensitive epigenomic profiling of open chromatin, DNA-binding proteins and nucleosome position. Nat Methods. 2013;10:1213–8.
24. Talbert PB, Henikoff S. Histone variants on the move: substrates for chromatin dynamics. Nat Rev Mol Cell Biol. 2017;18:115–26.
25. Gates LA, Foulds CE, O'Malley BW. Histone Marks in the "Driver"s Seat': Functional Roles in Steering the Transcription Cycle. Trends Biochem Sci. 2017;42:977–89.
26. Asensi-Fabado M-A, Amtmann A, Perrella G. Plant responses to abiotic stress: The chromatin context of transcriptional regulation. Biochim Biophys Acta. 2017;1860:106–22.
27. Eberharter A, Becker PB. Histone acetylation: a switch between repressive and permissive chromatin. Second in review series on chromatin dynamics. EMBO Rep. 2002;3:224–9.
28. Kim J-M, To TK, Ishida J, Matsui A, Kimura H, Seki M. Transition of chromatin status during the process of recovery from drought stress in Arabidopsis thaliana. Plant Cell Physiol. 2012;53:847–56.
29. Kim J-M, To TK, Ishida J, Morosawa T, Kawashima M, Matsui A, et al. Alterations of lysine modifications on the histone H3 N-tail under drought stress conditions in Arabidopsis thaliana. Plant Cell Physiol. 2008;49:1580–8.
30. Kumar SV, Wigge PA. H2A.Z-containing nucleosomes mediate the thermosensory response in Arabidopsis. Cell. 2010;140:136–47.
31. Sura W, Kabza M, Karlowski WM, Bieluszewski T, Kus-Slowinska M, Pawełoszek Ł, et al. Dual Role of the Histone Variant H2A.Z in Transcriptional Regulation of Stress-Response Genes. Plant Cell. 2017;29:791–807.
32. Cortijo S, Charoensawan V, Brestovitsky A, Buning R, Ravarani C, Rhodes D, et al. Transcriptional Regulation of the Ambient Temperature Response by H2A.Z Nucleosomes and HSF1 Transcription Factors in Arabidopsis. Mol Plant. 2017;10:1258–73.
33. Dai X, Bai Y, Zhao L, Dou X, Liu Y, Wang L, et al. H2A.Z Represses Gene Expression by Modulating Promoter Nucleosome Structure and Enhancer Histone Modifications in Arabidopsis. Mol Plant. 2017;10:1274–92.
34. Torres ES, Deal RB. The histone variant H2A. Z and chromatin remodeler BRAHMA act coordinately and antagonistically to regulate transcription and nucleosome dynamics in Arabidopsis. bioRxiv. Cold Spring Harbor Laboratory; 2018;243790.
35. Hajheidari M, Koncz C, Eick D. Emerging roles for RNA polymerase II CTD in Arabidopsis. Trends Plant Sci. 2013;18:633–43.

bioRxiv preprint doi: https://doi.org/10.1101/479980; this version posted November 27, 2018. The copyright holder for this preprint (which was not certified by peer review) is the author/funder, who has granted bioRxiv a license to display the preprint in perpetuity. It is made available under aCC-BY-NC-ND 4.0 International license.

36. Milligan L, Huynh-Thu VA, Delan-Forino C, Tuck A, Petfalski E, Lombraña R, et al. Strand-specific, high-resolution mapping of modified RNA polymerase II. Mol Syst Biol. 2016;12:874.
37. Phatnani HP, Greenleaf AL. Phosphorylation and functions of the RNA polymerase II CTD. Genes Dev. 2006;20:2922–36.
38. Jonkers I, Lis JT. Getting up to speed with transcription elongation by RNA polymerase II. Nat Rev Mol Cell Biol. 2015;16:167–77.
39. Hetzel J, Duttke SH, Benner C, Chory J. Nascent RNA sequencing reveals distinct features in plant transcription. Proc Natl Acad Sci U S A. 2016;113:12316–21.
40. Zhu J, Liu M, Liu X, Dong Z. RNA polymerase II activity revealed by GRO-seq and pNET-seq in Arabidopsis. Nat Plants [Internet]. 2018; Available from: http://dx.doi.org/10.1038/s41477-018-0280-0
41. Van Veen H, Vashisht D, Akman M, Girke T. Transcriptomes of eight Arabidopsis thaliana accessions reveal core conserved, genotype-and organ-specific responses to flooding stress. Plant [Internet]. Am Soc Plant Biol; 2016; Available from: http://www.plantphysiol.org/content/early/2016/05/15/pp.16.00472.abstract
42. de Lorenzo L, Sorenson R, Bailey-Serres J, Hunt AG. Noncanonical Alternative Polyadenylation Contributes to Gene Regulation in Response to Hypoxia. Plant Cell. 2017;29:1262–77.
43. Niedojadło J, Dełeńko K, Niedojadło K. Regulation of poly(A) RNA retention in the nucleus as a survival strategy of plants during hypoxia. RNA Biol. 2016;13:531–43.
44. Deal RB, Henikoff S. A simple method for gene expression and chromatin profiling of individual cell types within a tissue. Dev Cell. 2010;18:1030–40.
45. Maher KA, Bajic M, Kajala K, Reynoso M, Pauluzzi G, West DA, et al. Profiling of Accessible Chromatin Regions across Multiple Plant Species and Cell Types Reveals Common Gene Regulatory Principles and New Control Modules. Plant Cell. 2018;30:15–36.
46. Reynoso M, Pauluzzi G, Kajala K, Cabanlit S, Velasco J, Bazin J, et al. Nuclear transcriptomes at high resolution using retooled INTACT. Plant Physiol [Internet]. 2017; Available from: http://dx.doi.org/10.1104/pp.17.00688
47. Zanetti ME, Chang I-F, Gong F, Galbraith DW, Bailey-Serres J. Immunopurification of polyribosomal complexes of Arabidopsis for global analysis of gene expression. Plant Physiol. 2005;138:624–35.
48. Lu Z, Hofmeister BT, Vollmers C, DuBois RM, Schmitz RJ. Combining ATAC-seq with nuclei sorting for discovery of cis-regulatory regions in plant genomes. Nucleic Acids Res [Internet]. 2016; Available from: http://dx.doi.org/10.1093/nar/gkw1179
49. Sijacic P, Bajic M, McKinney EC, Meagher RB, Deal RB. Chromatin accessibility changes between Arabidopsis stem cells and mesophyll cells illuminate cell type-specific transcription factor networks [Internet]. bioRxiv. 2017 [cited 2018 Apr 5]. p. 213900. Available from: https://www.biorxiv.org/content/early/2017/11/03/213900.abstract
50. Ansari A, Hampsey M. A role for the CPF 3'-end processing machinery in RNAP II-dependent gene looping. Genes Dev. 2005;19:2969–78.
51. Ozsolak F, Poling LL, Wang Z, Liu H, Liu XS, Roeder RG, et al. Chromatin structure analyses identify miRNA promoters. Genes Dev. 2008;22:3172–83.
52. Frank A, Matiolli CC, Viana AJC, Hearn TJ, Kusakina J, Belbin FE, et al. Circadian Entrainment in Arabidopsis by the Sugar-Responsive Transcription Factor bZIP63. Curr Biol. 2018;28:2597–606.e6.
53. O'Malley RC, Huang S-SC, Song L, Lewsey MG, Bartlett A, Nery JR, et al. Cistrome and Epicistrome Features Shape the Regulatory DNA Landscape. Cell. 2016;166:1598.
54. Gibbs DJ, Md Isa N, Movahedi M, Lozano-Juste J, Mendiondo GM, Berckhan S, et al. Nitric oxide sensing in plants is mediated by proteolytic control of group VII ERF transcription factors. Mol Cell. 2014;53:369–79.

bioRxiv preprint doi: https://doi.org/10.1101/479980; this version posted November 27, 2018. The copyright holder for this preprint (which was not certified by peer review) is the author/funder, who has granted bioRxiv a license to display the preprint in perpetuity. It is made available under aCC-BY-NC-ND 4.0 International license.

55. Büttner M, Singh KB. Arabidopsis thaliana ethylene-responsive element binding protein (AtEBP), an ethylene-inducible, GCC box DNA-binding protein interacts with an ocs element binding protein. Proc Natl Acad Sci U S A. 1997;94:5961–6.
56. Loreti E, Poggi A, Novi G, Alpi A, Perata P. A genome-wide analysis of the effects of sucrose on gene expression in Arabidopsis seedlings under anoxia. Plant Physiol. 2005;137:1130–8.
57. Chang R, Jang CJH, Branco-Price C, Nghiem P, Bailey-Serres J. Transient MPK6 activation in response to oxygen deprivation and reoxygenation is mediated by mitochondria and aids seedling survival in Arabidopsis. Plant Mol Biol. 2012;78:109–22.
58. Baxter-Burrell A, Yang Z, Springer PS, Bailey-Serres J. RopGAP4-dependent Rop GTPase rheostat control of Arabidopsis oxygen deprivation tolerance. Science. 2002;296:2026–8.
59. Pucciariello C, Parlanti S, Banti V, Novi G, Perata P. Reactive oxygen species-driven transcription in Arabidopsis under oxygen deprivation. Plant Physiol. 2012;159:184–96.
60. Gonzali S, Loreti E, Cardarelli F, Novi G, Parlanti S, Pucciariello C, et al. Universal stress protein HRU1 mediates ROS homeostasis under anoxia. Nat Plants. 2015;1:15151.
61. Yeung E, van Veen H, Vashisht D, Sobral Paiva AL, Hummel M, Rankenberg T, et al. A stress recovery signaling network for enhanced flooding tolerance in Arabidopsis thaliana. Proc Natl Acad Sci U S A. 2018;115:E6085–94.
62. Banti V, Mafessoni F, Loreti E, Alpi A, Perata P. The heat-inducible transcription factor HsfA2 enhances anoxia tolerance in Arabidopsis. Plant Physiol. 2010;152:1471–83.
63. Kawaguchi R, Bailey-Serres J. mRNA sequence features that contribute to translational regulation in Arabidopsis. Nucleic Acids Res. 2005;33:955–65.
64. Roy B, von Arnim AG. Translational Regulation of Cytoplasmic mRNAs. Arabidopsis Book. 2013;11:e0165.
65. Mustroph A, Lee SC, Oosumi T, Zanetti ME, Yang H, Ma K, et al. Cross-kingdom comparison of transcriptomic adjustments to low-oxygen stress highlights conserved and plant-specific responses. Plant Physiol. 2010;152:1484–500.
66. Zhou J, Wang X, He K, Charron J-BF, Elling AA, Deng XW. Genome-wide profiling of histone H3 lysine 9 acetylation and dimethylation in Arabidopsis reveals correlation between multiple histone marks and gene expression. Plant Mol Biol. 2010;72:585–95.
67. Kumar SV. H2A.Z at the Core of Transcriptional Regulation in Plants. Mol Plant. 2018;11:1112–4.
68. Efroni I, Han S-K, Kim HJ, Wu M-F, Steiner E, Birnbaum KD, et al. Regulation of leaf maturation by chromatin-mediated modulation of cytokinin responses. Dev Cell. 2013;24:438–45.
69. Kosmacz M, Parlanti S, Schwarzländer M, Kragler F, Licausi F, Van Dongen JT. The stability and nuclear localization of the transcription factor RAP2.12 are dynamically regulated by oxygen concentration. Plant Cell Environ. 2015;38:1094–103.
70. Zid BM, O'Shea EK. Promoter sequences direct cytoplasmic localization and translation of mRNAs during starvation in yeast. Nature. 2014;514:117–21.
71. Banti V, Loreti E, Novi G, Santaniello A, Alpi A, Perata P. Heat acclimation and cross-tolerance against anoxia in Arabidopsis. Plant Cell Environ. Wiley Online Library; 2008;31:1029–37.
72. Kwak H, Lis JT. Control of transcriptional elongation. Annu Rev Genet. 2013;47:483–508.
73. Ding Y, Ndamukong I, Xu Z, Lapko H, Fromm M, Avramova Z. ATX1-generated H3K4me3 is required for efficient elongation of transcription, not initiation, at ATX1-regulated genes. PLoS Genet. 2012;8:e1003111.
74. Weng M, Yang Y, Feng H, Pan Z, Shen W-H, Zhu Y, et al. Histone chaperone ASF1 is involved in gene transcription activation in response to heat stress in Arabidopsis thaliana. Plant Cell Environ. 2014;37:2128–38.

bioRxiv preprint doi: https://doi.org/10.1101/479980; this version posted November 27, 2018. The copyright holder for this preprint (which was not certified by peer review) is the author/funder, who has granted bioRxiv a license to display the preprint in perpetuity. It is made available under aCC-BY-NC-ND 4.0 International license.

75. Fennoy SL, Nong T, Bailey-Serres J. Transcriptional and post-transcriptional processes regulate gene expression in oxygen-deprived roots of maize. Plant J. Wiley Online Library; 1998;15:727–35.
76. Karmodiya K, Krebs AR, Oulad-Abdelghani M, Kimura H, Tora L. H3K9 and H3K14 acetylation co-occur at many gene regulatory elements, while H3K14ac marks a subset of inactive inducible promoters in mouse embryonic stem cells. BMC Genomics. 2012;13:424.
77. Yang W, Wightman R, Meyerowitz EM. Cell Cycle Control by Nuclear Sequestration of CDC20 and CDH1 mRNA in Plant Stem Cells. Mol Cell. 2017;68:1108–19.e3.
78. Koroleva OA, Calder G, Pendle AF, Kim SH, Lewandowska D, Simpson CG, et al. Dynamic behavior of Arabidopsis eIF4A-III, putative core protein of exon junction complex: fast relocation to nucleolus and splicing speckles under hypoxia. Plant Cell. 2009;21:1592–606.
79. Lokdarshi A, Conner WC, McClintock C, Li T, Roberts DM. Arabidopsis CML38, a Calcium Sensor That Localizes to Ribonucleoprotein Complexes under Hypoxia Stress. Plant Physiol. 2016;170:1046–59.
80. Sato F, Kitajima S, Koyama T. Ethylene-induced gene expression of osmotin-like protein, a neutral isoform of tobacco PR-5, is mediated by the AGCCGCC eft-sequence. Plant Cell Physiol. Oxford University Press; 1996;37:249–55.
81. van Dongen JT, Licausi F. Oxygen sensing and signaling. Annu Rev Plant Biol. 2015;66:345–67.
82. Voesenek LACJ, Bailey-Serres J. Flooding tolerance: O2 sensing and survival strategies. Curr Opin Plant Biol. 2013;16:647–53.
83. Licausi F, Van Dongen JT, Giuntoli B, Novi G, Santaniello A, Geigenberger P, et al. HRE1 and HRE2, two hypoxia-inducible ethylene response factors, affect anaerobic responses in Arabidopsis thaliana. Plant J. Wiley Online Library; 2010;62:302–15.
84. Watson JA, Watson CJ, McCann A, Baugh J. Epigenetics, the epicenter of the hypoxic response. Epigenetics. 2010;5:293–6.
85. LaGory EL, Giaccia AJ. The ever-expanding role of HIF in tumour and stromal biology. Nat Cell Biol. 2016;18:356–65.
86. Buck MJ, Raaijmakers LM, Ramakrishnan S, Wang D, Valiyaparambil S, Liu S, et al. Alterations in chromatin accessibility and DNA methylation in clear cell renal cell carcinoma. Oncogene. 2014;33:4961–5.
87. Chervona Y, Costa M. The control of histone methylation and gene expression by oxidative stress, hypoxia, and metals. Free Radic Biol Med. 2012;53:1041–7.
88. Kim S-H, Jeong J-W, Park JA, Lee J-W, Seo JH, Jung B-K, et al. Regulation of the HIF-1α stability by histone deacetylases. Oncol Rep. Spandidos Publications; 2007;17:647–51.
89. Blais JD, Filipenko V, Bi M, Harding HP, Ron D, Koumenis C, et al. Activating transcription factor 4 is translationally regulated by hypoxic stress. Mol Cell Biol. 2004;24:7469–82.
90. Young RM, Wang S-J, Gordan JD, Ji X, Liebhaber SA, Simon MC. Hypoxia-mediated selective mRNA translation by an internal ribosome entry site-independent mechanism. J Biol Chem. 2008;283:16309–19.
91. ENCODE Project Consortium. An integrated encyclopedia of DNA elements in the human genome. Nature. 2012;489:57–74.
92. Schmidl C, Rendeiro AF, Sheffield NC, Bock C. ChIPmentation: fast, robust, low-input ChIP-seq for histones and transcription factors. Nat Methods. 2015;12:963–5.
93. Kumar R, Ichihashi Y, Kimura S, Chitwood DH, Headland LR, Peng J, et al. A High-Throughput Method for Illumina RNA-Seq Library Preparation. Front Plant Sci. 2012;3:202.
94. Lawrence M, Huber W, Pagès H, Aboyoun P, Carlson M, Gentleman R, et al. Software for computing and annotating genomic ranges. PLoS Comput Biol. 2013;9:e1003118.
95. Heinz S, Benner C, Spann N, Bertolino E, Lin YC, Laslo P, et al. Simple combinations of lineage-determining transcription factors prime cis-regulatory elements required for macrophage and B cell identities. Mol Cell. 2010;38:576–89.

bioRxiv preprint doi: https://doi.org/10.1101/479980; this version posted November 27, 2018. The copyright holder for this preprint (which was not certified by peer review) is the author/funder, who has granted bioRxiv a license to display the preprint in perpetuity. It is made available under aCC-BY-NC-ND 4.0 International license.

96. Cao J, Packer JS, Ramani V, Cusanovich DA, Huynh C, Daza R, et al. Comprehensive single-cell transcriptional profiling of a multicellular organism. Science. 2017;357:661–7.
97. Girke T. systemPipeR: NGS workflow and report generation environment. UC Riverside https://github com/tgirke/systemPipeR [Internet]. 2014; Available from: http://www.bioconductor.org/packages/release/bioc/html/systemPipeR.html
98. Morgan M, Carey V, Lawrence M. BiocParallel: Bioconductor facilities for parallel evaluation. R package version 0 4. 2014;1.
99. Bernd Bischl, Michel Lang, Olaf Mersmann, Jörg Rahnenführer, Claus Weihs. BatchJobs and BatchExperiments&58; Abstraction Mechanisms for Using R in Batch Environments. J Stat Softw. 2015;64:1–25.
100. McCarthy DJ, Chen Y, Smyth GK. Differential expression analysis of multifactor RNA-Seq experiments with respect to biological variation. Nucleic Acids Res. 2012;40:4288–97.
101. Warnes GR, Bolker B, Bonebakker L, Gentleman R, Huber W, Liaw A, et al. gplots: Various R programming tools for plotting data. R package version. 2009;2:1.
102. Wickham H. ggplot2: Elegant Graphics for Data Analysis. Springer Science & Business Media; 2009.
103. Neuwirth E. RColorBrewer: colorbrewer palettes. R package version. 2011;1.
104. Wickham H, Francois R. dplyr: A grammar of data manipulation. R package version 0 4. 2015;3.
105. Durinck S, Huber W. biomaRt: Interface to BioMart databases (eg Ensembl, COSMIC, Wormbase and Gramene). R package version. 2.
106. Yu G, Wang L-G, He Q-Y. ChIPseeker: an R/Bioconductor package for ChIP peak annotation, comparison and visualization. Bioinformatics. 2015;31:2382–3.
107. Lawrence M, Gentleman R, Carey V. rtracklayer: an R package for interfacing with genome browsers. Bioinformatics. 2009;25:1841–2.
108. Krijthe JH. Rtsne: T-distributed stochastic neighbor embedding using Barnes-Hut implementation. R package version 0 13, URL https://github com/jkrijthe/Rtsne. 2015;
109. Kolde R. Pheatmap: pretty heatmaps. R package version. 2012;61.
110. Meyer D, Dimitriadou E, Hornik K, Weingessel A, Leisch F. e1071: Misc Functions of the Department of Statistics (e1071), TU Wien, 2014. R package version. 2015;1–6.
111. Maechler M. Finding Groups in Data'': Cluster Analysis Extended Rousseeuw et. Documentation for software package The Comprehensive R Archive Network (CRAN): Wien [Internet]. 2018; Available from: ftp://128.61.111.11/pub/CRAN/web/packages/cluster/cluster.pdf
112. Morgan M, Anders S, Lawrence M, Aboyoun P, Pagès H, Gentleman R. ShortRead: a bioconductor package for input, quality assessment and exploration of high-throughput sequence data. Bioinformatics. 2009;25:2607–8.
113. Morgan M, Pages H, Obenchain V, Hayden N. Rsamtools: Binary alignment (BAM), FASTA, variant call (BCF), and tabix file import. R package version. 2016;1.
114. Kim D, Pertea G, Trapnell C, Pimentel H, Kelley R, Salzberg SL. TopHat2: accurate alignment of transcriptomes in the presence of insertions, deletions and gene fusions. Genome Biol. 2013;14:R36.
115. Gordon A, Hannon GJ. Fastx-toolkit. FASTQ/A short-reads preprocessing tools (unpublished) http://hannonlab cshl edu/fastx_toolkit. 2010;5.
116. Andrews S, Others. FastQC: a quality control tool for high throughput sequence data. 2010;
117. Bailey TL, Boden M, Buske FA, Frith M, Grant CE, Clementi L, et al. MEME SUITE: tools for motif discovery and searching. Nucleic Acids Res. 2009;37:W202–8.
118. Ramírez F, Ryan DP, Grüning B, Bhardwaj V, Kilpert F, Richter AS, et al. deepTools2: a next generation web server for deep-sequencing data analysis. Nucleic Acids Res. 2016;44:W160–5.

bioRxiv preprint doi: https://doi.org/10.1101/479980; this version posted November 27, 2018. The copyright holder for this preprint (which was not certified by peer review) is the author/funder, who has granted bioRxiv a license to display the preprint in perpetuity. It is made available under aCC-BY-NC-ND 4.0 International license.

119. Krzywinski M, Schein J, Birol I, Connors J, Gascoyne R, Horsman D, et al. Circos: an information aesthetic for comparative genomics. Genome Res. 2009;19:1639–45.
120. Quinlan AR, Hall IM. BEDTools: a flexible suite of utilities for comparing genomic features. Bioinformatics. 2010;26:841–2.
121. Li H. A statistical framework for SNP calling, mutation discovery, association mapping and population genetical parameter estimation from sequencing data. Bioinformatics. 2011;27:2987–93.
121. Li H. A statistical framework for SNP calling, mutation discovery, association mapping and population genetical parameter estimation from sequencing data. Bioinformatics. 2011;27:2987–93.

bioRxiv preprint doi: https://doi.org/10.1101/479980; this version posted November 27, 2018. The copyright holder for this preprint (which was not certified by peer review) is the author/funder, who has granted bioRxiv a license to display the preprint in perpetuity. It is made available under aCC-BY-NC-ND 4.0 International license.

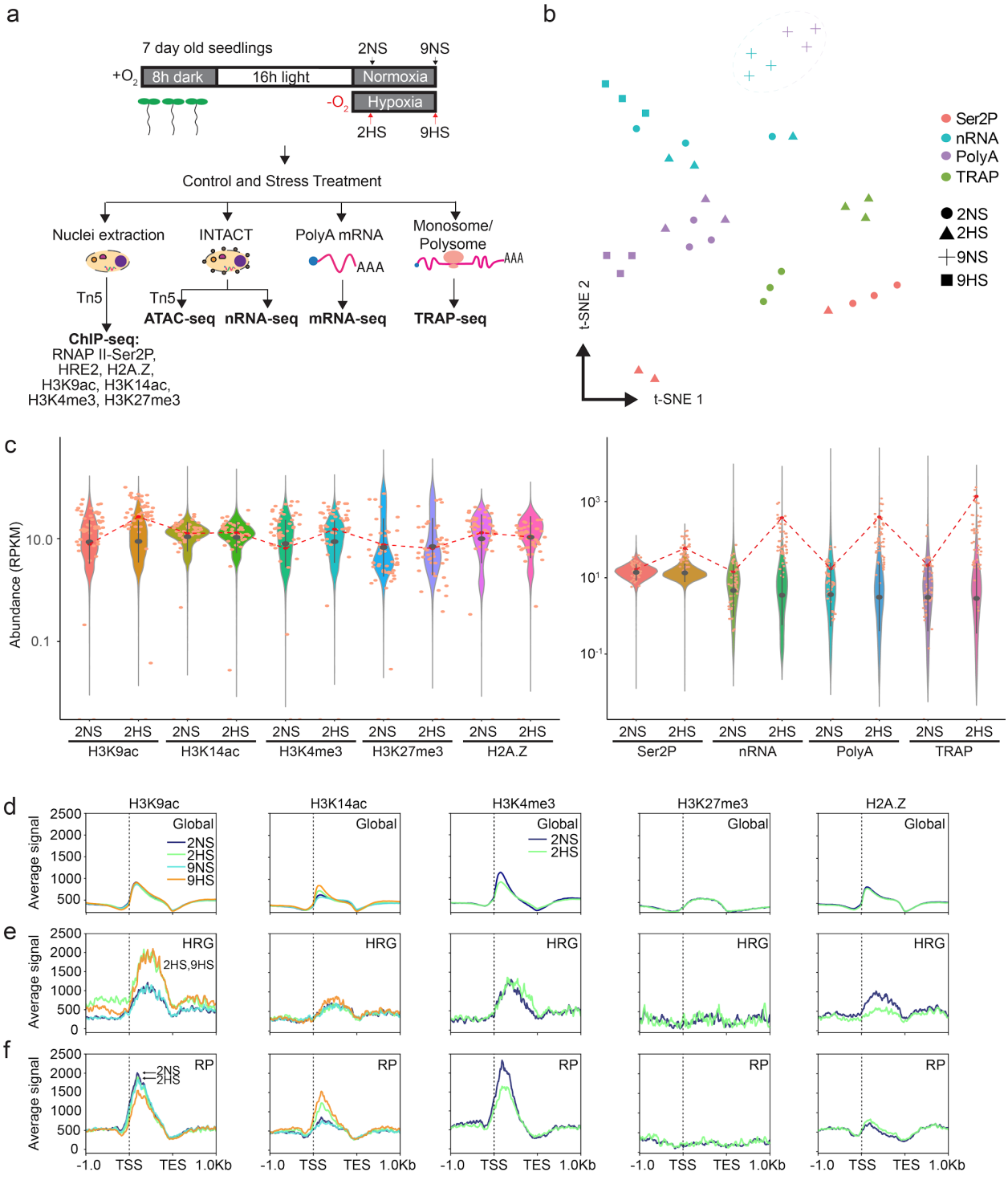

bioRxiv preprint doi: https://doi.org/10.1101/479980; this version posted November 27, 2018. The copyright holder for this preprint (which was not certified by peer review) is the author/funder, who has granted bioRxiv a license to display the preprint in perpetuity. It is made available under aCC-BY-NC-ND 4.0 International license.

Fig. 1 Multiscale chromatin and RNA gene regulatory analyses of control (normoxic) and hypoxic seedlings of *Arabidopsis*. **a** Schematic of experiments performed. Seven-day-old seedlings were subjected to control (normoxic) (2NS, 9NS) or hypoxic stress (2HS, 9HS) conditions. Vertical arrows indicate time of harvest. Chromatin immunopurification (ChIP) was performed to evaluate genomic regions bound by the Ser2 phospho-isoform of RNA Polymerase II (Ser2P), the Histone 2 variant H2A.Z, modified Histone 3 (H3K4me3, H3K27me3, H3K9ac, H3K14ac), and the group VII Ethylene Responsive Factor (ERF) transcription factor HYPOXIA RESPONSIVE ERF 2 (HRE2). Isolation of Nuclei TAgged in specific Cell Types (INTACT) purified nuclei were used for Assay for Transposase Accessible Chromatin (ATAC) and evaluation of nuclear RNA. Ribosome-associated mRNA was obtained by Translating Ribosome Affinity Purification (TRAP). **b** Reproducibility of individual replicates related to nascent transcription (Ser2P) and RNA (nuclear [nRNA], polyadenylated mRNA [polyA], ribosome-associated polyA mRNA [TRAP]) by use of t-Distributed stochastic neighbor embedding (t-SNE). **c** Violin plots displaying genome-wide abundance (reads per kilobase per million reads [RPKM]) of histone and mRNA-related outputs for control (2NS) and short-term hypoxic (2HS) treatments. Mean ± SD are depicted within violins in gray. RPKM values for the 49 core hypoxia-responsive upregulated genes (HRGs) [17] are plotted as orange dots. The HRG, *ALCOHOL DEHYDROGENASE 1* (*ADH1*) is tracked as a red line. **d-f** Read distributions of histone modifications/variant genome wide **d**, for HRGs **e** and 246 cytosolic ribosomal proteins (RPs) **f**. Read distributions are plotted from 1 kb upstream to 1 kb downstream of gene units defined by the transcription start site (TSS) and transcription end site (TES). **g** Distribution of transposase hypersensitive sites (THS) on genomic features for each condition. **h-j** Average distribution of chromatin accessibility for **h** protein-coding genes, **i** HRGs, and **j** RPs determined by ATAC-seq.

bioRxiv preprint doi: https://doi.org/10.1101/479980; this version posted November 27, 2018. The copyright holder for this preprint (which was not certified by peer review) is the author/funder, who has granted bioRxiv a license to display the preprint in perpetuity. It is made available under aCC-BY-NC-ND 4.0 International license.

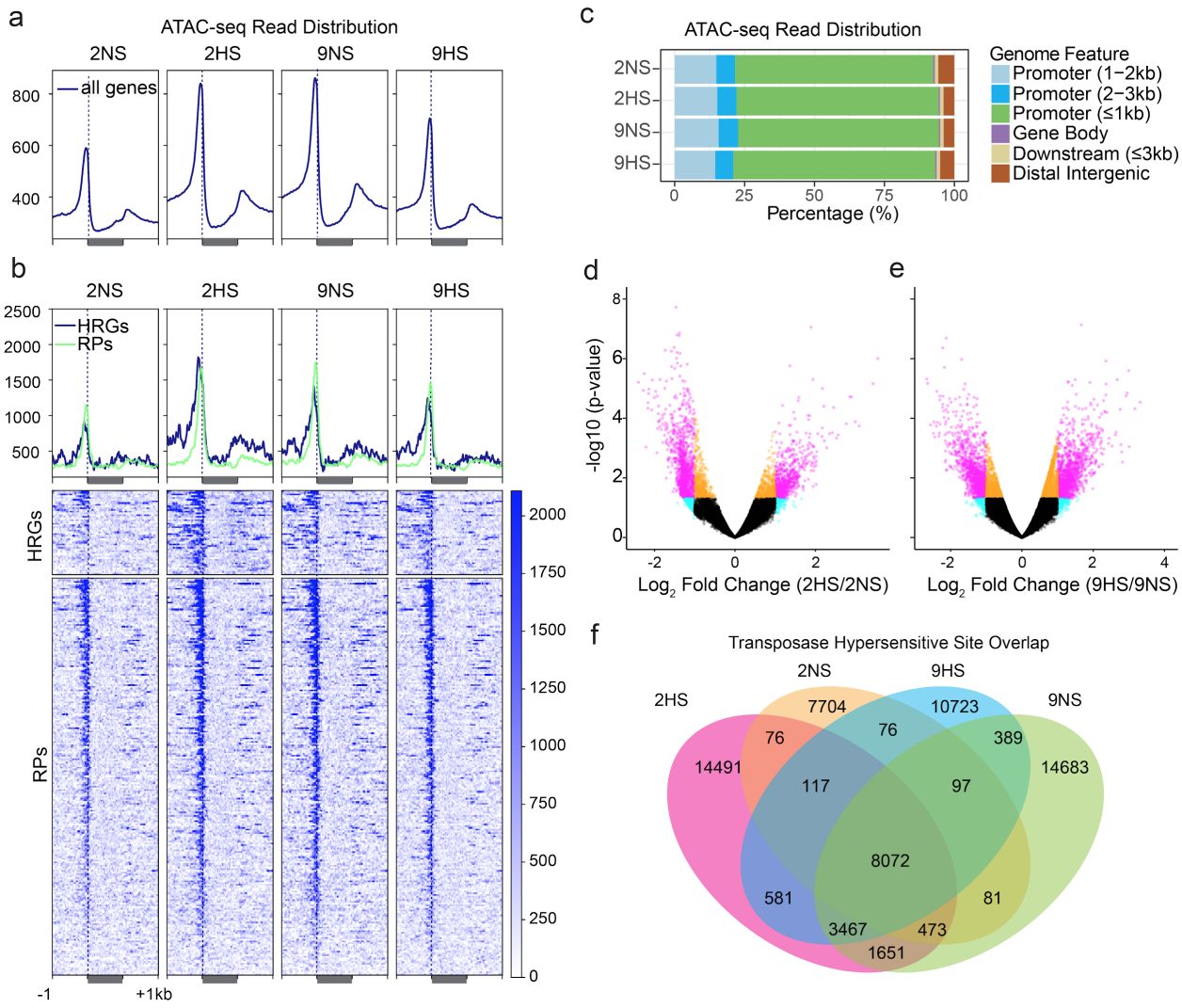

Fig. 2 Regions of chromatin accessibility determined by Transposase-Accessible Chromatin using sequencing (ATAC-seq) are dynamically regulated by hypoxic stress. **a-b** Average ATAC-seq read distribution of chromatin accessibility for **a** protein-coding genes, **b** HRGs, and RPs determined by ATAC-seq. **c** Distribution of transposase hypersensitive sites (THSs) on genomic features for each condition. **d-e** Volcano plot of $\log_2$ fold change in THSs identifiable under two conditions and the significance value of their difference. Genes indicated in pink meet the criteria of $\log_2$ fold change value > |1|, 0.05 < p. value. **f** Overlap in THSs identified for each of four conditions.

bioRxiv preprint doi: https://doi.org/10.1101/479980; this version posted November 27, 2018. The copyright holder for this preprint (which was not certified by peer review) is the author/funder, who has granted bioRxiv a license to display the preprint in perpetuity. It is made available under aCC-BY-NC-ND 4.0 International license.

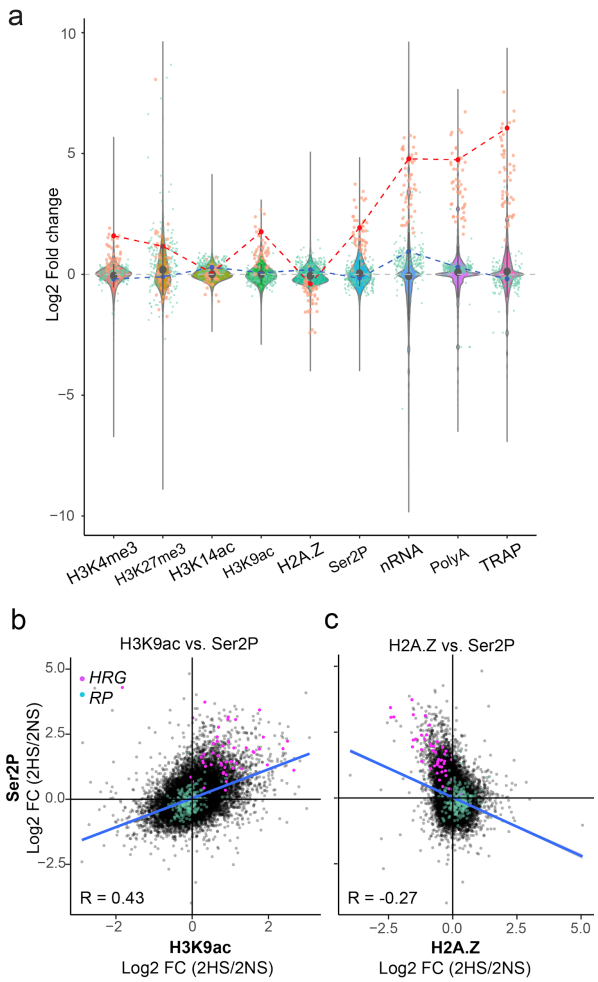

Fig. 3 Short term hypoxic stress promotes pronounced changes in chromatin, transcription and nascent transcripts that are not uniformly reflected in transcript steady-state abundance or translation. Comparison of genome-wide data for chromatin and RNA for 2 h hypoxic stress (2HS) relative to the normoxic control (2NS). **a** Violin plots of $\log_2$ fold change (2HS/2NS) of histone, RNAPII-Ser2P and RNA outputs. The 49 core Hypoxia-Responsive Genes (HRGs) [17] are plotted as orange dots with *ALCOHOL DEHYDROGENASE 1* (*ADH1*) depicted in red and tracked between datasets (red dashed line). Cytosolic ribosomal proteins (RPs) are plotted in blue, with *RIBOSOMAL PROTEIN 37B* tracked between datasets (blue dashed line). Mean ± SD are depicted within violins as a dark gray dashed line **b** Comparison of $\log_2$ fold change (2HS/2NS) between H2A.Z on the gene body and Ser2P on the gene body. **c** Comparison of $\log_2$ fold change (FC) (2HS/2NS) between H3K9ac and Ser2P on the gene body. For b and c, HRGs are plotted in pink and RPs in blue; the Pearson's coefficient of determination is shown.

bioRxiv preprint doi: https://doi.org/10.1101/479980; this version posted November 27, 2018. The copyright holder for this preprint (which was not certified by peer review) is the author/funder, who has granted bioRxiv a license to display the preprint in perpetuity. It is made available under aCC-BY-NC-ND 4.0 International license.

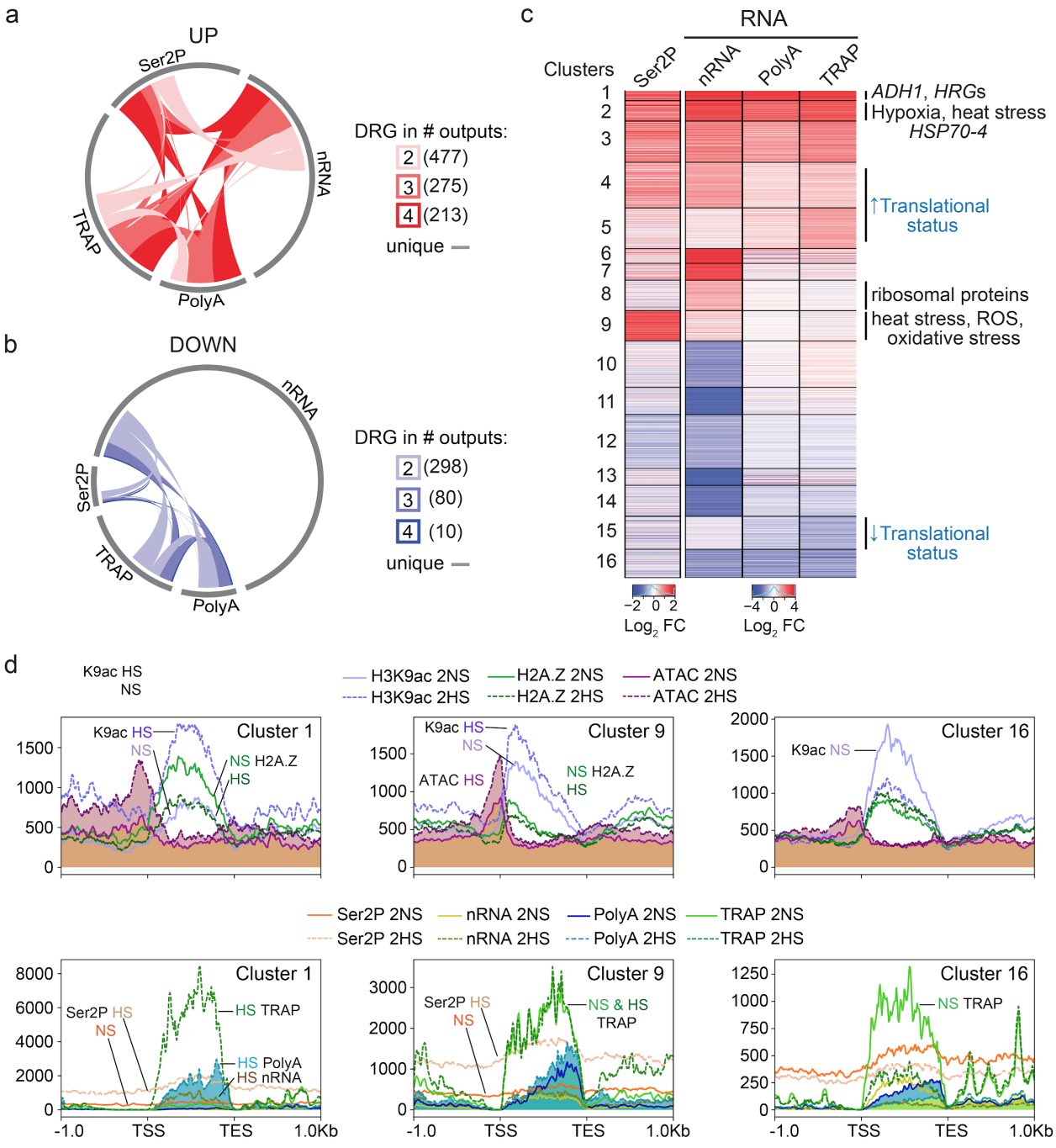

Fig. 4 Multi-scale analysis of hypoxia-regulated genes reveals concordant and discordant patterns of gene regulation. Number of **a** up- and **b** down-differentially regulated genes (DRGs) in response to hypoxic stress (|log$_2$ fold change| > 1; FDR < 0.05) identified in each of the four readouts related to RNA: Ser2P ChIP, nRNA, polyA RNA, and TRAP RNA. Arc of circle circumference indicated by the grey line represents the DRGs in each of the four readouts. Genes differentially regulated in 2 to 4 readouts were tabulated (number in parentheses) and depicted by links within the circle. Genes differentially regulated in only one readout are represented by unlinked grey lines. **c** Heatmap showing similarly regulated genes based on four assays of gene activity. Partitioning around medoids (PAM) clustering of 3,042 differentially regulated genes; 16 clusters. Selected enriched Gene Ontology terms are shown at right (p

bioRxiv preprint doi: https://doi.org/10.1101/479980; this version posted November 27, 2018. The copyright holder for this preprint (which was not certified by peer review) is the author/funder, who has granted bioRxiv a license to display the preprint in perpetuity. It is made available under aCC-BY-NC-ND 4.0 International license.

adj. < 1.47e-09), |FC| > 1, FDR < 0.05. Clusters displaying increased or decreased translational status (ribosome-associated [TRAP] relative to total abundance [polyA]) are shown. **d** Average signal of various chromatin and RNA outputs for genes of three clusters plotted from 1 kb upstream of the transcription start site (TSS) to 1 kb downstream of the transcript end site (TES) for the 2 hour (2NS, 2HS) timepoints. Signal scale of graphs differ. Dashed lines used to plot hypoxic stress data. Upper panel, ATAC-seq data shaded. Lower panel 2HS polyA data shaded.

bioRxiv preprint doi: https://doi.org/10.1101/479980; this version posted November 27, 2018. The copyright holder for this preprint (which was not certified by peer review) is the author/funder, who has granted bioRxiv a license to display the preprint in perpetuity. It is made available under aCC-BY-NC-ND 4.0 International license.

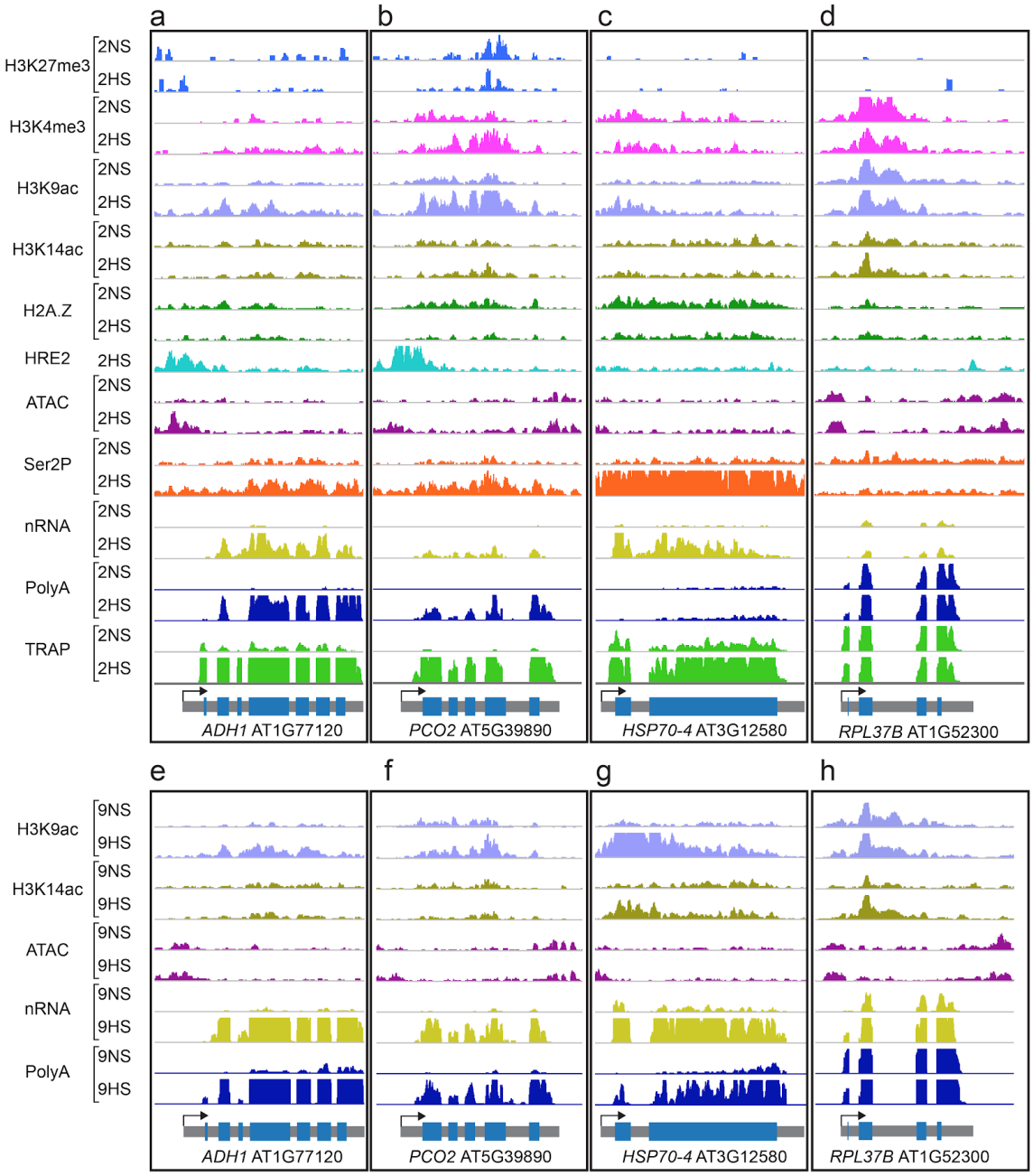

Fig. 5. Genome browser view of normalized read coverage of histone, ATAC-seq, RNAPII-Ser2P, HRE2-chromatin immunopurification and RNA outputs for representative genes. a-d Normoxia (2NS) and 2 h hypoxic stress (2HS). **e-h** 9NS and 9HS samples. **a,e** *ALCOHOL DEHYDROGENASE 1* (*ADH1*), **b,f** *PLANT CYSTEINE OXIDASE 2* (*PCO2*), **c,g** *HEAT SHOCK PROTEIN 70-4* (*HSP70-4*) and **d,h** *RIBOSOMAL PROTEIN L37B* (*RPL37B*). The maximum read scale value used for chromatin based and RNA based outputs is equivalent for all genes depicted. At bottom, the transcription unit is shown in grey with the transcription start site marked with an arrow. *PCO2* shows a stronger decline in H2A.Z than *ADH1* in response to hypoxia at 2HS (*PCO2*, -1.15 $\log_2$ FC; *ADH1*, -0.33 $\log_2$ FC) and demonstrates an example of elevated H3K4me3 under hypoxic stress.

bioRxiv preprint doi: https://doi.org/10.1101/479980; this version posted November 27, 2018. The copyright holder for this preprint (which was not certified by peer review) is the author/funder, who has granted bioRxiv a license to display the preprint in perpetuity. It is made available under aCC-BY-NC-ND 4.0 International license.

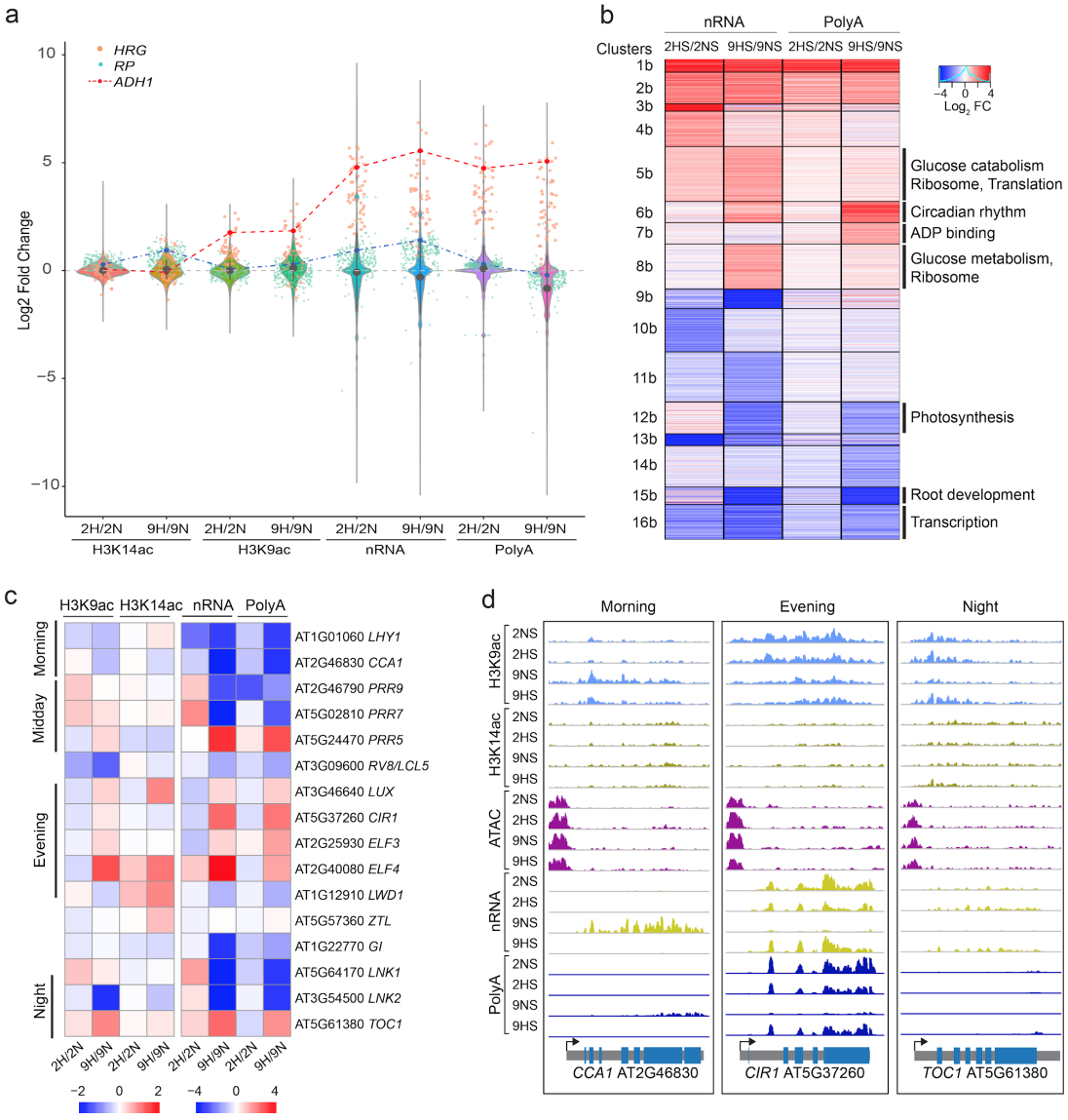

Fig. 6. Prolonged hypoxia leads to further variation in epigenetic, transcriptional and posttranscriptional regulation. a Violin plots comparing $\log_2$ fold change of two histone and two mRNA outputs at the 2h (2HS/2NS) and 9h timepoints (9HS/9NS) as plotted in Figure 1b. The *HRGs* are plotted as orange dots with *ADH1* depicted in red and tracked between datasets (red dashed line). *RPs* are plotted in blue, with *RIBOSOMAL PROTEIN 37B*. Mean ± SD depicted within violins as a dark gray dashed line. **b** Heatmap showing similarly regulated genes based on two RNA readouts. Partitioning around medoids (PAM) clustering of 3,897 differentially regulated genes; 16 clusters. Selected enriched Gene Ontology terms are shown at right (p adj. < 1.37E-06), |FC| > 1, FDR < 0.05. **c** Heatmap of chromatin and RNA readouts of select circadian regulated genes under short and prolonged hypoxic stress. Heatmap scales between chromatin and RNA based readouts differ. **d** Brower views of a morning (*CIRCADIAN CLOCK ASSOCIATED 1*, CCA1), evening (*CIRCADIAN 1*, CIR1), and night (*TIMING OF CAB EXPRESSION 1*, TOC1) expressed genes. RNA scale of *TOC1* is three-fold lower than the scale used for *CCA1* and *CIR1* due to low transcript abundance.

bioRxiv preprint doi: https://doi.org/10.1101/479980; this version posted November 27, 2018. The copyright holder for this preprint (which was not certified by peer review) is the author/funder, who has granted bioRxiv a license to display the preprint in perpetuity. It is made available under aCC-BY-NC-ND 4.0 International license.

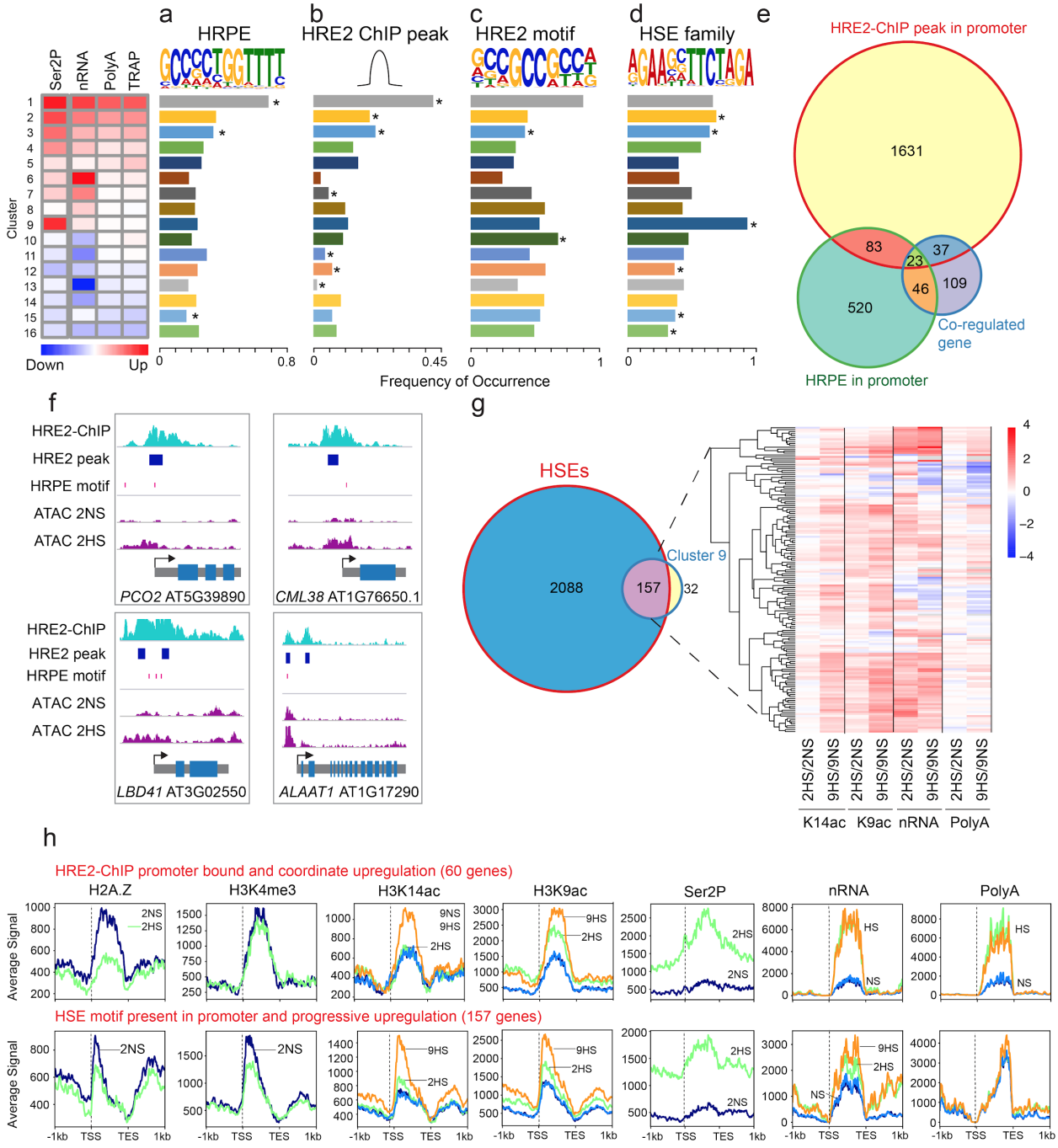

Fig. 7. Regulation of hypoxic responses by two ERFVII and HSF TF families. **a-d** Motif and peak enrichment in the promoter regions (1 kb upstream to 500 bp downstream of the TSS) of genes in clusters identified in Fig. 4c for **a**. Hypoxia Responsive Promoter Element (HRPE), **b**. HRE2-ChIP peaks, **c** HRE2-motif, and **d.** Heat Shock sequence Elements (HSE). Frequency of motif and peak occurrence was calculated as # motifs per # genes in cluster. Clusters with significant enrichment were identified by two-tailed Fisher's exact test $p < 0.05$. **e.** Overlap of genes containing HRE2-ChIP peaks and HRPE within promoter regions and the coordinately upregulated genes. **f**. Genome browser view of select *HRGs* (*PLANT CYSTEINE OXIDASE2, PCO2*; *CALMODULIN-LIKE 38, CML38*; *LOB-DOMAIN CONTAINING PROTEIN 41, LBD41*; *ALANINE AMINO TRANSFERASE1, AAT1*). The locations of

bioRxiv preprint doi: https://doi.org/10.1101/479980; this version posted November 27, 2018. The copyright holder for this preprint (which was not certified by peer review) is the author/funder, who has granted bioRxiv a license to display the preprint in perpetuity. It is made available under aCC-BY-NC-ND 4.0 International license.

HRE2-ChIP peaks and HRPEs are depicted as a horizontal blue box and vertical red line, respectively. **g**. Venn diagram of DRGs containing promoter HSEs and cluster 9 genes in Fig. 4c. Heatmap of log_2 FC values for H3K14ac, H3K9ac, nRNA, and polyA RNA for 2HS/2NS and 9HS/9NS is depicted for the union of genes. **h,i** Average signal of chromatin and RNA readouts for **h,** HRE2 bound genes with coordinate upregulation and **i,** genes with progressive upregulation (cluster 9) containing promoter HSEs. Average signal is plotted from 1 kb upstream of the transcription start site (TSS) to 1 kb downstream of the transcript end site (TES).

bioRxiv preprint doi: https://doi.org/10.1101/479980; this version posted November 27, 2018. The copyright holder for this preprint (which was not certified by peer review) is the author/funder, who has granted bioRxiv a license to display the preprint in perpetuity. It is made available under aCC-BY-NC-ND 4.0 International license.

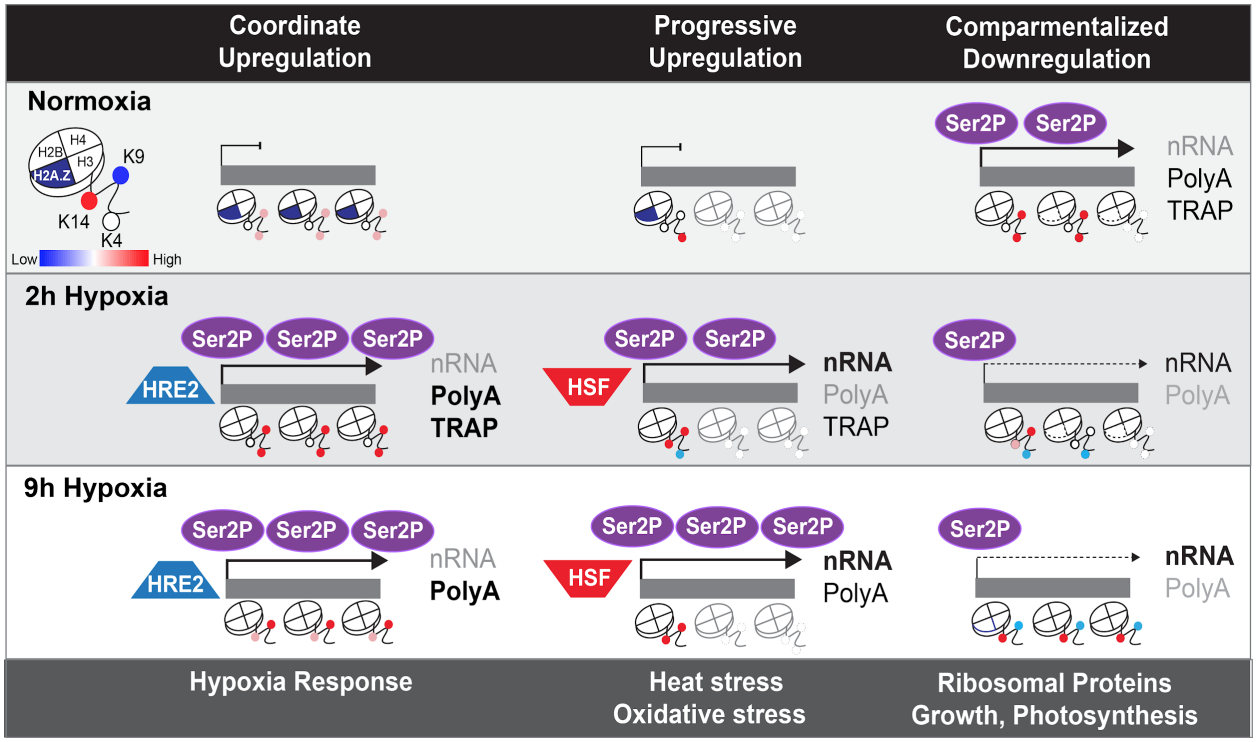

Fig. 8. Model of four dominant patterns of nuclear regulation in response to short term and prolonged hypoxic stress. Genes with coordinate upregulation from chromatin to translation, many of which are bound by the transcription factor HRE2, are characterized by H2A.Z eviction, H3K4me3, H3K9ac. Genes with progressive upregulation include many associated with heat and oxidative stress responses. These are lowly transcribed under normoxia (nonstress conditions); their transcription increases in response to brief hypoxia (2h hypoxia) as shown by high association with RNAPII-Ser2P and elevation of nuclear transcripts (nRNA), some of which are incompletely spliced. Although polyadenylated (polyA) transcripts of these genes are low abundance and primarily 3' biased, they are typically associated with ribosomes (TRAP). Progressively upregulated genes have strong 5' bias in histone marks, hypoxia-triggered H2A.Z eviction, H3K9ac elevation and H3K4me3 reduction. Many are targets of HSFs. Genes with compartmentalized downregulation include many associated with growth and photosynthesis. Maintained Ser2P and nRNA levels under the stress indicate these continue to be transcribed, acquire greater H3K14ac and sustain H3K9ac. Cartoons illustrates histone modifications as defined by the key. Transcript abundance ranges from limited (grey) to abundant (black, bold). HRE2, Hypoxia-Responsive ERF 2; HSF, Heat Shock Factor transcriptional activator; Ser2P, RNAPII with the Ser2P modification.

bioRxiv preprint doi: https://doi.org/10.1101/479980; this version posted November 27, 2018. The copyright holder for this preprint (which was not certified by peer review) is the author/funder, who has granted bioRxiv a license to display the preprint in perpetuity. It is made available under aCC-BY-NC-ND 4.0 International license.

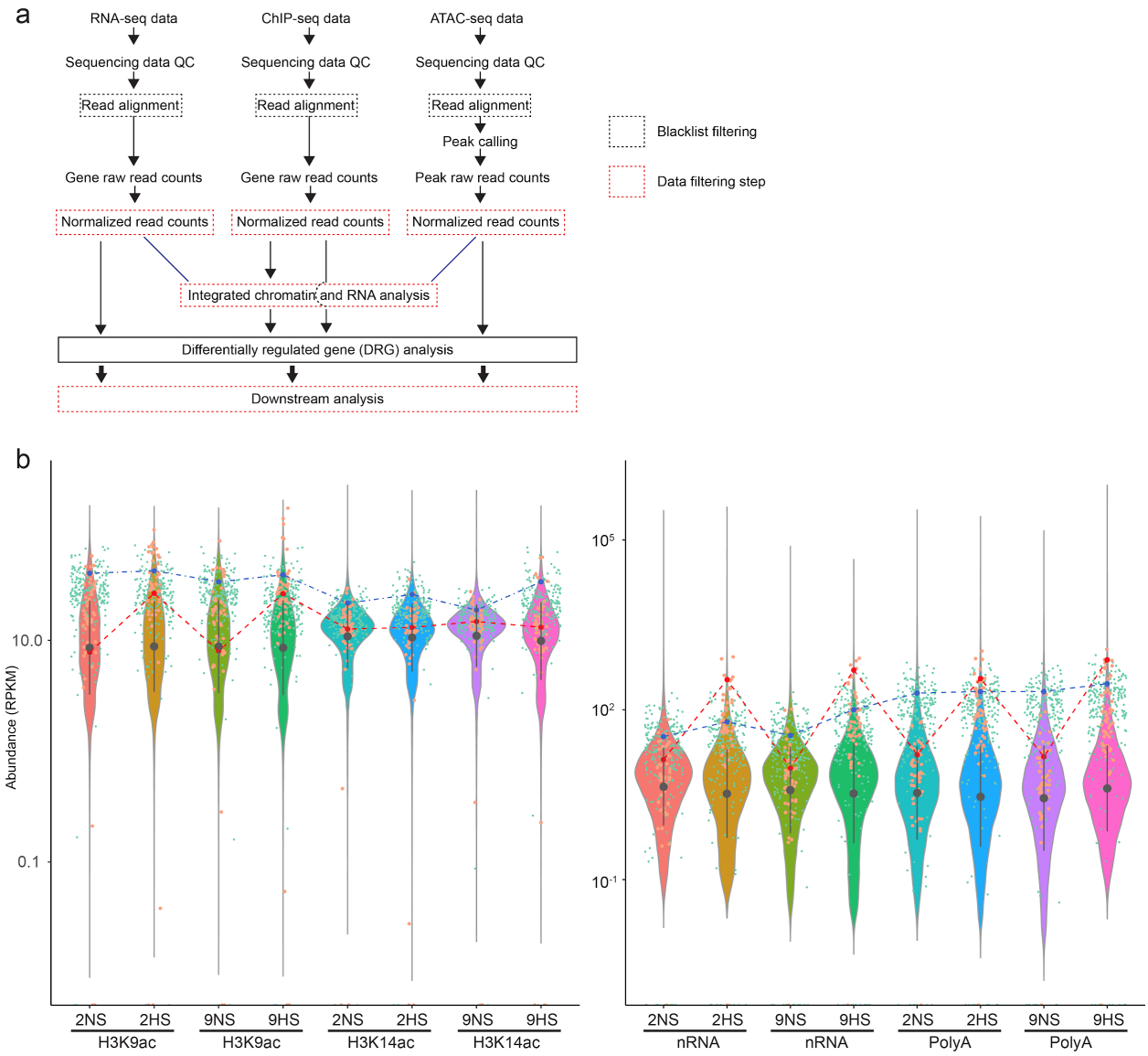

Figure S1. Expanded overview of the multiscale chromatin and RNA gene regulatory analyses. a Schematic of library types and data analysis performed on 7-day-old seedlings subjected to control (normoxic) (2NS, 9NS) or hypoxic stress (2HS, 9HS) as shown in Fig 1a. Control seedlings were compared to hypoxia stress seedlings independently within each chromatin- and RNA-based dataset. Low abundance reads were filtered (< 2 CPM). Differentially regulated genes were identified and utilized for downstream analyses. The chromatin and RNA datasets were also analyzed in combination. **b** Violin plots comparing distribution of genome-wide abundance (reads per kilobase per million reads [RPKM]) of histone and mRNA-related outputs for control (2NS, 9NS) and hypoxic (2HS, 9HS) treatments for all readouts assayed at 9HS. RPKM values for the 49 core hypoxia responsive upregulated genes (HRGs) [17] are plotted as orange dots. The HRG, *ALCOHOL DEHYDROGENASE 1* (*ADH1*) is tracked as a red line. RPKM values for cytosolic ribosomal proteins (RPs) are plotted in blue, with *RIBOSOMAL PROTEIN 37B* tracked between datasets (blue dashed line). Mean ± SD are depicted within violins as a dark gray dashed line.

bioRxiv preprint doi: https://doi.org/10.1101/479980; this version posted November 27, 2018. The copyright holder for this preprint (which was not certified by peer review) is the author/funder, who has granted bioRxiv a license to display the preprint in perpetuity. It is made available under aCC-BY-NC-ND 4.0 International license.

Figure S2 (on two pages)

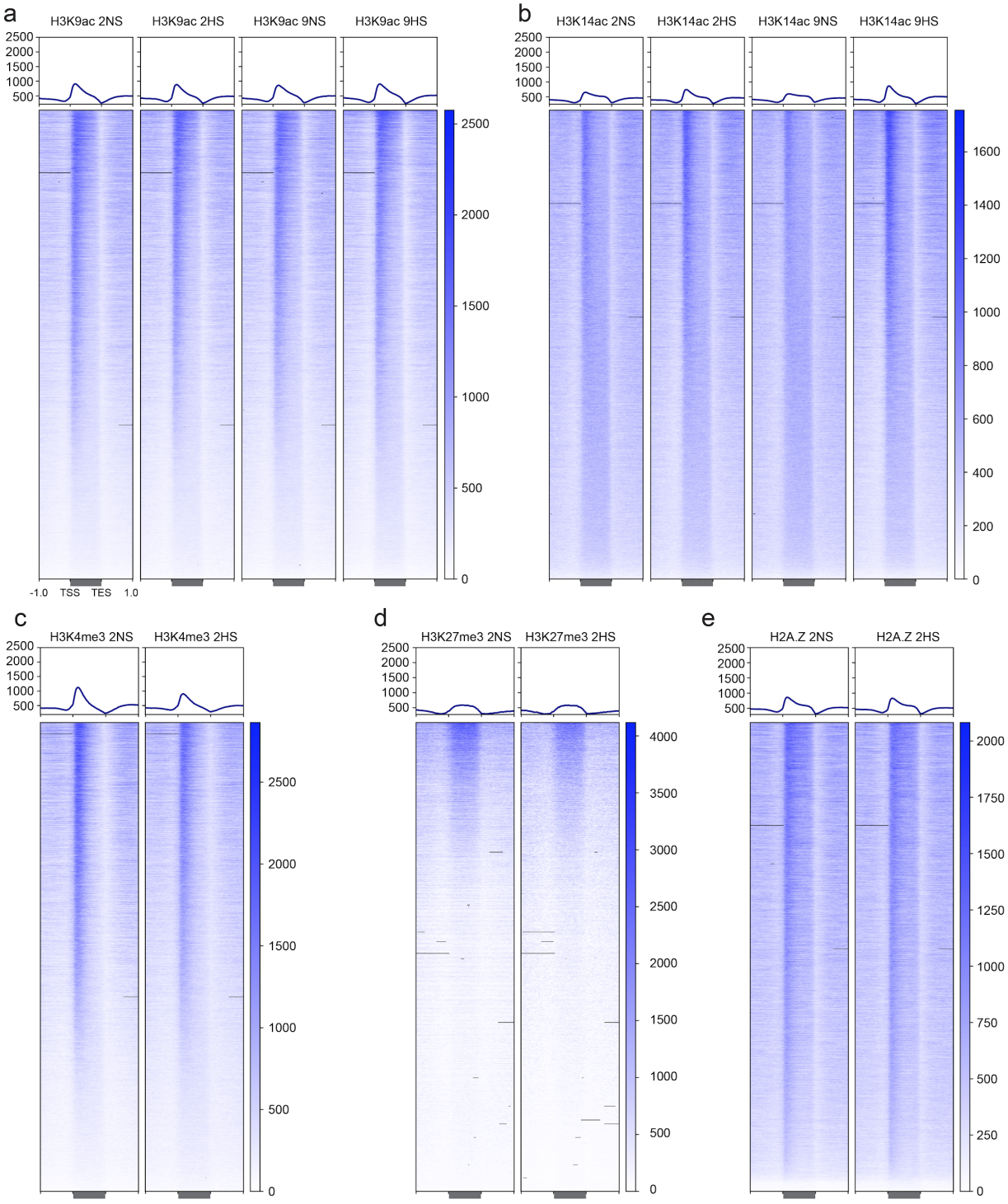

bioRxiv preprint doi: https://doi.org/10.1101/479980; this version posted November 27, 2018. The copyright holder for this preprint (which was not certified by peer review) is the author/funder, who has granted bioRxiv a license to display the preprint in perpetuity. It is made available under aCC-BY-NC-ND 4.0 International license.

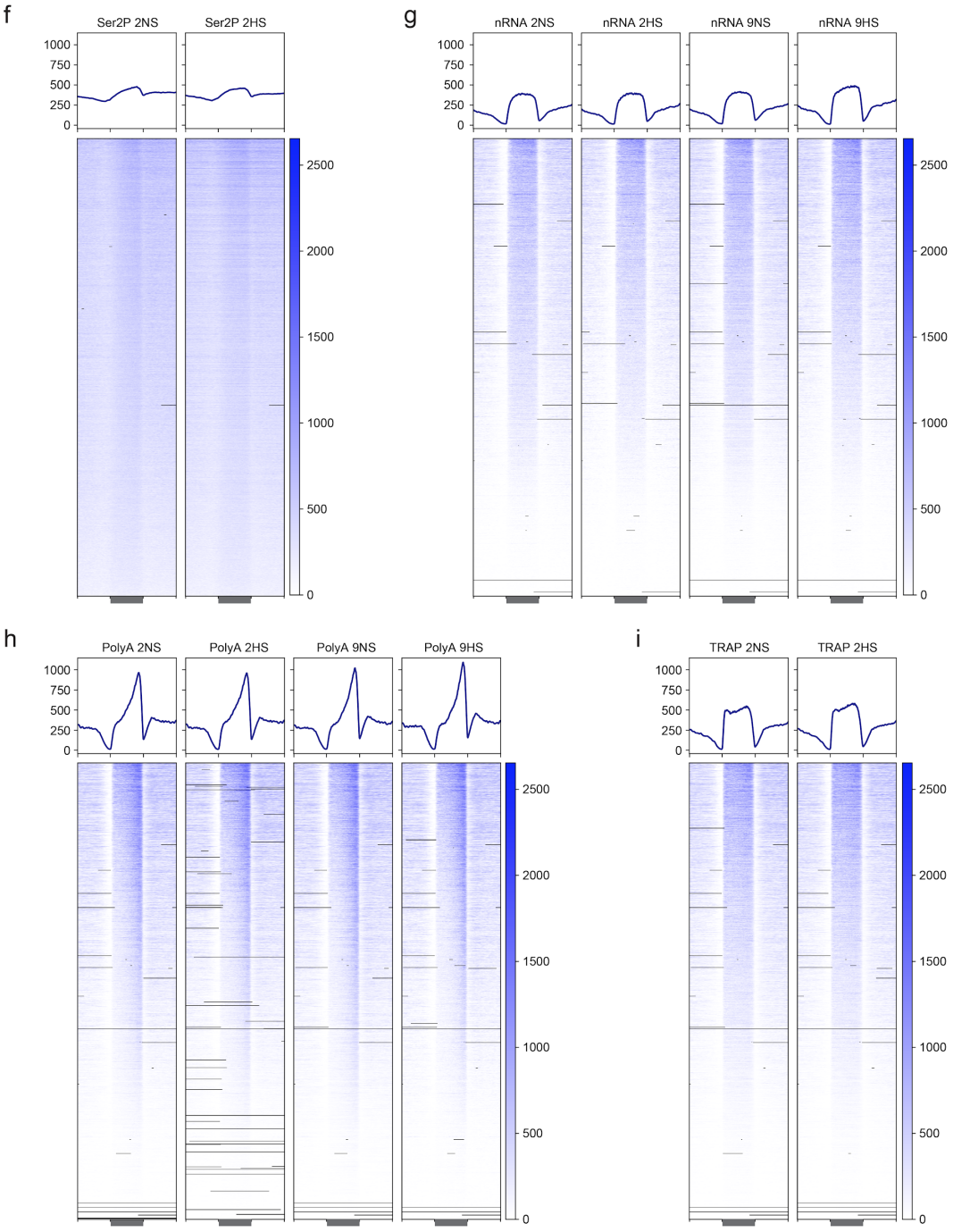

Figure S2. Average signal plots and heat maps for the global distribution of reads of chromatin and RNA data. a-h The genomic region from 1 kb upstream of the transcription start site (TSS) to 1 kb downstream of the transcription end site (TES) is depicted for each histone modification and variant, RNAPII-Ser2P (Ser2P), nuclear RNA (nRNA), polyadenylated RNA (polyA RNA) and ribosome-associated RNA (TRAP RNA) for nonstress (2NS, 9NS) and hypoxia (2HS, 9HS) stressed seedlings. Each heat map ranks genes from the highest signal (top) to the lowest (bottom). Heatmap intensity scale values differ between plots of different readouts and are shown. Blacklisted regions of the genome with disproportionately high reads are tabulated in Table S5 and depicted as a black line.

bioRxiv preprint doi: https://doi.org/10.1101/479980; this version posted November 27, 2018. The copyright holder for this preprint (which was not certified by peer review) is the author/funder, who has granted bioRxiv a license to display the preprint in perpetuity. It is made available under aCC-BY-NC-ND 4.0 International license.

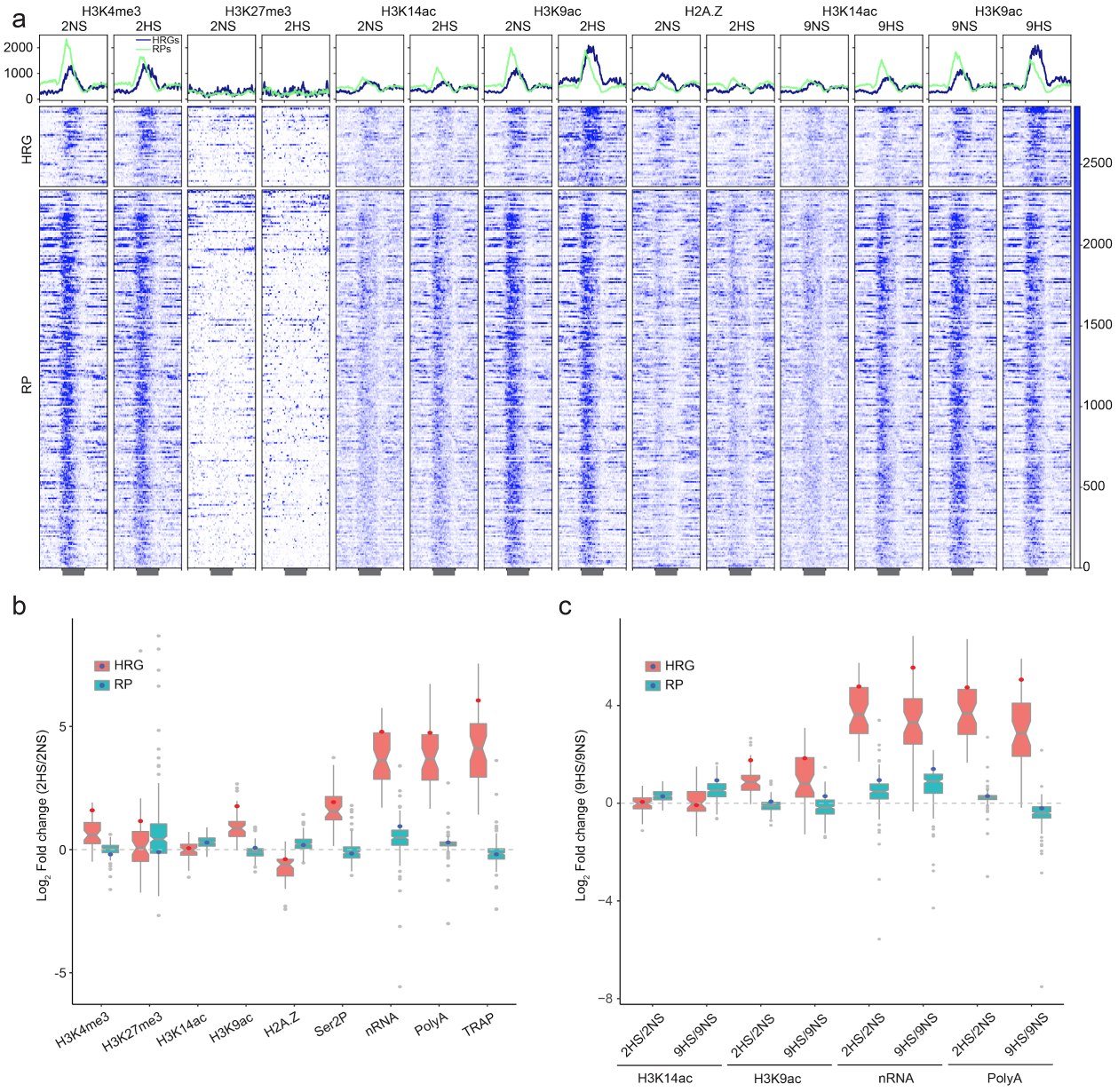

Figure S3. Multi-level evaluation of histone and gene regulation activity of the *HRG*s and *RP*s. a The average signal profile and read distribution heatmap for *HRG*s (blue) and *RPs* (green) is depicted for each histone dataset and condition. Analysis of the hypoxia responsive genes (*HRG*s) (n=49) and cytosolic ribosomal protein genes (n=223). Each row in the heat map represents an individual gene; gene order is the same in all plots. **b,c** Box plots of log_2 fold change assayed for (**b**) short (2 h) and (**c**) prolonged (9 h) hypoxic stress compared to control (2HS/2NS, 9HS/9NS). Data for *ADH1* is indicated as a red dot and that of *RPL37B* is indicated as a blue dot. Range of dataset and upper and lower quantiles are depicted within each boxplot.

bioRxiv preprint doi: https://doi.org/10.1101/479980; this version posted November 27, 2018. The copyright holder for this preprint (which was not certified by peer review) is the author/funder, who has granted bioRxiv a license to display the preprint in perpetuity. It is made available under aCC-BY-NC-ND 4.0 International license.

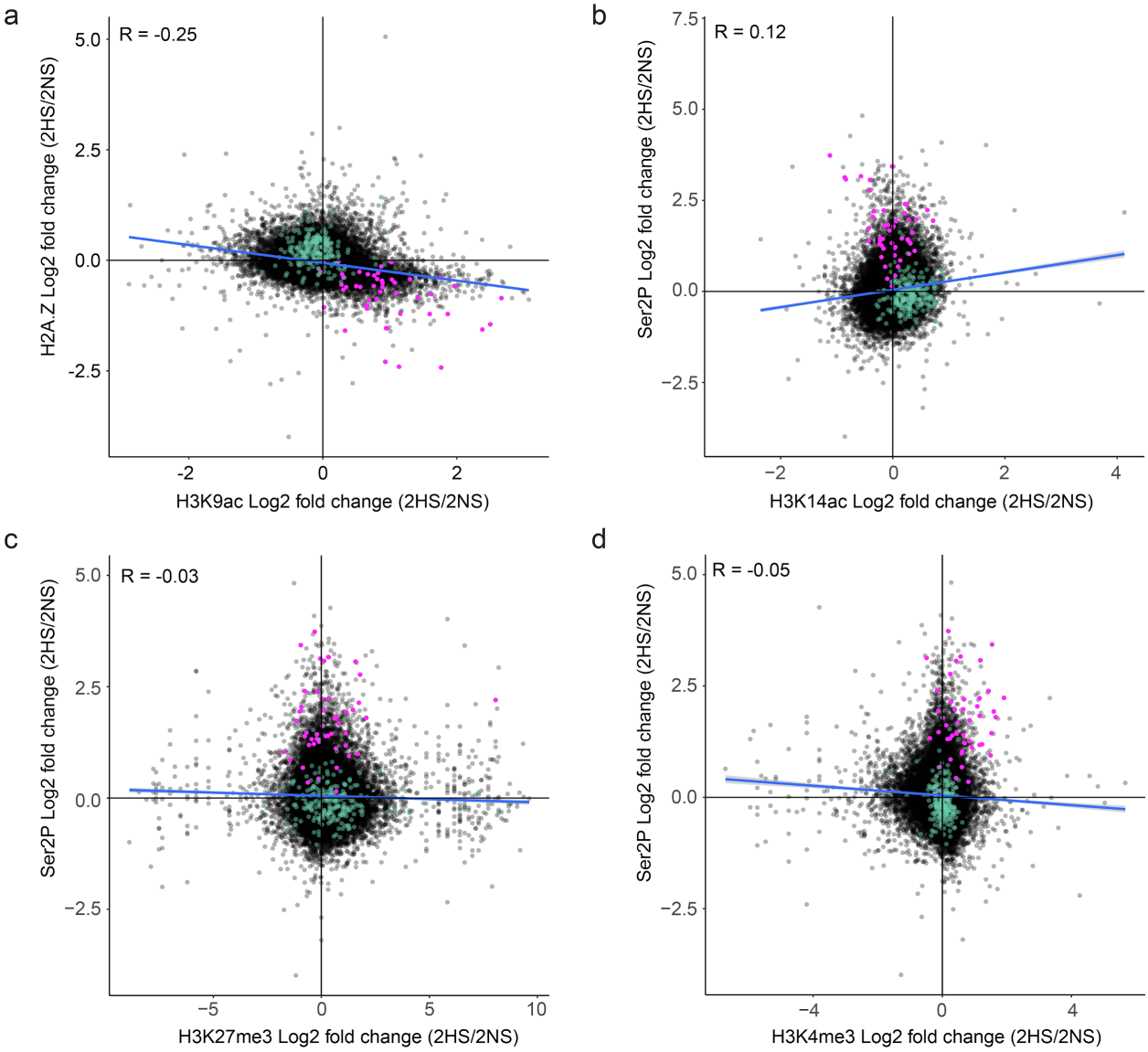

Figure S4. Evidence of cooperative association between H2A.Z eviction and H3K9ac and the relation between Histone H3 modification and RNAPII engagement. Plots comparing genome-wide changes in histone modifications and RNAP-Ser2P on individual gene bodies in response to hypoxia. **a** Comparison of $\log_2$ fold change (2HS/2NS) values of H3K9ac and H2A.Z association on gene bodies. **b-d** Comparison of $\log_2$ fold change (2HS/2NS) values of (**b**) H3K14ac, (**c**) H3K27me3, and (**d**) H3K4me3 and Ser2P on gene bodies. In all panels, *HRG*s are plotted in pink and *RP*s in green; the Pearson correlation coefficient for all genes is shown and the slope depicted with a blue line.

bioRxiv preprint doi: https://doi.org/10.1101/479980; this version posted November 27, 2018. The copyright holder for this preprint (which was not certified by peer review) is the author/funder, who has granted bioRxiv a license to display the preprint in perpetuity. It is made available under aCC-BY-NC-ND 4.0 International license.

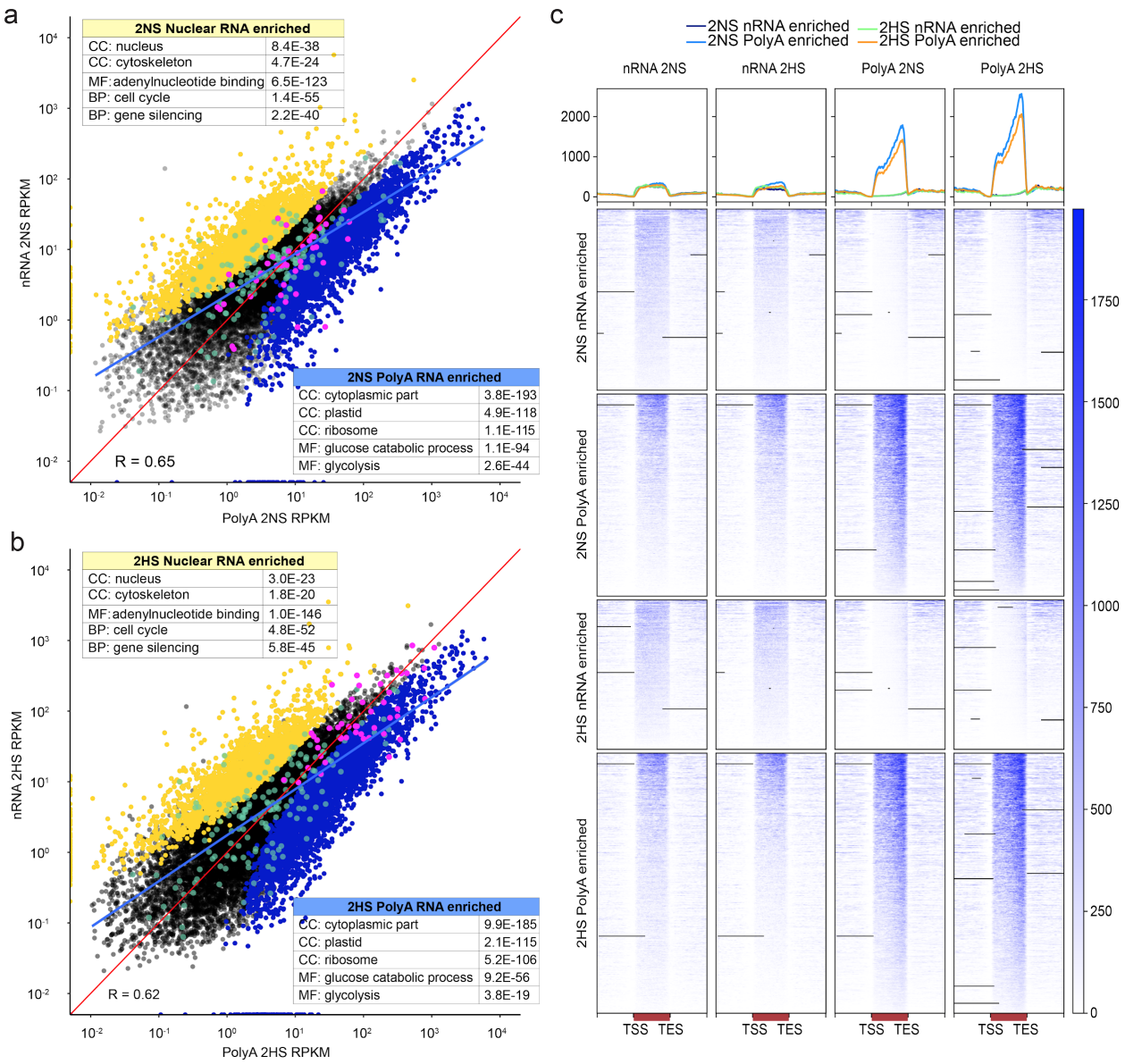

Figure S5. Genome-wide comparison of nRNA to polyA RNA demonstrates nuclear and cytoplasmic enrichment of transcripts under two conditions. **a, b** Scatterplot of normalized read values (per kilobase per million reads; RPKM) on genes in nRNA and polyA RNA populations at (**a**) 2NS and (**b**) 2HS. Transcripts enriched in nRNA (yellow; 2NS: 2,855, 2HS: 2,377) or polyA RNA (blue; 2NS: 3,139, 2HS: 4,029) are depicted ($|\log_2 FC > 1|$, $p < 0.05$). *HRG*s and *RP*s are also indicated in pink and green, respectively. The genome-wide Pearson correlation coefficient is shown and the slope depicted with a blue line. The red line is a slope of 1. Inserted tables describe representative Gene Ontology categories that are over-represented in nuclear RNA and polyA under the two conditions (data from Table S2). Many of the same groups of cell component (CC) and molecular (MF) were over-represented in the nRNA and polyA RNA populations obtained in the same manner in rice [46]. **c** Average signal profile and read distribution heatmap of nRNA-enriched and polyA-enriched transcripts at 2NS and 2HS.

bioRxiv preprint doi: https://doi.org/10.1101/479980; this version posted November 27, 2018. The copyright holder for this preprint (which was not certified by peer review) is the author/funder, who has granted bioRxiv a license to display the preprint in perpetuity. It is made available under aCC-BY-NC-ND 4.0 International license.

Figure S6 (on two pages)

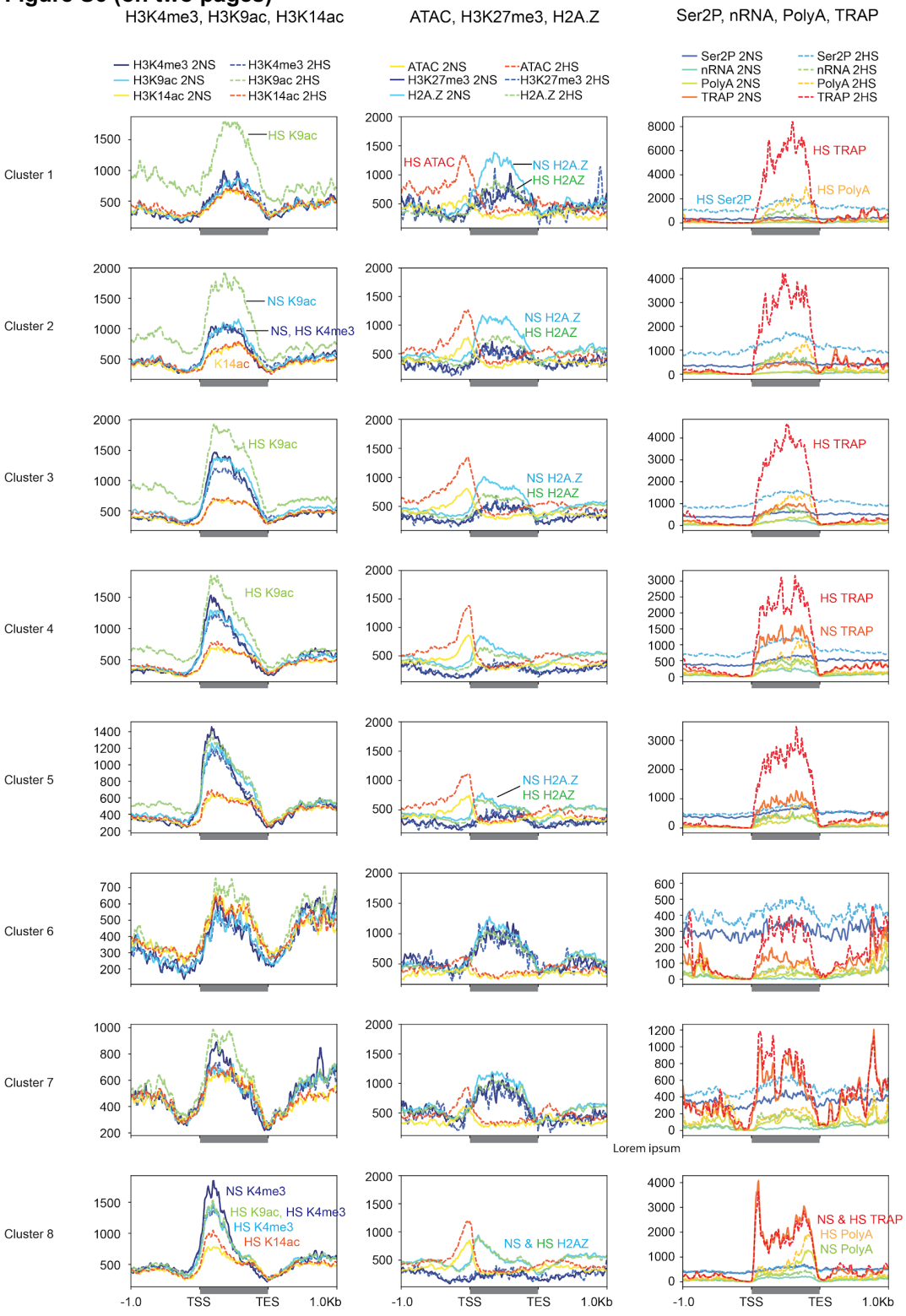

bioRxiv preprint doi: https://doi.org/10.1101/479980; this version posted November 27, 2018. The copyright holder for this preprint (which was not certified by peer review) is the author/funder, who has granted bioRxiv a license to display the preprint in perpetuity. It is made available under aCC-BY-NC-ND 4.0 International license.

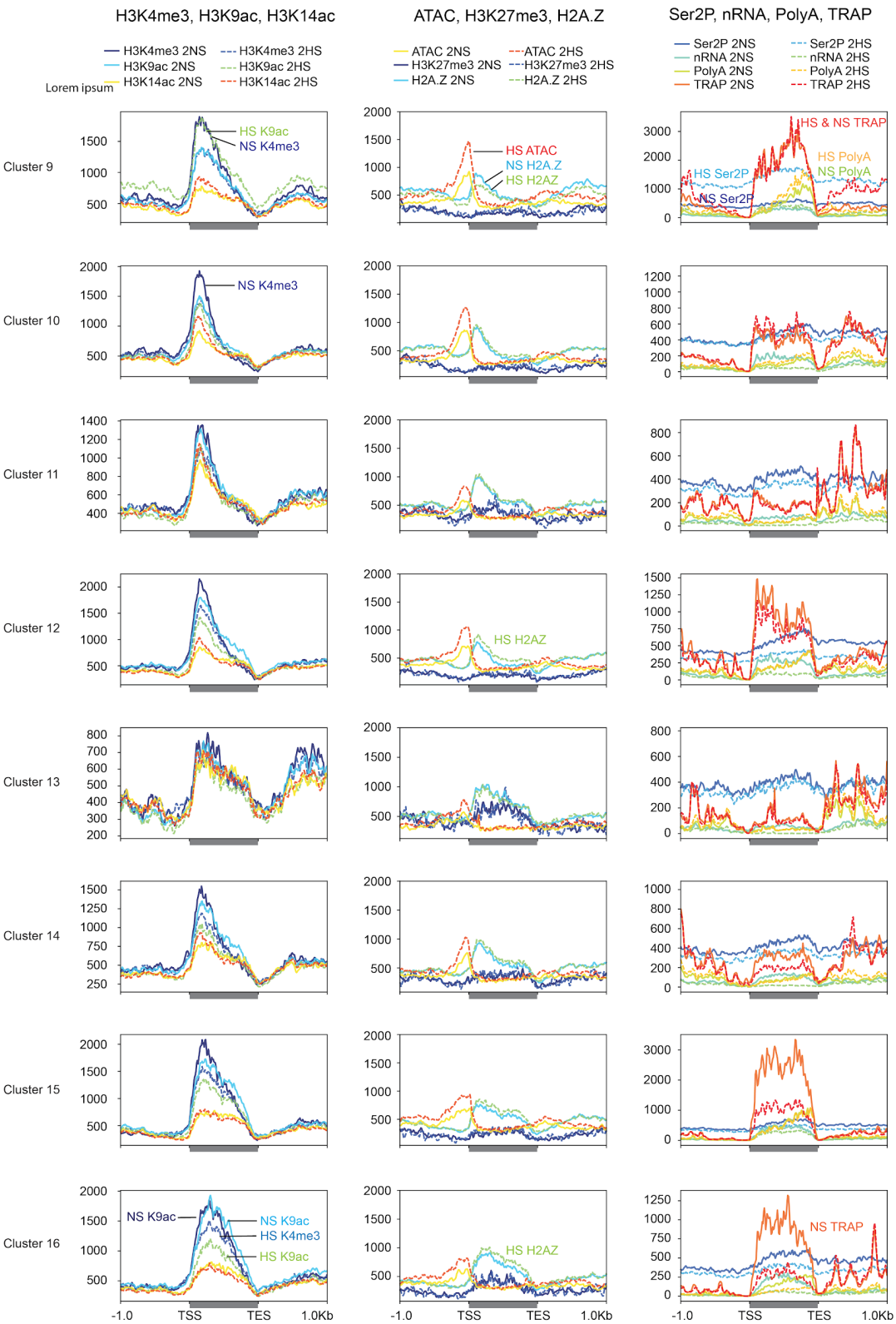

Figure S6. Distinctions in histones, RNAPII-Ser2P and RNA levels on genes that are co-regulated in response to hypoxic stress. Average signal of chromatin and RNA outputs for clustered genes identified from the 2HS comparison in Fig. 4c. Hypoxic sample data are dashed lines. Signal values are plotted from 1 kb upstream of the TSS to 1 kb downstream of the TES. Signal scale of graphs may differ.

bioRxiv preprint doi: https://doi.org/10.1101/479980; this version posted November 27, 2018. The copyright holder for this preprint (which was not certified by peer review) is the author/funder, who has granted bioRxiv a license to display the preprint in perpetuity. It is made available under aCC-BY-NC-ND 4.0 International license.

Figure S7 (on two pages)

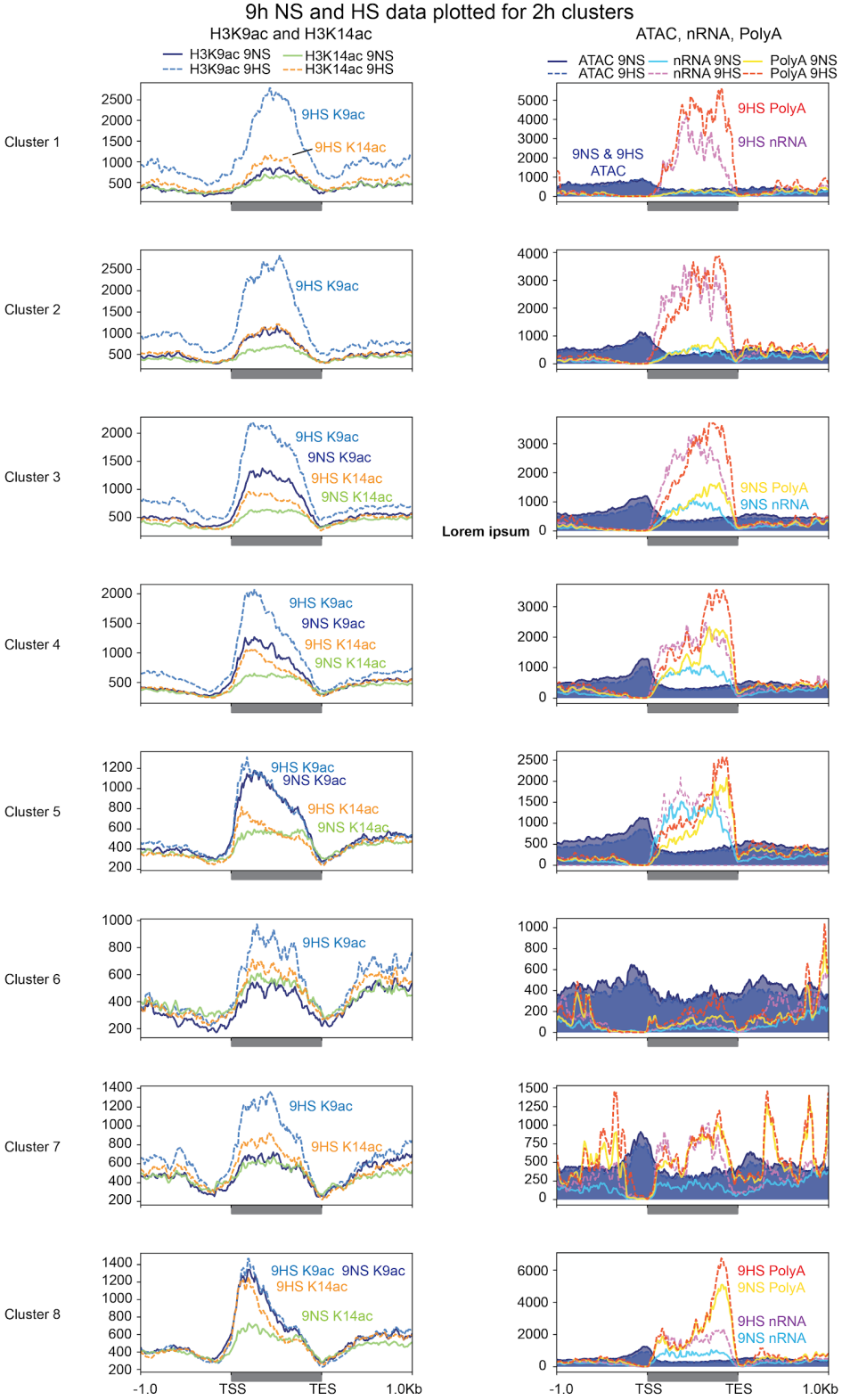

bioRxiv preprint doi: https://doi.org/10.1101/479980; this version posted November 27, 2018. The copyright holder for this preprint (which was not certified by peer review) is the author/funder, who has granted bioRxiv a license to display the preprint in perpetuity. It is made available under aCC-BY-NC-ND 4.0 International license.

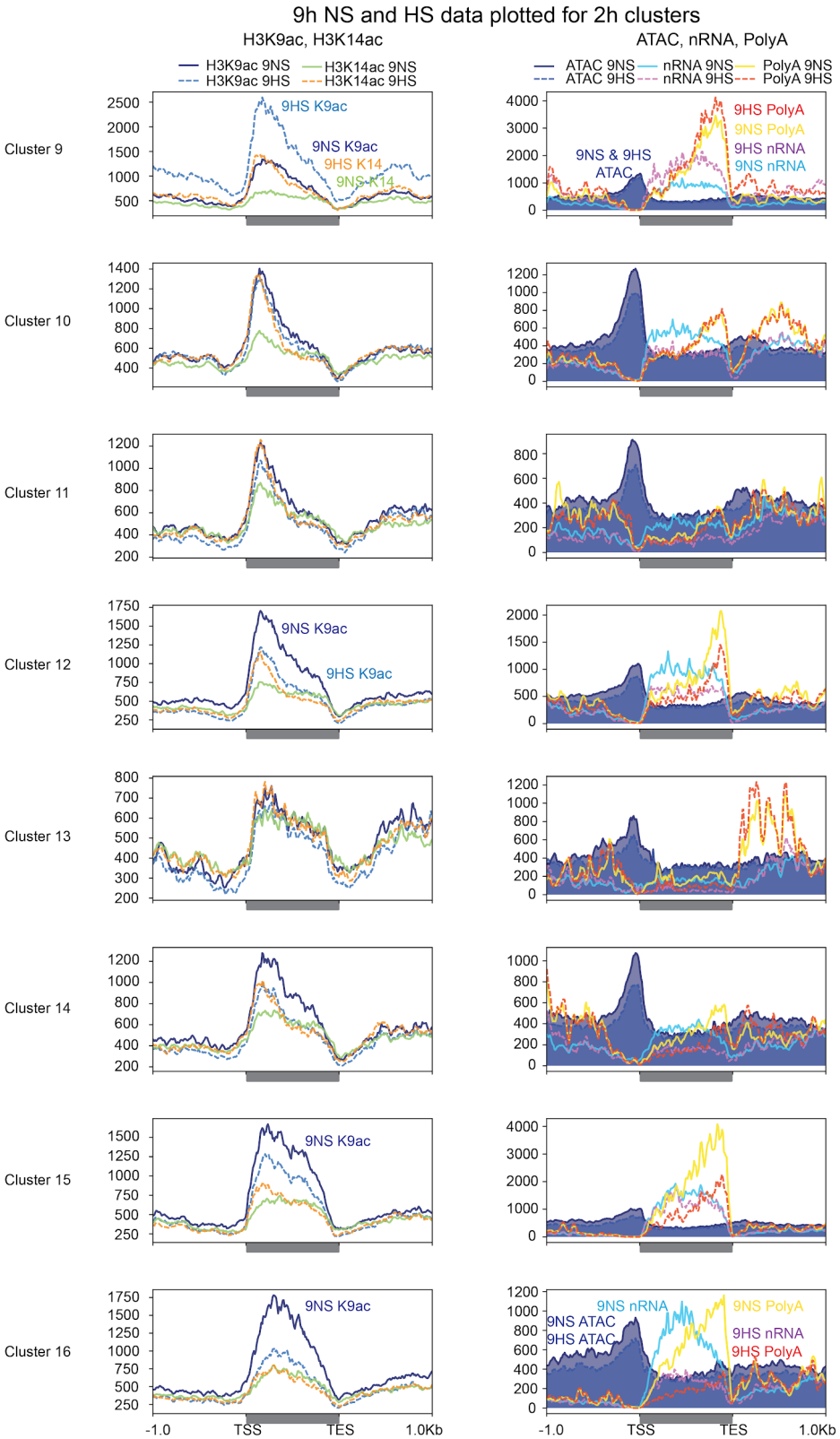

Figure S7. Progressive regulation of variations in gene activity in response to hypoxia. Average signal of chromatin and RNA outputs for clustered genes identified from the 9HS (9HS/9NS) comparison in Fig. 4c. Plotting is as described for Figure S6.

bioRxiv preprint doi: https://doi.org/10.1101/479980; this version posted November 27, 2018. The copyright holder for this preprint (which was not certified by peer review) is the author/funder, who has granted bioRxiv a license to display the preprint in perpetuity. It is made available under aCC-BY-NC-ND 4.0 International license.

Figure S8 (on two pages)

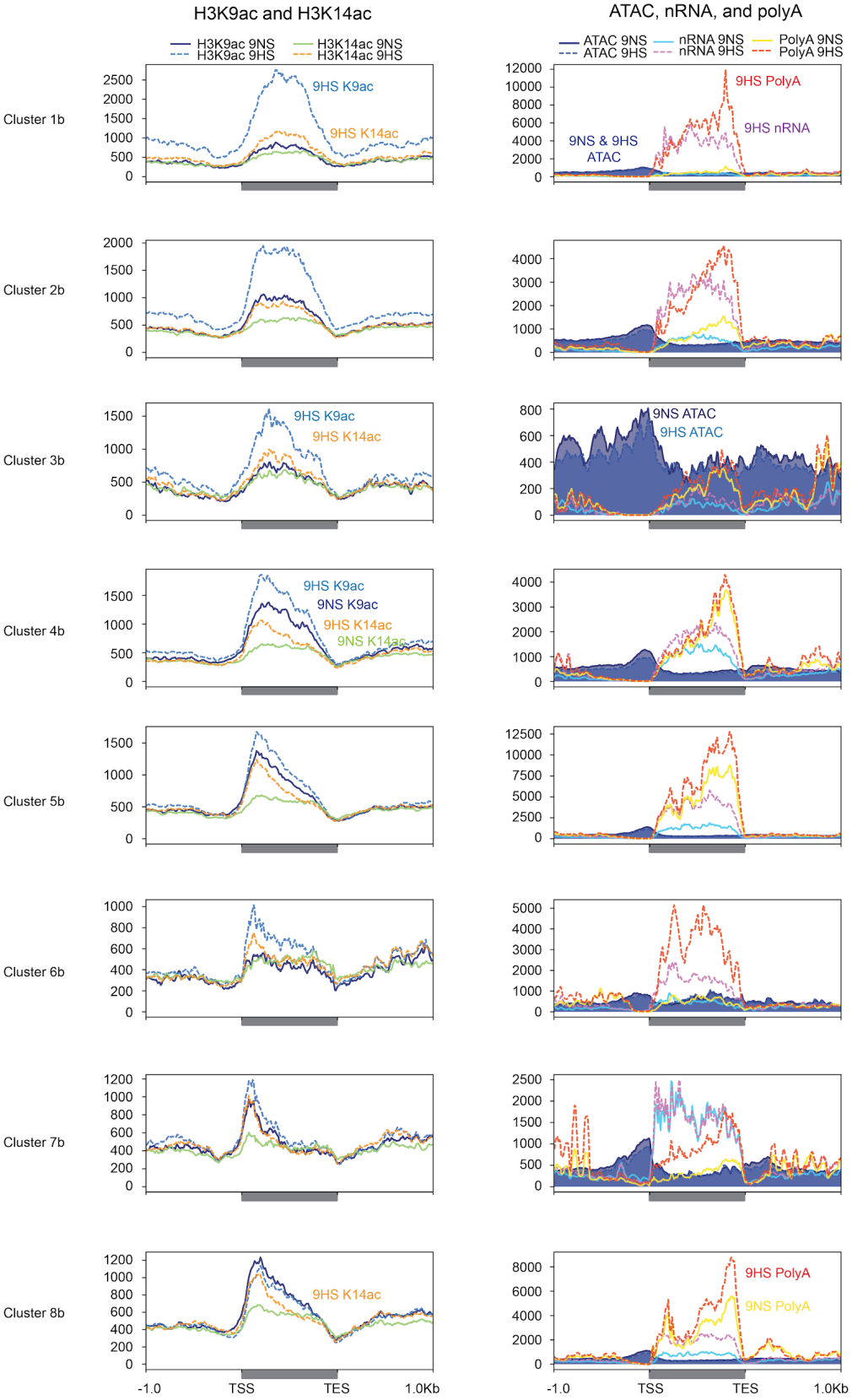

bioRxiv preprint doi: https://doi.org/10.1101/479980; this version posted November 27, 2018. The copyright holder for this preprint (which was not certified by peer review) is the author/funder, who has granted bioRxiv a license to display the preprint in perpetuity. It is made available under aCC-BY-NC-ND 4.0 International license.

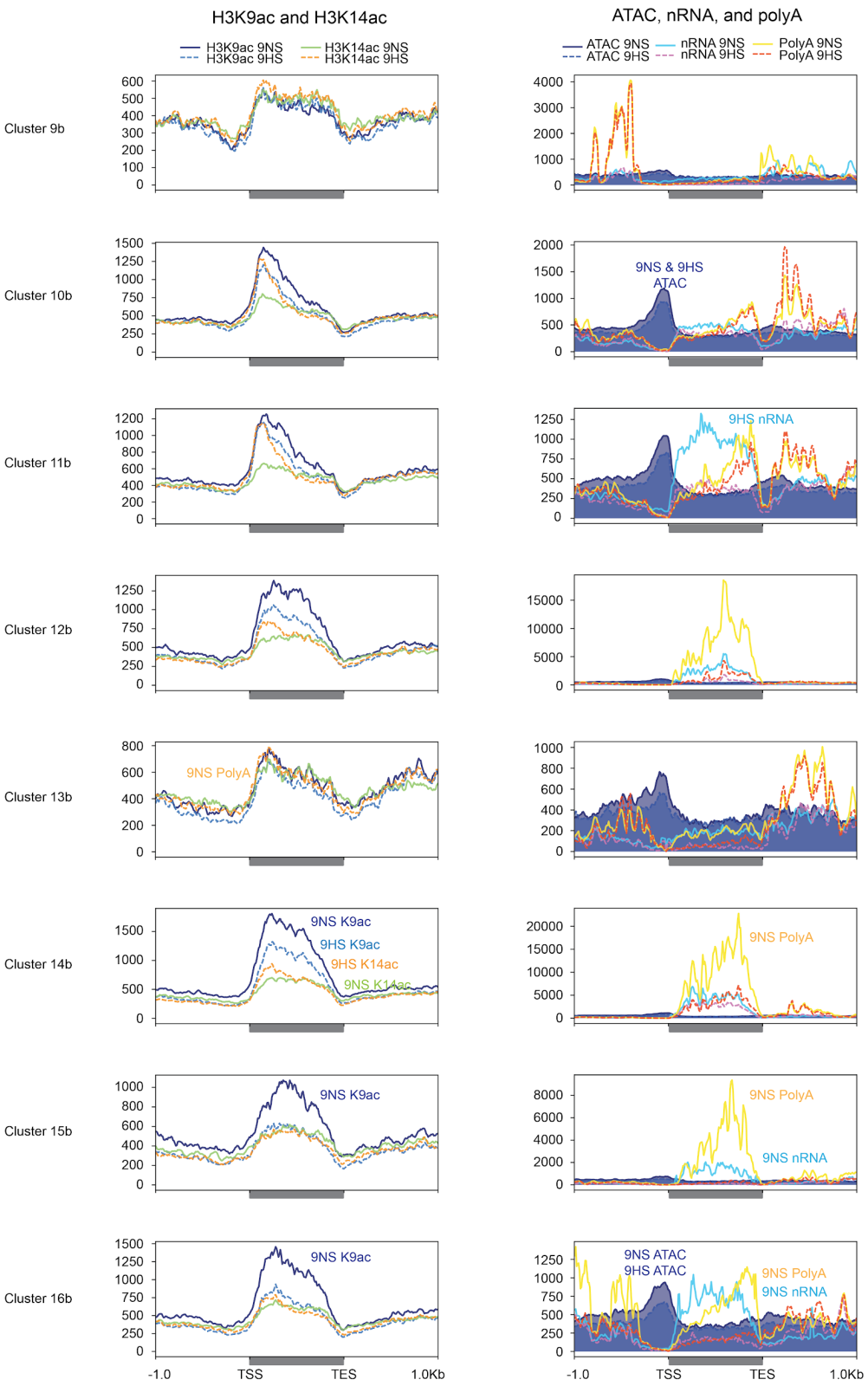

Figure S8. Histone and gene activity comparisons of genes co-regulated after 9 h of hypoxic stress. Average signal of chromatin and RNA data for co-regulated gene clusters identified from the 9 h hypoxic stress comparison (9HS/9NS) in Fig. 6b. Plotting is as described for Figure S6.

bioRxiv preprint doi: https://doi.org/10.1101/479980; this version posted November 27, 2018. The copyright holder for this preprint (which was not certified by peer review) is the author/funder, who has granted bioRxiv a license to display the preprint in perpetuity. It is made available under aCC-BY-NC-ND 4.0 International license.

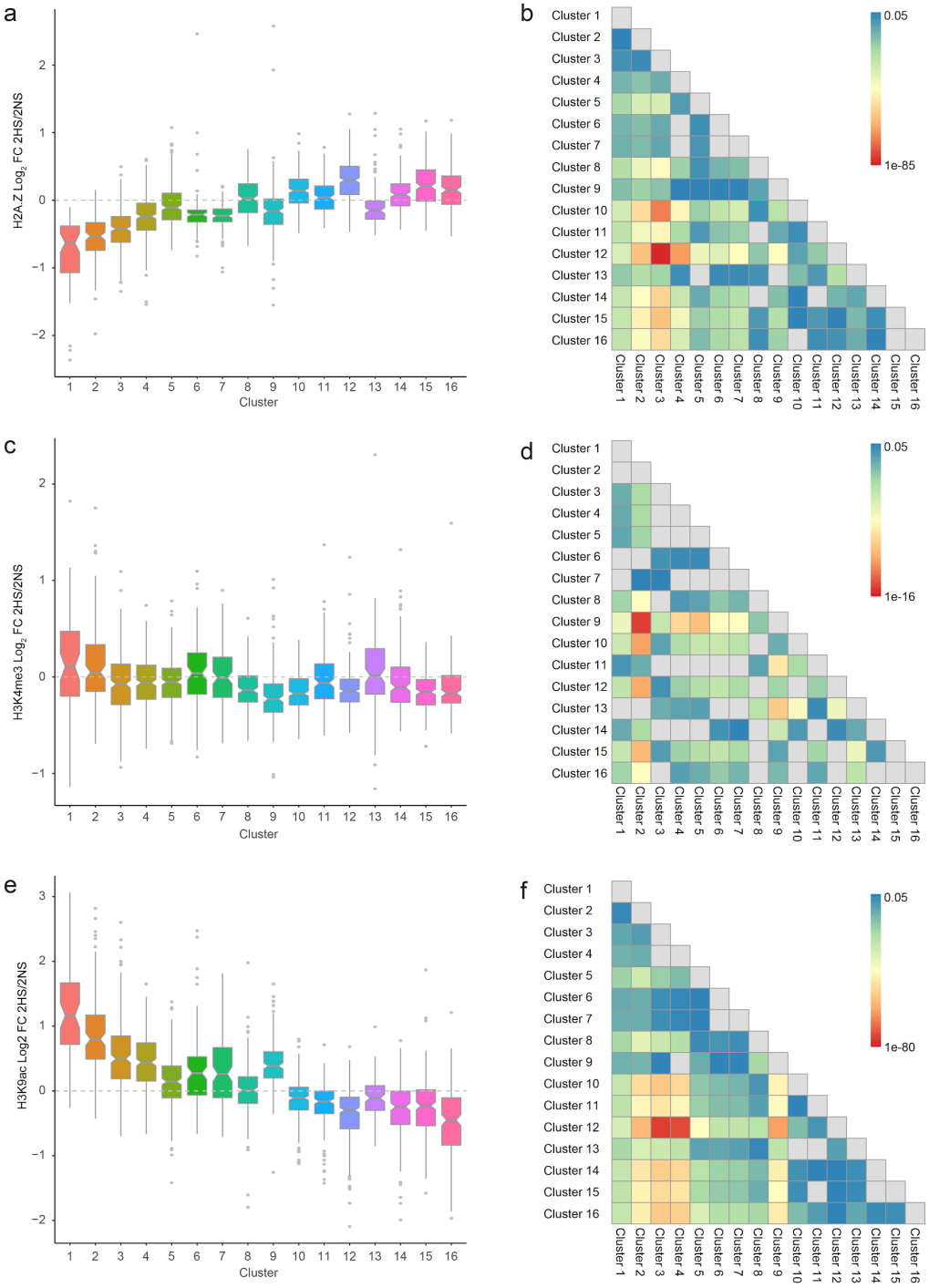

Figure S9. Quantitative analysis of dynamics in histone modifications of co-regulated gene clusters after 2 h of hypoxic stress. a, c, e Box plots of log_2 fold change in response to 2 h hypoxic stress of H2A.Z, H3K4me3 and H3K9ac for the 16 clusters shown in Panels **b**, **d**, **f** provide Wilcoxon signed rank test values of gene clusters in an all by all matrix. Grey boxes denote no significant difference between clusters. Heatmap scale depicts significance values of $p < 0.05$.

bioRxiv preprint doi: https://doi.org/10.1101/479980; this version posted November 27, 2018. The copyright holder for this preprint (which was not certified by peer review) is the author/funder, who has granted bioRxiv a license to display the preprint in perpetuity. It is made available under aCC-BY-NC-ND 4.0 International license.

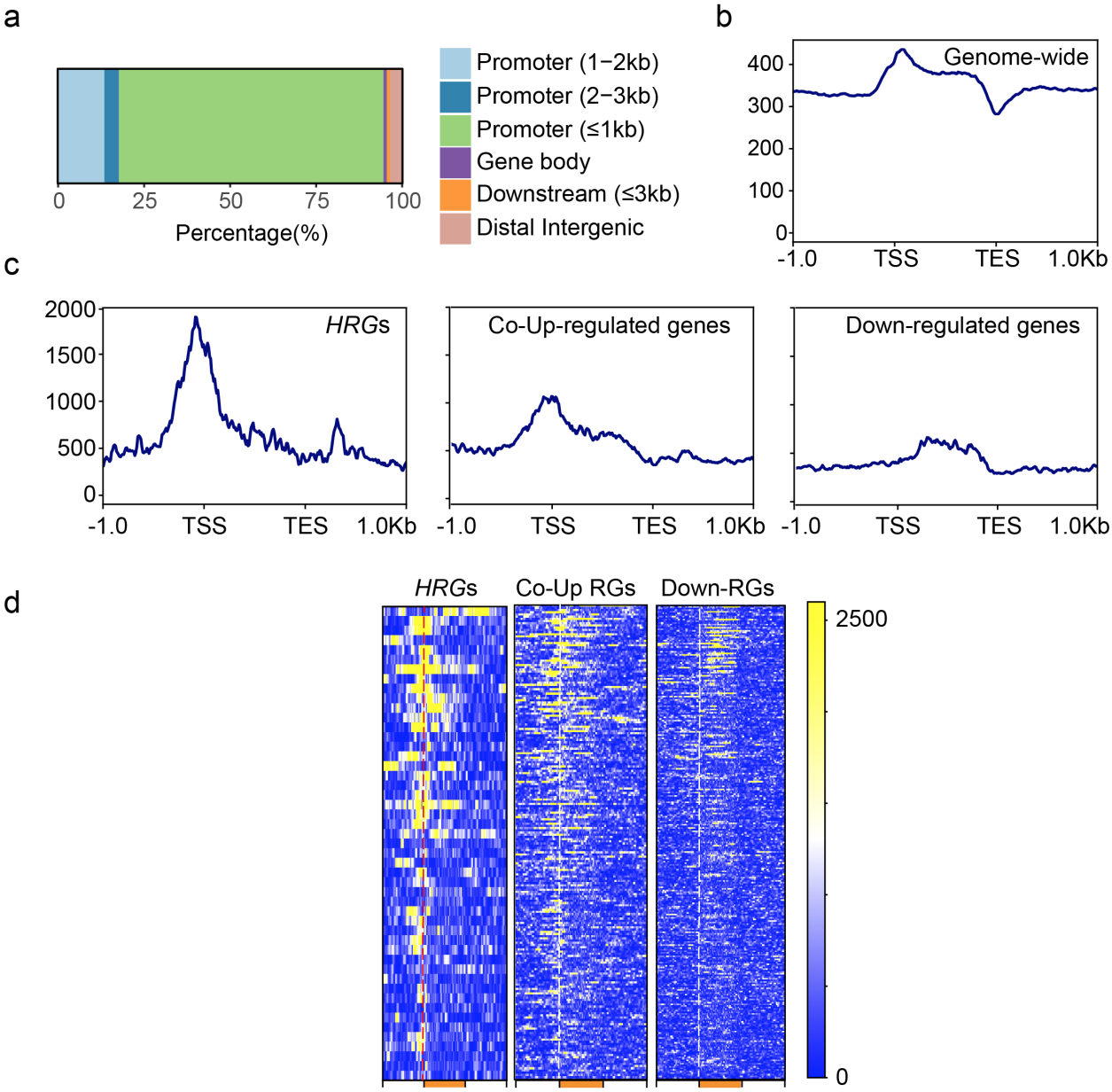

Figure S10. Genome-wide binding dynamics of HRE2 determined by ChIP-seq. **a** Distribution of HRE2 peaks on genomic features. **b, c** Average HRE2-ChIP read distribution in regions spanning 1 kb upstream to 1 kb downstream of gene features: **b** genome wide and **c** for the *HRG*s, Coordinately upregulated genes (Co-Up), and Down regulated genes (RGs). **d** Heat map of the HRE2- ChIP reads for genes in each group (*HRG*s) (n=49) and co-UP (n=213, and down-RGs (n=297). Each row in the heat map represents an individual gene; gene order is the same in all plots.

bioRxiv preprint doi: https://doi.org/10.1101/479980; this version posted November 27, 2018. The copyright holder for this preprint (which was not certified by peer review) is the author/funder, who has granted bioRxiv a license to display the preprint in perpetuity. It is made available under aCC-BY-NC-ND 4.0 International license.

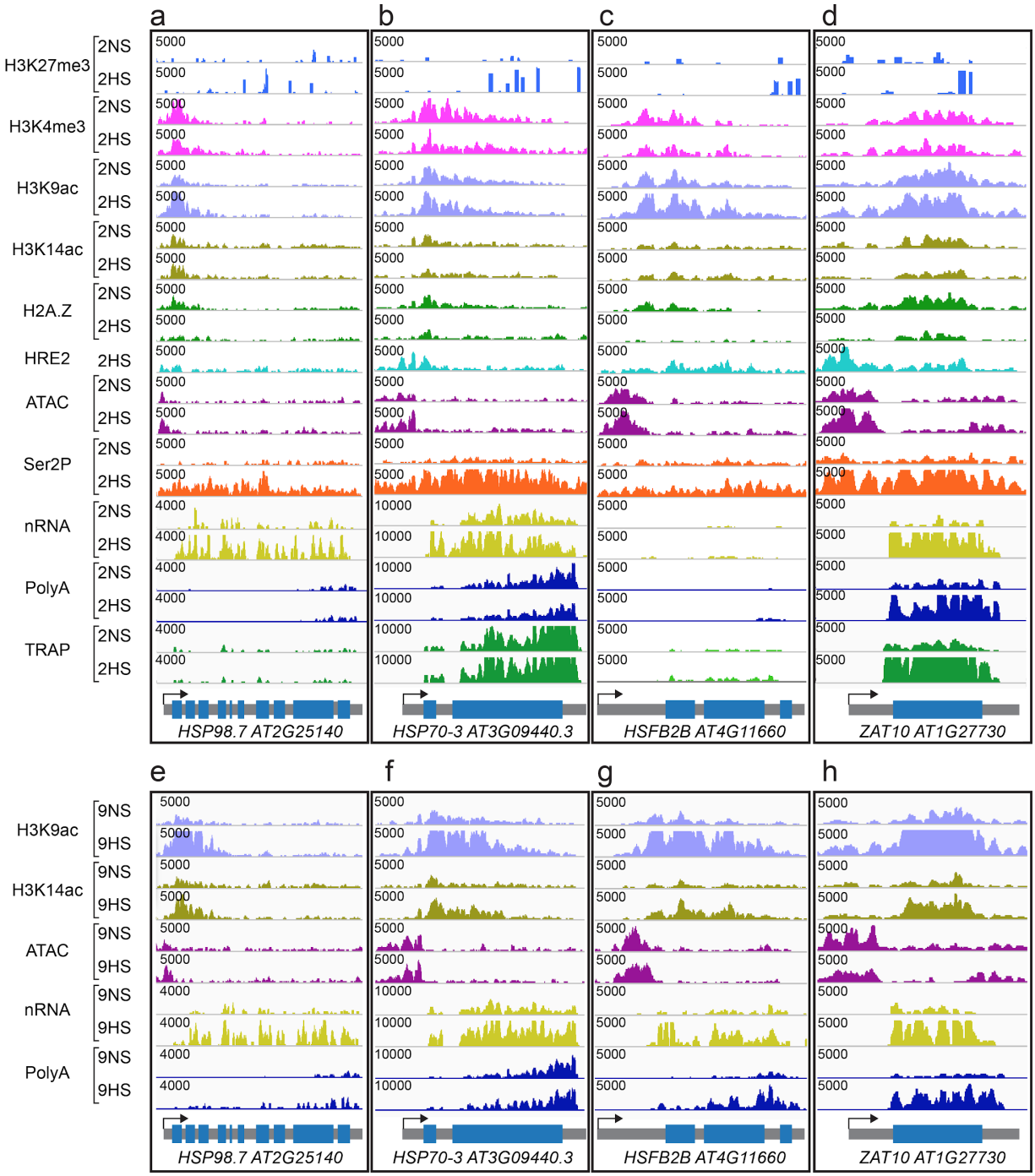

Figure S11. **Genome browser view of normalized read coverage of histone, ATAC-seq, RNAPII-Ser2P, HRE2-chromatin immunopurification and RNA outputs for representative genes of cluster 9. a-d** Normoxia (2NS) and 2 h hypoxic stress (2HS). **e-h** 9NS and 9HS samples. **a,e** *HEAT SHCOK PROTEIN (HSP) 98-7* **b,f** *HSP70-3,* **c,g** *HEAT SHOCK TRANSCRIPTION FACTOR B2B* and **d,h** *ZAT10.* The maximum read scale value used for chromatin based and RNA based outputs is provided. At bottom, the transcription unit is shown in grey with the transcription start site marked with an arrow.